3-21-2019

Simulation and Piloted Simulator Study of an Automatic Ground Collision Avoidance System for Performance Limited Aircraft

James D. Carpenter

Simulation and Piloted Simulator Study of an Automatic Ground Collision Avoidance System for Performance Limited Aircraft

THESIS

James D. Carpenter, Capt, USAF

AFIT-ENY-MS-19-M-207

DEPARTMENT OF THE AIR FORCE
AIR UNIVERSITY

AIR FORCE INSTITUTE OF TECHNOLOGY

Wright-Patterson Air Force Base, Ohio

AFIT-ENY-MS-19-M-207

Simulation and Piloted Simulator Study of an Automatic Ground Collision Avoidance System for Performance Limited Aircraft

THESIS

Presented to the Faculty

Department of Aeronautics and Astronautics

Graduate School of Engineering and Management

Air Force Institute of Technology

Air University

Air Education and Training Command

in Partial Fulfillment of the Requirements for the

Degree of Master of Science in Aeronautical Engineering

James D. Carpenter, B.S.M.E.

Capt, USAF

March 21, 2019

AFIT-ENY-MS-19-M-207

Simulation and Piloted Simulator Study of an Automatic Ground Collision Avoidance System for Performance Limited Aircraft

THESIS

James D. Carpenter, B.S.M.E.
Capt, USAF

Committee Membership:

Richard G. Cobb, Ph.D.
Chair

Bradley S. Liebst, Ph.D.
Member

Donald L. Kunz, Ph.D.
Member

Abstract

The F-16 Automatic-Ground Collision Avoidance System (Auto-GCAS) has been a resounding success since implementation in Nov 2014, saving 8 pilots and 7 aircraft from Controlled Flight into Terrain (CFIT). However, there is no implemented Auto-GCAS for "heavy" performance limited aircraft. This research endeavors to expand on the success of F-16 Auto-GCAS to other aircraft in the Air Force inventory such as the C-130, C-17, and B-1. MIL-STD-1797 classifies performance limited aircraft as large, heavy, and low to medium maneuverability. Using a stitched Learjet-25D model (LJ-25D), an Auto-GCAS algorithm was developed to predict multiple escape-maneuver trajectories, compare these paths to digital terrain elevation data (DTED), and trigger the most aggressive escape path upon predicted terrain collision. Multiple numerical integration methods were compared to balance computational speed vs. accuracy. The Adams-Bashforth multi-step method showed improved accuracy and increased speed than the previous Euler Explicit method. Simulations in a modified DTED terrain map evaluated differences in Auto-GCAS algorithm design, principally forward look-ahead time. Results showed extending the forward look-ahead time past 45 s did not decrease collision prevention, but changing the trigger activation to the forward-open method successfully reduced the number of collisions. An algorithm was developed to vary trajectory prediction based on airspeed and performance variables without increasing computational cost. This Trajectory Prediction Algorithm (TPA) was able to extend the forward climb look-ahead time approximately 20 seconds at slower airspeeds and successfully escape a box canyon where previous methods failed. Preliminary pilot feedback was collected through a piloted simulator study at Air Force Research Laboratory's (AFRL) Multi-Crew Cockpit Simulator (MCCS).

Acknowledgements

Dedicated to all those who have been lost in ground collision accidents, and to my family, friends, and colleague's for their critical thinking, listening and encouragement

I specifically want to thank several people for their contribution to this research. Many thanks to Dr. Cobb for his guidance and enthusiasm towards this research topic. His expertise and instruction throughout this program was truly an honor to learn under. The previous and continued efforts of the Auto-GCAS community have astonished me and I am glad to be a small part of this very important and life saving effort. The successful implementation by the AFRL ACAT team on F-16 Auto-GCAS is validation of the positive impact engineering can have on people's lives. The previous work accomplished by Col Suplisson, Major Trombetta, and Capt Gahan was inspirational to helping to transfer Auto-GCAS to performance limited aircraft. Additionally, at NASA Armstrong I appreciated the time with Mark Skoog discussing his research, Mark is a great problem solver who can see the road ahead in Auto-GCAS designs. Last but not least, thank you to Stephanie Simon, Zach Demers, and Tom Danube at AFRL/RQQ who assisted in integration of the Auto-GCAS algorithm into a working simulator. No Nerds, No Birds!

James D. Carpenter

Table of Contents

Page

Abstract iv

Acknowledgements v

List of Figures ix

List of Tables xiii

I. Introduction 1

1.1 Motivation 1
1.2 Problem Statement and Research Objectives 3
1.3 Methodology Outline 4
1.4 Assumptions and Limitations 5
1.5 Document Outline 6

II. Literature Review 7

2.1 Auto-GCAS Overarching Design 7
2.1.1 Framework Principles 7
2.1.2 Conflict Detection and Resolution 8
2.2 Existing Terrain Awareness and Warning System 12
2.2.1 GPWS Mode 2 - Excessive Closure to Terrain 13
2.2.2 EGPWS Mode 2 - Terrain look-ahead Alerting 14
2.3 Aircraft Model Types: 3-Degree of Freedom Point Mass vs. 6-Degree of Freedom 15
2.4 Reference Frames and Coordinate Systems 18
2.5 Digital Elevation Model - Terrain Elevation 22
2.6 Auto-GCAS Research and Implementation 24
2.6.1 F-16 Auto-GCAS System 24
2.6.2 NASA Small Unmanned Aerial Vehicle Auto-GCAS System 26
2.7 AFIT Auto-GCAS Academic and Flight Test Research 28
2.8 Existing Display and Warning Settings for Terrain Avoidance 30
2.9 Flight Path Prediction: Selected Numerical Integration Methods 32
2.9.1 Building Blocks of a Numerical Integration 33
2.9.2 Classification of Numerical Integration 34
2.9.3 Euler Explicit (Forward Euler) Method 37
2.9.4 Runge-Kutta Method 37
2.9.5 Adams-Bashforth Method 40

Page

2.10 Chapter II Summary 41

III. Simulation Methodology 42

3.1 Learjet 6-DOF System Model 42
3.2 Implementation of LJ-25D Model in Auto-GCAS Algorithm 45
3.2.1 LJ-25D State Propagation 46
3.2.2 LJ-25D State Dimensions 48
3.2.3 LJ-25D Collision Detection 48
3.2.4 LJ-25D Collision Resolution and Maneuvers 49
3.2.5 LJ-25D Multiple-Conflicts 50
3.3 Numerical Integration Methods Used for Comparison 50
3.3.1 Euler Solver 53
3.3.2 Adams-Bashforth Solver 54
3.3.3 MATLAB ode2 Solver 55
3.3.4 MATLAB ode3 Solver 55
3.3.5 MATLAB ode4 Solver 56
3.3.6 MATLAB ode5 Solver 57
3.3.7 MATLAB ode45 Solver 58
3.4 System Under Test and Measures of Performance 60
3.4.1 Description of LJ-25D Auto-GCAS algorithm 60
3.4.2 Down Selection of Integration Methods 62
3.4.3 Measure of Performance (MOP): Comparison of LJ-25D Auto-GCAS Models 64
3.5 Chapter III Summary 67

IV. Simulation Results 68

4.1 Predicted Aircraft Trajectory Integration Comparison 68
4.2 Euler and Adams-Bashforth Off-Nominal Integration Comparison 73
4.2.1 Trim Condition 1 73
4.2.2 Trim Condition 2 76
4.2.3 Trim Condition 3 79
4.3 Comparison of Extending Forward Look-Ahead Time 81
4.4 Time Varying Paths 86
4.5 Chapter IV Summary 89

V. Piloted Simulator Study Methodology and Results 91

5.1 Piloted Simulator Study - MCCS 91
5.1.1 Nuisance Boundary 92
5.1.2 Pilot Displays and Warnings 94
5.2 Piloted Simulator Study Results 98

Page

5.2.1 Time to Impact 98
5.2.2 Feedback on System Operation 102
5.3 Chapter V Summary 106

VI. Conclusions and Recommendations 107

6.1 Contributions to Research Goals 107
6.2 Predicted Aircraft Trajectory Integration Methods 109
6.3 Simulation Results in Terrain Test Matrix 109
6.4 Time Varying TPA 110
6.5 Piloted Simulator Study 111
6.6 Recommendations for Future Auto-GCAS Design 111
6.7 Conclusion 113

Appendix A. Path Integration Comparison for Steady-Level Flight 114

Appendix B. Euler vs Adams-Bashforth Path Integration Comparison for Off-Nominal Flight 118

Appendix C. Test Terrain for Extended Forward Look-Ahead Time: Euler vs Adams-Bashforth Integration Comparison 125

Appendix D. Piloted Study Test Plan in AFRL Multi-Crew Cockpit Simulator (MCCS) 129

List of Figures

Figure		Page
1	State Propagation Methods for Conflict Detection and Resolution Methods [11]	9
2	Ground Proximity Warning System Mode 2 - Excessive Closure to Terrain Warning Envelopes [17]	13
3	Enhanced Ground Proximity Warning System Mode 2 - Terrain Caution and Warning Envelopes [16]	15
4	Earth geoid and definition of height [21]	19
5	Earth Centered Earth Fixed (ECEF) Coordinate Frame [21]	20
6	Aircraft Body and Wind axes Reference Frame [21]	21
7	Aircraft Body and Wind axes Reference Frame [21]	21
8	(a) Tip-Tilt DEM Data and (b) Typical Thinned DEM Data [25]	23
9	Output of NASA GEDACS compression algorithm for DEM data [25]	24
10	F-16 Auto-GCAS Terrain Scanning and Binning Process[12]	25
11	Nuisance Determination: Time Available vs. Pilot Anxiety Rating [26]	26
12	SUAV Escape-Maneuvers and Selection [25]	27
13	SUAV Top-view of Escape-Maneuvers with P-factor [25]	27
14	SUAV Scan Zone Overlaying DTED Posts [25]	28
15	SUAV Post Scanning Technique to search DTED height [25]	28
16	Auto-GCAS Chevrons Closing to Warn Impending Activation [29]	31

Figure Page

17 Auto-GCAS Activated with Break "X" and "FLYUP" on HUD [29] 31

18 Enhanced Ground Proximity Warning System - Peaks Color Code [17] 32

19 Enhanced Ground Proximity Warning System - Peaks Heads-Down Display [17] 32

20 Euler Explicit Method for solving ODE initial value problems [35] 37

21 4^{th} Order Runge-Kutta Explicit Method for solving ODE initial value problems [35] 40

22 Auto-GCAS System Architecture [10] 46

23 Auto-GCAS Refresh Rate [12] 47

24 DTED Nearest Interpolation (Continuous Grid) vs. DTED Post Terrain (Discrete Grid) 49

25 Auto-GCAS Algorithm Varying Path Lengths Based on Escape-Maneuver Performance 62

26 Modified DTED Terrain for Simulation Comparison (Front Wall Not Shown) 64

27 Modified DTED Terrain Simulation Example Run 65

28 Level Left Accuracy vs. Speed Integration Comparison for Steady-Level Flight 69

29 Climbing Left Accuracy vs. Speed Integration Comparison for Steady-Level Flight 70

30 Forward Climb Accuracy vs. Speed Integration Comparison for Steady-Level Flight 72

31 Level Left Accuracy vs. Speed Comparison for Trim Condition 1 74

32 Climbing Left Accuracy vs. Speed Comparison for Trim Condition 1 75

Figure Page

33 Forward Climb Accuracy vs. Speed Comparison for Trim Condition 1 76

34 Level Left Accuracy vs. Speed Comparison for Trim Condition 2 77

35 Climbing Left Accuracy vs. Speed Comparison for Trim Condition 2 78

36 Forward Climb Accuracy vs. Speed Comparison for Trim Condition 2 79

37 Climbing Right Euler Integration at Trim Condition 3 - Maximum RSS Error vs. Time 81

38 Simulation of First-Open Trigger Activation showing (a) Flightpath and (b) Height Above Terrain profiles 85

39 Simulation of Forward-Open Trigger Activation showing (a) Flightpath and (b) Height Above Terrain profiles 86

40 Wasted Computation Time for Trajectory Prediction - Stalled Flight Conditions 86

41 *AB Varying* Auto-GCAS Algorithm Flying Towards Boxed Canyon 88

42 *AB30 45FC* Auto-GCAS Algorithm Flying Towards Boxed Canyon 89

43 View of the Multi-Crew Cockpit Simulator (MCCS) [44] 91

44 Collision Point Scan Area 93

45 Level Left Turn: Time Available at Anxiety Point vs. Time Available at Min Distance Point 95

46 HUD Symbology for Pre-Initiation of Auto-GCAS Algorithm [44] 96

47 HUD Symbology for Initiation of Auto-GCAS Algorithm [44] 96

48 Four PFD Designs for Piloted Simulator Study 97

Figure Page

49 Level Left Minimum Distance Time to Collision at Anxiety Point 99

50 Climbing Left Minimum Distance Time to Collision at Anxiety Point 100

51 Forward Climb Minimum Distance Time to Collision at Anxiety Point 100

52 Climbing Right Minimum Distance Time to Collision at Anxiety Point 101

53 Level Right Minimum Distance Time to Collision at Anxiety Point 101

54 Test Subject 6 - Level Left Escape-Maneuvers and Projected Time to Collision Points 129

55 Test Subject 6 - Climbing Left Escape-Maneuvers and Projected Time to Collision Points 130

56 Test Subject 6 - Forward Climb Escape-Maneuvers and Projected Time to Collision Points 131

57 Test Subject 6 - Climbing Right Escape-Maneuvers and Projected Time to Collision Points 132

58 Test Subject 6 - Level Right Escape-Maneuvers and Projected Time to Collision Points 133

List of Tables

Table		Page
1	Digital Terrain Elevation Data (DTED) Accuracy [24, 12]	23
2	Constants of third-order Runge-Kutta methods [35] [39]	39
3	LJ-25D Auto-GCAS TPA Escape-Maneuvers [10]	47
4	Proposed Escape-Maneuvers Propagation Times [13]	48
5	Butchers Tableau for Dormand-Prince 5th Order Runge-Kutta [42]	58
6	Butchers Tableau for Dormand-Prince ode45 Solver [42]	59
7	LJ-25D Auto-GCAS Algorithm Differences	61
8	Level Left Integration Comparison with 0.015s time step	70
9	Climbing Left Integration Comparison with 0.015s time step	71
10	Forward Climb Integration Comparison with 0.015s time step	71
11	Trim Condition 3: Best Approximations for Trajectory Prediction	80
12	Overall LJ-25D Auto-GCAS Extending Forward Look-Ahead Time	82
13	Varying Safety Buffer: LJ-25D Auto-GCAS Extending Forward Look-Ahead Time	83
14	Varying Initial Airspeed: LJ-25D Auto-GCAS Extending Forward Look-Ahead Time	84
15	Boxed Canyon Simulation Comparison	87
16	Anxiety Rating For Time Available Determination [26]	94
17	Piloted Simulator Study - Overall Rating for PFD Displays	104

List of Symbols

α	Angle of Attack
α_e	Angle of Attack, Equilibrium
β	Sideslip Angle
δ_f	Flap Deflection
ρ	Scheduling Parameter Vector
γ	Flight Path Angle
$\dot{\gamma}$	Flight Path Angle, Time Rate of Change
ψ	Heading Angle
$\dot{\psi}$	Heading Angle, Time Rate of Change
θ	Pitch Angle
$\dot{\theta}$	Pitch Angle Rate
ϕ	Bank Angle
$\dot{\phi}$	Bank Angle Rate
ψ	Yaw Angle
$\dot{\phi}$	Yaw Angle Rate
g	Acceleration of Gravity
$\dot{h}$	Aircraft Climb Rate
I	Moment of Inertia
D	Drag
L	Lift
T	Thrust
L	Roll Moment
M	Pitch Moment
N	Yaw Moment
X	Aircraft Horizontal Force
Y	Aircraft Lateral Force
Z	Aircraft Vertical Force
p	Aircraft Body Roll Rate
$\dot{p}$	Aircraft Body Roll Acceleration

q	Aircraft Body Pitch Rate
$\dot{q}$	Aircraft Body Pitch Acceleration
r	Aircraft Body Yaw Rate
$\dot{r}$	Aircraft Body Roll Acceleration
u	Aircraft Horizontal Velocity
$\dot{u}$	Aircraft Horizontal Acceleration
v	Aircraft Lateral Velocity
$\dot{v}$	Aircraft Lateral Acceleration
w	Aircraft Vertical Velocity
$\dot{w}$	Aircraft Vertical Acceleration
x	Horizontal Position
$\dot{x}$	Horizontal Velocity
y	Lateral Position
$\dot{y}$	Lateral Velocity
z	Vertical Position
$\dot{z}$	Vertical Velocity
V_t	Aircraft Body Velocity Vector
V	Airspeed
$\dot{V}$	Airspeed Acceleration
v_{w_x}	Wind Speed, Horizontal
v_{w_y}	Wind Speed, Lateral
v_{w_z}	Wind Speed, Vertical

List of Acronyms

ACAS	Air Collision Avoidance System
AGL	Above Ground Level
AFIT	Air Force Institute of Technology
AFRL	Air Force Research Laboratory
ATM	Air Traffic Management
AoA	Angle of Attack
Auto-GCAS	Automatic Ground Collision Avoidance System
CDR	Conflict Detection and Resolution
CG	Center of Gravity
CFIT	Controlled Flight Into Terrain
CICTT	Commercial International Common Taxonomy Team
CL	Climbing Left
CR	Climbing Right
CRM	Crew Resource Management
DCM	Direction Cosine Matrix
DEM	Digital Elevation Model
DGM	Digital Ground Model
DoD	Department of Defense
DOF	Degree of Freedom
DTED	Digital Terrain Elevation Data
DSM	Digital Surface Model
DSOC	Defense Safety Oversight Council
ECEF	Earth-Centered Earth-Fixed
EGI	Embedded Global Positioning System Inertial Navigation System
EGPWS	Enhanced Ground Proximity Warning System
ENU	East-North-Up
FAA	Federal Aviation Administration
FC	Forward Climb
ft	Feet

FRRP	Fighter Risk Reduction Program
GEDACS	Global Elevation Data Adaptive Compression System
GPWS	Ground Proximity Warning System
HAT	Height Above Terrain
HDD	Heads Down Display
HUD	Heads Up Display
IATA	International Air Transport Association
ICAS	Integrated Collision Avoidance System
IVP	Initial Value Problem
KTAS	Knots True Air Speed
KIAS	Knots Indicated Air Speed
LJ-25D	Learjet Aircraft, Model Type 25D
LL	Level Left
LR	Level Right
LPV	Linear Paraemter Varying
LRRA	Low Range Radar Altimeter
MATLAB	MATrix LABoratory
MCCS	Multi-Crew Cockpit Simulator
NASA	National Aeronautical and Space Administration
NED	North-East-Down
NGA	National Geospatial-Intelligence Agency
ODE	Ordinary Differential Equations
PARS	Pilot Activated Recovery System
PFD	Primary Flight Display
RMS	Root Mean Square
s	Seconds
SRTM	Shuttle Radar Topography Mission
SUAV	Small Unmanned Aerial Vehicle
TAWS	Terrain Awareness and Warning System
TPA	Trajectory Prediction Algorithm
TPS	Test Pilot School
UAV	Unmanned Aerial Vehicle
WGS-84	World Geodetic System 1984

Simulation and Piloted Simulator Study of an Automatic Ground Collision Avoidance System for Performance Limited Aircraft

I. Introduction

1.1 Motivation

Controlled Flight into Terrain (CFIT) remains a leading cause of fatalities and loss of aircraft for both Department of Defense (DoD) and civilian aircrew. The Federal Aviation Administration (FAA) defines CFIT as "An accident or incident in which the airplane, under the flightcrew's control, is inadvertently flown into terrain, obstacles, or water without either sufficient or timely flightcrew awareness to prevent the event, or both"[1]. The International Air Transport Association (IATA) identifies causes of CFIT as human performance deficiencies (Crew Resource Management (CRM), non-compliance with standard operating procedures, and inadequate flight planning and management), loss of situational awareness, target fixation, meteorological, and physiological incapacity [2]. CFIT accidents are rarely survivable and, despite the low number of occurrences, result in high fatality fatalities, aircraft loss and related damage. A 2006 report analyzing 124 United States Air Force (USAF) Class A Mishaps from 1993 - 2002 showed CFIT resulted in 59 destroyed aircraft, 132 fatalities, and a financial loss of $1.94 Billion (Fiscal Year 2001 $)[3]. Breaking down by aircraft category, fighter aircraft accounted for 23 CFIT accidents and multi-crewed platforms accounted for 14 CFIT accidents [3]. The United States Air Force Academy business case study between 1992 - 2015, found that within the DoD there were 28 C-130 Class A mishaps, of which five of these were identified as CFIT mishaps and Auto-GCAS

preventable, costing 34 lives [4]. Extending into the civilian sector, among all forms of air transport, NASA reported data between 2001 and 2010 finding 19.8% of aircraft accidents were CFIT, accounting for 46% of aircraft fatalities [5]. The IATA CFIT Accident Analysis Report [2] from 2008 to 2017, analyzed civilian sector accidents for aircraft over 12.5k lbs gross-take-off weight. While the IATA identified 47 CFIT accidents (6% of reported aviation accidents), these this resulted in 892 fatalities (28% of total fatal accidents) [2]. Additionally, the Commercial International Common Taxonomy Team (CICTT) tracks commercial jet CFIT accidents, where between 2008 and 2017, 636 fatalities were caused by CFIT (24% of total fatal accidents and 26% of all fatalities) [6].

CFIT affects all aviation communities. Another solution in addition to existing warning systems and CRM training needs to be implemented to reduce the percentage of CFIT accidents within commercial and military aircraft operations. The DoD addressed this is in 2003 when Defense Secretary Rumsfeld established an executive action to reduce military accidents by 50% in two years [7] and in 2005 a goal of reducing CFIT mishaps by 75% was established [8]. The resulting F-16 Automatic-Ground Collision Avoidance System (Auto-GCAS) developed between 2007 and 2014 has been a resounding success since implementation in Nov 2014 – saving 8 pilots and 7 aircraft from CFIT [9]. But what about "heavy" performance limited aircraft in the Air Force inventory such as the C-130, C-17, and B-1? There currently is no implemented Auto-GCAS to prevent CFIT for heavy performance limited aircraft. With the advancement of flight control computers and increased processing capability, it is feasible to implement the next step in terrain avoidance. The aircraft's flight control computer should be enabled to act automatically on the monitoring and warning systems already in place to control the aircraft temporarily away from terrain. Aircraft autopilot's acting on calculated aircraft projected state data is the difference between

an automatic warning system and a warning system. However, automatic controls come with considerable responsibility to design a robust system that acts reliably, timely, nuisance free, and ultimately at the discretion of the pilot.

1.2 Problem Statement and Research Objectives

The challenge is to reduce and eventually eliminate controlled flight into terrain (CFIT) for heavy performance limited aircraft. Expanding the F-16 Auto-GCAS to heavy aircraft requires designing a specific heavy Auto-GCAS algorithm with multiple escape-maneuvers. Additionally, Auto-GCAS designs need to assist aircrew who perform low-level flying missions and operate in mountainous terrain. The research objective is to extend the capabilities successfully proven in the fighter Auto-GCAS to a heavier aircraft platform labeled as a performance limited aircraft. Specific research objectives were:

(1) Expand the previous 3-Degree of Freedom (DOF) aircraft point model to a 6-DOF aircraft model

(2) Explore path predictions longer than 30 seconds to determine if the longer times help avoid becoming trapped in a boxed canyon

(3) Examine different path integration methods to improve computation time while maintaining accuracy, specifically to get an adaptive time solver, compare to MATLAB's ode45 solver as the truth source.

(4) Develop adaptive maneuvers with time varying prediction lengths.

(5) Evaluate initial display concepts that can be incorporated into future pilot system design and assess autopilot nuisance criteria in a simulator.

This research seeks to advance existing Auto-GCAS algorithms to include forward climbs with lateral escape-maneuvers suitable for performance limited heavy aircraft, and ultimately act as the ultimate wingman to the aircraft crew by constantly mon-

itoring and automatically acting, if needed, to avoid collisions with terrain.

1.3 Methodology Outline

The methodology to explore the research objectives of increasing computation speed while increasing collision prediction accuracy and forward look-ahead time for box canyon scenarios is the following. Using the a stitched Learjet aircraft model (LJ-25D) and existing algorithm developed by Gahan [10], a numerical integration comparison between different integration methods was conducted. This was to down-select a method that provided good prediction accuracy while maintaining computation speed. Then, a comparison of extending the forward look-ahead time was conducted to determine the impact increased escape-maneuver lengths would have in avoiding terrain. Additionally, a piloted simulator study was conducted to receive initial pilot feedback on Auto-GCAS algorithm operation and displays. The specific research methodology was:

(1) Update existing algorithm code to execute simulations in a modified terrain map to determine impact of extending forward look-ahead times.

(2) Implement multiple aircraft escape-maneuver trajectory prediction algorithms (TPA) to compare accuracy vs. speed of execution. The different integration methods were compared initially in a straight-level aircraft position and also in off-nominal conditions.

(3) Implement varying path lengths to speed up algorithm.

(4) Change trigger selection criteria to avoid chatter of design and early handback.

(5) Establish nuisance boundary of LJ-25D model in a piloted simulator study, write a simulator test plan and develop prototype display designs, and verify if the existing algorithm meets pilot nuisance criteria.

1.4 Assumptions and Limitations

The trajectory integration and simulations did not factor in wind or turbulence models, although the code has the capability to incorporate those. The speed of algorithm execution is compared using computer clock speed as a comparison performance metric. Therefore the computer on which the algorithm is loaded will determine how many operations per second the algorithm can run. Translating speed of operation from the desktop computer to an aircraft flight computer was not within the scope of this work.

The LJ-25D is a stitched model and therefore does not have continuous state properties. Interpolations between flight tested data points is required. That converted LJ-25D Simulink model to MATLAB is assumed to accurately represent the actual aircraft. The LJ-25D model also assumed a rigid aircraft and is not subjected to aeroelastic effects. The aircraft state variables in simulation do not factor in changing mass for fuel burn due to the length of simulation, however the mass information can be relayed through the aircraft control computer when implemented on an operation aircraft. The LJ-25D engine model does not factor in throttle position delay or engine spool time to reach a different power setting. Therefore the autopilot algorithm assumes instantaneous engine control between the current setting and maximum power executed for the escape-maneuvers.

Digital Terrain Elevation Data (DTED) Level 1 was used, which has approximately 300 ft spacing between elevation posts. The DTED post was made into a continuous grid through a nearest approximation method in order to calculate terrain elevation not at a latitude / longitude DTED post.

1.5 Document Outline

Chapter II provides relevant technical background regarding conflict detection resolution models, aircraft equations of motion, aircraft reference frames, Auto-GCAS research and implemented designs, and numerical integration methods used for trajectory prediction. The chapter highlights the compounding research on Auto-GCAS by previous Air Force Institute of Technology (AFIT) students.

Chapter III describes the specific LJ-25D aircraft model used, an explanation of 6-DOF aircraft equations of motions used for numerical integration, an explanation of the specific numerical integration methods used to predict future aircraft path trajectories, and the simulation tested digital terrain map.

Chapter IV contains the data and analysis for the path integration comparison and simulations of varying algorithm designs.

Chapter V summarizes the piloted research study methodology and results. The study collected a time to impact for the LJ-25D aircraft and also feedback on displays for pilot situational awareness.

Chapter VI summarizes the research findings, highlights significance of results, and provides recommendations for future research.

Appendix A - Path Integration Comparison for Steady-Level Flight

Appendix B - Euler vs. Adams-Bashforth Path Integration Comparison for Off-Nominal Flight

Appendix C - Test Terrain for Extended Forward Look-Ahead Time: Euler vs. Adams-Bashforth Integration Comparison

Appendix D - Piloted Study Test Plan in Air Force Research Laboratory's (AFRL) Multi-Crew Cockpit Simulator (MCCS)

II. Literature Review

Chapter Overview

This chapter provides an in depth review of Auto-GCAS and similar research. The majority of aircraft collision avoidance focuses on air-to-air avoidance for air traffic control and also for flight path planning. The majority of interest in automatic ground collision avoidance has been focused within the DoD and National Aeronautics and Space Administration (NASA). The final research covered shows the progression of Auto-GCAS application from previous AFIT students. Additionally, a review of the underlying aircraft dynamic reference frames, digital terrain data, geodesics, and the LJ-25D model is conducted.

2.1 Auto-GCAS Overarching Design

2.1.1 Framework Principles.

The framework of the Auto-GCAS algorithm had to fit within the overarching design limits presented by Griffin et al. [8] during the Fighter Risk Reduction Program (FRRP):

1. Do No Harm
2. Do Not Impede Mission Performance
3. Avoid Ground Collisions

These are presented in order of importance. First, the Auto-GCAS algorithm can not harm the aircraft by making the performance worse nor increase the risk for a mishap. The algorithm must have integrity monitoring methods to disable the algorithm if unsafe bounds are reached. Second, the Auto-GCAS algorithm can not interfere with mission operations by impeding aircrew tasks (making tasks more difficult) and also displaying premature or early warnings (which will be tuned out by

pilots, rendering system information obsolete). Third, the algorithm must successfully evade collision with terrain through all phases of the algorithm. The airborne Conflict Detection and Resolution (CDR) systems reviewed by Kuchar and Yang [11] illustrate this third design point by breaking an algorithm into three different phases required to successfully accomplish collision avoidance. The CDR model consists of: (1) Prediction: anticipating and diagnosing future conflicts within a predetermined acceptable search limit, (2) Communication: notification of the conflict to a human operator, and (3) Resolution: assisting the operator in avoiding the future conflict [11]. The heavy Auto-GCAS algorithm designs by Colonel Suplisson [12], Major Trombetta [13], and Capt Gahan [10] presented later in section 2.7 all include these basic CDR design phases to varying degrees.

2.1.2 Conflict Detection and Resolution.

Kuchar and Yang [11] reviewed 68 CDR models and determined six categories where CDR methods differed: (1) State Propagation, (2) State Dimensions, (3) Conflict Detection, (4) Conflict Resolution, (5) Resolution Maneuvers, and (6) Multiple Conflicts.

2.1.2.1 State Propagation.

The CDR model's reliability is directly related to the model's ability to predict the aircraft's future trajectory [11]. The FAA report on aircraft trajectory prediction errors by Mondolini goes even further to highlight the importance, "...high quality and time aircraft trajectory predictions - the cornerstone of current and future automation systems " [14].

Figure 1 (a) shows a nominal state propagation method where aircraft states are extrapolated based on current position, and translational and rotational rates. The

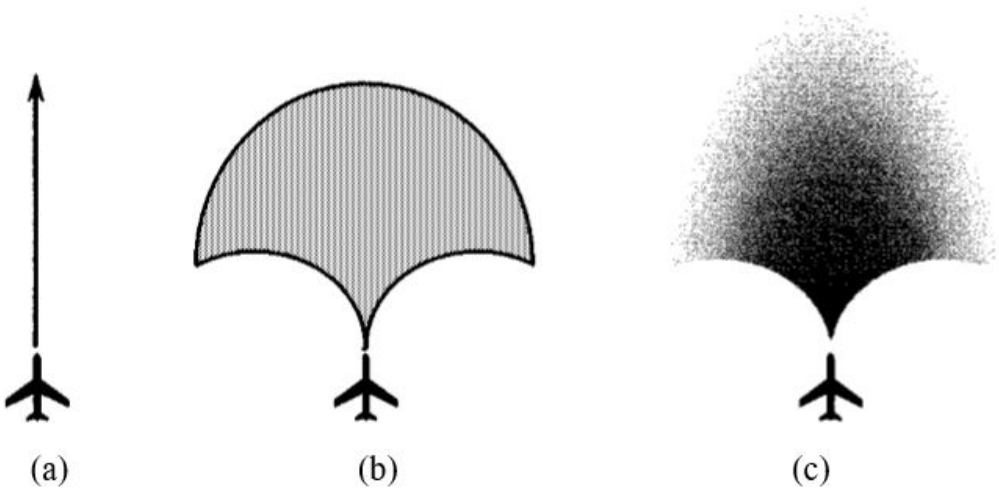

Figure 1. State Propagation Methods for Conflict Detection and Resolution Methods [11]

nominal projection does not account for uncertainties in aircraft behaviour which factor into longer path prediction models and is usually managed by adding a safety buffer or minimum missed distance / time threshold [11]. Figure 1 (b) shows a worst-case state propagation method where a collection of projections are combined into a forward scanning boundary to form a wider field of view than the nominal path propagation. This is the most conservative approach in that it disregards probability of a path and any intrusion into the forward boundary is determined to be a conflict regardless of likelihood of that path being flown [11]. CDR models using this method need a defined "look-ahead projection time" [11] that define a search boundary, requiring nuisance evaluation and terrain analysis to determine a reasonable projection time. Figure 1 (c) shows a probabilistic state propagation method where aircraft states are assigned a likelihood of position occurrence, and therefore conflicts that are detected fall within a certain probability of occurring versus a worst case scenario or single nominal solution [11].

2.1.2.2 State Dimensions.

The state dimensions indicate which plane (horizontal, vertical, or a combination of both) the algorithm projects aircraft position and searches for conflicts to include missed distances [11, 12]. The majority of CDR models utilize horizontal (typically air-to-air traffic collision avoidance) or a combination of horizontal and vertical, with only the Ground Proximity Warning System (GPWS) measuring conflicts in a purely vertical plane [11]. Utilizing a three dimensional spatial state dimension of the aircraft is critical for Auto-GCAS path propagation, but the conflict detection can still vary between using a horizontal, vertical, or combined approach to terrain collision prediction. At a minimum, for a ground collision avoidance system, the vertical plane needs to be factored in for collision detection [12].

2.1.2.3 Conflict Detection.

Conflict detection is concerned with the identification of a conflict and relaying this information to the operator in the form of an alert [11]. The basis for a detection alert is predefined by a threshold value. For a collision avoidance system, the threshold value can be a time to conflict, a minimum missed distance, or a safe operating range distance. Determining the conflict detection threshold for an Auto-GCAS is a combination of the forward-look-ahead time and the safety threshold of terrain. It is important to note the distinct difference between conflict detection and resolution. Detection identifies the conflict, but that does not mean an action has been taken or is planned to take place. Resolution acts on the detection to solve the conflict, and also defines the level of input required by the operator.

2.1.2.4 Conflict Resolution and Resolution Maneuvers.

Conflict resolution can be prescribed, optimized, modeled as a force field, manual, or non-existent [11]. Prescribed resolutions are fixed maneuvers during system design and do not vary based on current state information. The optimized approach incorporates cost functions which typically minimize control or state variables, but is dependent on the current state input to determine a solution. Optimal is always preferred as a solution but often requires more computational expense that may or may not be operationally feasible. Manual resolutions "allow the user to generate potential conflict resolution solutions and obtain feedback as to whether the trail solution is acceptable" [11]. This allows more control to the operator to solve conflicts and the CDR model will provide feedback indicating if the conflict detected is getting worse or better. The resolution maneuver specifically details the conflict resolution execution. The maneuver dimensions can include turns, vertical climbs, speed changes, or a combination of multiple maneuvers [11]. Resolution maneuvers will depend on the type of aircraft and performance capabilities. For example a high performance fighter aircraft (F-16, F-18, F-22, F-35,etc) may only need a single resolution maneuver to avoid all conflicts. Whereas a low to medium performance aircraft (C-130, C-17, B-1, General Aviation, etc) may need multiple resolution maneuvers to include climbs and lateral turns [12].

2.1.2.5 Multiple Conflicts.

Kuchar and Yang [11] referred to multiple conflicts in the pure air-to-air model of projected collisions with multiple aircraft. The paper explains two different decision making models as pairwise and global; pairwise meaning a sequential conflict resolution method whereas global is a simultaneous conflict resolution method [11]. This can be extrapolated to ground collision since the Auto-GCAS algorithm has

multiple resolution maneuvers, there can be multiple terrain collision conflicts at a given time. Therefore, the system algorithm has to decide priorities for which resolution maneuver to choose, or perhaps factor in the simultaneous collision conflicts to create a new resolution maneuver. With the development of the Integrated Collision Avoidance System (ICAS) combining Air Collision Avoidance Systems (ACAS) with ground collision avoidance systems, there are combinations of multiple conflicts that include air and ground conflicts [15].

2.2 Existing Terrain Awareness and Warning System

Kuchar and Yang [11] characterized CDR methods and outlined the overarching design principles. The specific CDR method pertinent to Auto-GCAS is Honeywell Aerospace's Ground Proximity Warning System (GPWS), which falls under the general FAA category of Terrain Awareness and Warning System (TAWS). This CDR method is currently in use by the USAF on the C-130 and C-17 platforms, through their respective avionics modernization programs.

GPWS has seven basic modes: (1) excessive descent rate, (2) excessive closure to terrain, (3) altitude loss after takeoff, (4) unsafe terrain clearance, (5) excessive deviation below glideslope, (6) advisory callouts, and (7) windshear alerting [16]. The basic GPWS has many enhanced features but the following are three primary features that make the GPWS an Enhanced Ground Proximity Warning System (EPGWS): (1) terrain clearance floor, (2) terrain look-ahead alerting, and (3) predictive wind shear [16]. The design characteristics of Honeywell's EGPWS relevant to Auto-GCAS are GPWS Mode 2 - excessive closure to terrain, and EGPWS Mode 2 - terrain look-ahead alerting.

2.2.1 GPWS Mode 2 - Excessive Closure to Terrain.

The radar altimeter is used to determine above ground level (AGL) altitude, and this GPWS mode is used to protect aircraft from rapidly rising terrain [17] by measuring the AGL closure rate in feet per minute. The system is broken into two configurations: (1) a climbout, cruise, and initial approach (flaps not in landing configuration yet and aircraft not on glideslope centerline), and (2) normal landing approach maneuvers (flaps in landing configuration and gears down) [17]. There are two AGL envelope boundaries that correspond with different warning measures (ref Figure 2); "TERRAIN TERRAIN" is the first audio-visual cue for breaking the first AGL closure rate envelope minimum, and "PULL UP" is the second audio-visual cue for breaking the second AGL closure rate envelope minimum [17].

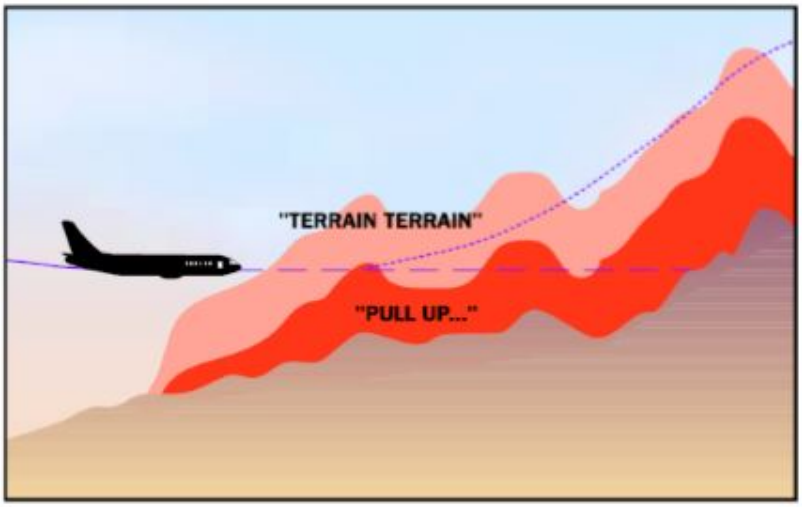

Figure 2. Ground Proximity Warning System Mode 2 - Excessive Closure to Terrain Warning Envelopes [17]

The system envelope minimums vary as a function of the aircraft speed. To reduce pilot warning nuisance, the mode is broken into operational sub-modes based on flight phases where audio-visual cues go away after certain conditions are met (either aircraft gaining 300ft of barometric altitude, 45 seconds of warnings, a decreasing trend in closure rate, or landing flap position is changed) [17]. If the Auto-GCAS system

is to be integrated into aircraft that currently operate with GPWS, the automatic activation should closely correspond to when the second AGL closure rate envelope is breached.

2.2.2 EGPWS Mode 2 - Terrain look-ahead Alerting.

This feature allows for predictive terrain avoidance warning to allow greater situational awareness for pilot resolution to a conflict. This mode has two different envelope warning boundaries, or ribbons, that correspond to a search area forward of the aircraft, "These ribbons [warning boundaries] project down, forward, then up from the aircraft with a width start at 1/4 nm and extending out at $\pm$ 3° laterally, more if turning. The look-down and up angles are a function of the aircraft flight path angle, and the look-down distance a function of the aircraft's altitude with respect to the nearest or destination runway" [17]. Figure 3 below shows the terrain look-ahead alerting range 3.

The normal look-ahead distance varies with airspeed but for the warning ribbon it corresponds approximately to 30 seconds, whereas the look-ahead distance for the caution ribbon is approximately 60 seconds [17]. The tactical version for military flying is roughly 50% shorter than the normal mode, which is intended to reduce pilot nuisance for low-level operations [18]. The EGPWS prioritizes the terrain warnings from GPWS mode 2 via the Low Range Radar Altimeter (LRRA) readings over the EGPWS mode 2 terrain look-ahead alerting [19]. LRRA is used to detect AGL altitude directly underneath the aircraft, which limits the forward-look-ahead ability of terrain prediction [19]. The combination of using LRRA and a digital terrain for 3-Dimensional terrain prediction (as used in the EGPWS) increases redundancy. However, a few disadvantages of LRRA are (1) emission of electrical energy, making the aircraft more visible to adversaries, (2) LRRA is not perfectly reliable for

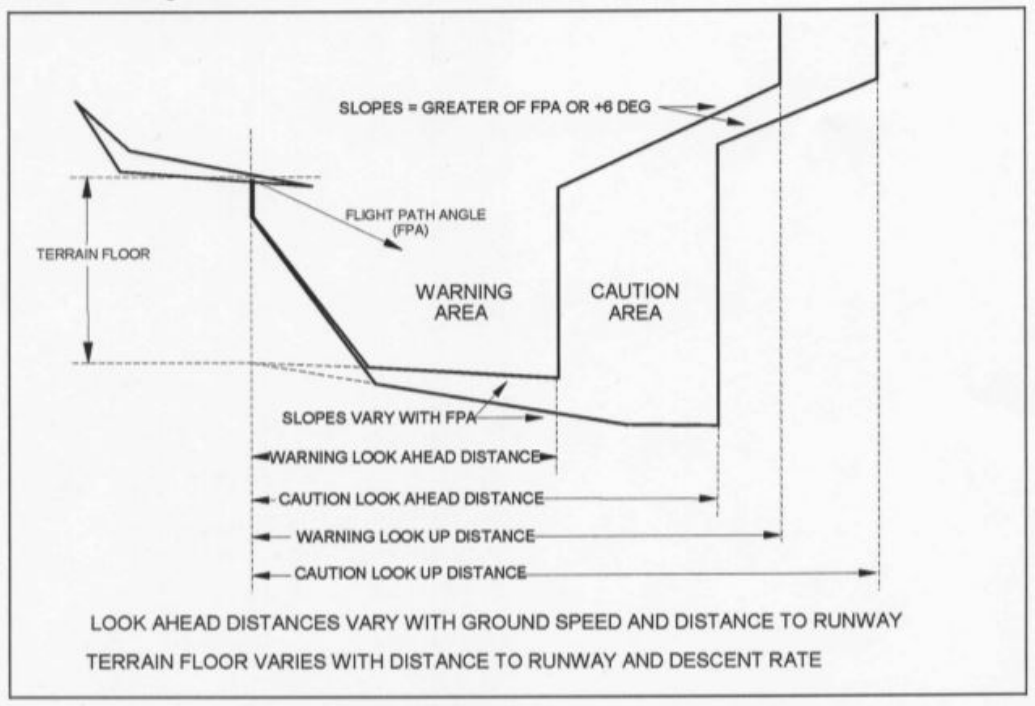

Figure 3. Enhanced Ground Proximity Warning System Mode 2 - Terrain Caution and Warning Envelopes [16]

AGL readings when in banks, and (3) there may be erratic radar altimeter readings causing false altimeter readings and terrain warnings. An example of deficient radar altimeter readings was the Norwegian C-130J crash in 2012, where one crash error was attributed to interference between the two radar altimeters and also reflection from snow / ice on the ground causing false AGL readings [18].

2.3 Aircraft Model Types: 3-Degree of Freedom Point Mass vs. 6-Degree of Freedom

In order to develop a conflict detection and resolution model, a working aircraft model is required. The air-to-air avoidance systems primarily use a 3-DOF point mass model as the significant quantity of data required and higher frequency dynamics for higher order models are not necessary to predict air traffic collisions [14].

The 3-DOF point mass model incorporates aircraft forces and longitudinal accel-

erations, but excludes the moments and angular accelerations [14] and therefore will not as accurately predict the higher order aircraft dynamics. The equations for a 3-DOF point mass model common for aircraft simulation are outlined below [12]:

$$\dot{x} = V\cos\gamma\cos\psi + v_{w_x} \tag{1}$$

$$\dot{y} = V\cos\gamma\sin\psi + v_{w_y} \tag{2}$$

$$\dot{z} = V\sin\gamma + v_{w_z} \tag{3}$$

$$\dot{V} = \frac{T\cos\alpha - D - Mg\sin\gamma}{M} \tag{4}$$

$$\dot{\gamma} = \frac{(T\sin\alpha + L)\cos\mu - Mg\cos\gamma}{MV} \tag{5}$$

$$\dot{\psi} = \frac{(T\sin\alpha + L)\sin\mu}{MV\cos\gamma} \tag{6}$$

where x, y, and z are the aircraft position, V is the airspeed, γ = flight path angle, μ = bank angle, α = Angle of Attack (AoA), g = acceleration of gravity, T = Thrust, M = mass, D = drag, L = lift, v_w = wind speed (in the x, y, z directions respectively), ψ = heading angle, and anything with a dot over it represents a time rate of change.

In a 6-DOF system, the forces and moments on the aircraft are modeled and the resulting longitudinal and lateral accelerations are computed [14]. The 6-DOF systems includes the following state variables that are required to be known as initial conditions into the Auto-GCAS path prediction integration:

$$y = [u, v, w, p, q, r, \phi, \theta, \psi, x, y, z] \tag{7}$$

where y is the state vector; u, v, and w are the aircraft body horizontal, lateral, and vertical velocities; p, q, and r are the aircraft body roll, pitch, and yaw rates; ϕ, θ, ψ, are the aircraft body roll, pitch, and yaw Euler angles; and x, y, and z are the

aircraft body horizontal, lateral, and vertical position.

The following are the 6-DOF rigid body equations of motion derived through Newton's 2nd Law from Nelson's text [20]:

Force Equations:

$$X - mg\sin\theta = m(\dot{u} + qw - rv) \tag{8}$$

$$Y + mg\cos\theta\sin\phi = m(\dot{v} + ru - pw) \tag{9}$$

$$Z + mg\cos\theta\cos\phi = m(\dot{w} + pv - qu) \tag{10}$$

where X, Y, Z, are the horizontal, lateral, and vertical forces; $\dot{u}$, $\dot{v}$, and $\dot{w}$ are the aircraft body horizontal, lateral, and vertical accelerations; m = mass; g = gravity; and the remaining terms are from the state vector definitions in Equation (7) above.

Moment Equations:

$$L = I_x\dot{p} - I_{xz}\dot{r} + qr(I_z - I_y) - I_{xz}pq \tag{11}$$

$$M = I_y\dot{q} + rq(I_x - I_z) + I_{xz}(p^2 - r^2) \tag{12}$$

$$N = -I_{xz}\dot{p} + I_z\dot{r} + pq(I_y - I_x) + I_{xz}qr \tag{13}$$

where L, M, N, are the roll, pitch, and yaw moments; $\dot{p}$, $\dot{q}$, and $\dot{r}$ are the aircraft body roll, pitch, and yaw accelerations; I are the products of inertia; and the remaining terms are from the state vector definitions in Equation (7) above.

Body angular velocities in terms of Euler angles / rates:

$$p = \dot{\phi} - \dot{\psi}\sin\theta \tag{14}$$

$$q = \dot{\theta}\cos\phi + \dot{\psi}\cos\theta\sin\phi \tag{15}$$

$$r = \dot{\psi}\cos\theta\cos\phi - \dot{\theta}\sin\phi \tag{16}$$

where $\dot{\theta}$, $\dot{\phi}$, $\dot{\psi}$, are the pitch, roll, and yaw angle rates; and the remaining terms are from the state vector definitions in Equation (7) above.

Euler rates in terms of Euler angles and body angular velocities:

$$\dot{\theta} = q\cos\phi - r\sin\theta \tag{17}$$

$$\dot{\phi} = p = q\sin\phi\tan\theta + r\cos\theta\tan\theta \tag{18}$$

$$\dot{\psi} = (q\sin\phi + r\cos\phi)\sec\theta \tag{19}$$

where $\dot{\theta}$, $\dot{\phi}$, $\dot{\psi}$, are the pitch, roll, and yaw angle rates; and the remaining terms are from the state vector definitions in Equation (7) above.

2.4 Reference Frames and Coordinate Systems

When discussing any aircraft dynamic problem it is important to delineate between the different reference frames and coordinate systems. Additionally, when discussing navigation problems it is important to define Earth shape and rotation in order to accurately approximate terrain surfaces. The National Geospatial-Intelligence Agency (NGA) provides the support for the DoD's oblate-spheroidal-Earth model, called the World Geodetic System 1984 (WGS-84) [21]. The geoid is defined as the "equipotential surface of the Earth's gravity field that coincides with the undisturbed mean sea level, extended continuously underneath the continents" [21]. Since the Earth's geoid undulates across the surface, the oblate-spheroidal-Earth model varies in surface level approximations, causing a small deviation in height between the Earth

model and actual Earth geoid surface. Figure 4 demonstrates this difference in height between the geoid and spheroidal model of the Earth.

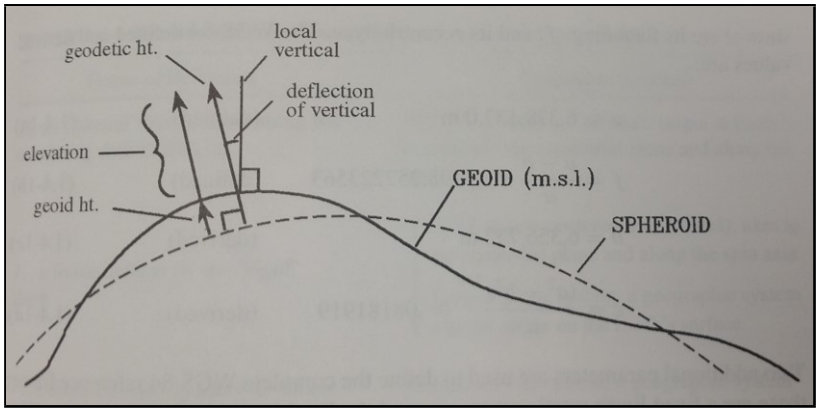

Figure 4. Earth geoid and definition of height [21]

Elevation is measured from the difference between the geodetic height and the geoid height at every given latitude and longitude value on the Earth. The worldwide average deviation of the geoid from the spheroid is approximately 30 meters when considering root-mean-square of 1° x 1° grids of the Earth [21]. Therefore factoring in the geoid height is necessary for an Auto-GCAS algorithm to be active, especially in low-level terrain. The geoid height comes from the geodetic coordinate system. In Figure 5, the geodetic height is normal to the spheroidal model for a given geodetic latitude (ϕ) and longitude (ℓ) [21]. Provided a set of geodetic latitude and longitude, an associated terrain elevation can be pulled from the Digital Elevation Model (DEM). The local navigation frame for the aircraft is called the geographic coordinate frame and is either a North-East-Down (NED) or East-North-Up (ENU) axes nomenclature [21]. Conversion between local navigation coordinates and geodetic coordinates is important for terrain height comparison (aircraft altitude and finding the height of the geodetic surface).

Earth-Centered Earth-Fixed (ECEF) is the frame defined by the rigid Earth, where the axes are in the equatorial plane and along the Earth spin axis. For low-

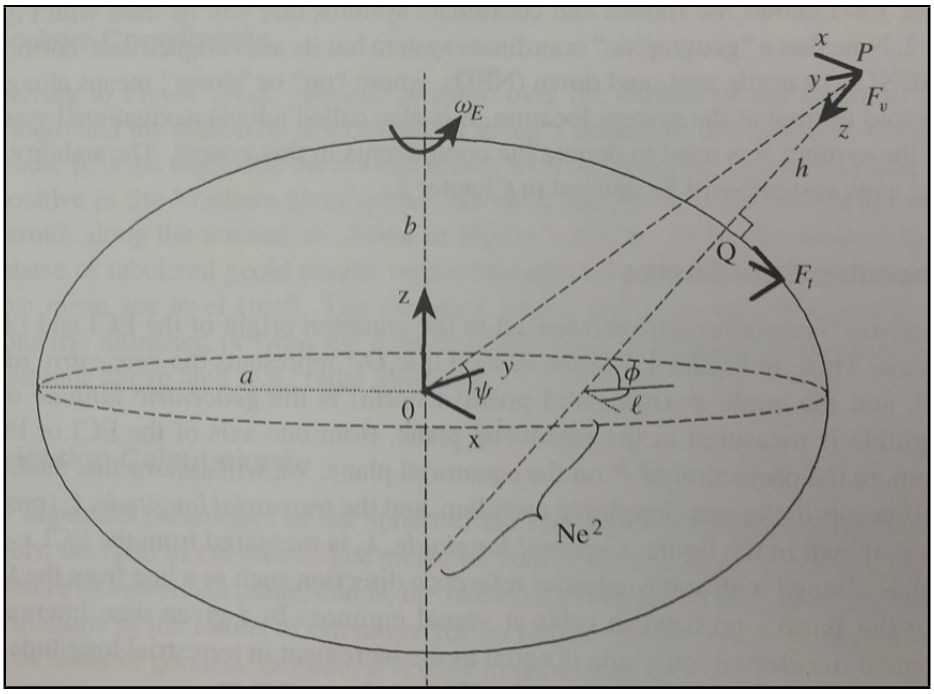

Figure 5. Earth Centered Earth Fixed (ECEF) Coordinate Frame [21]

speed simulation over small portions of the Earth, a flat Earth approximation can be considered which means the Earth's rotation compared to the aircraft are considered to be equivalent [21]. The equations of motion are based in the inertial reference frame and any rotations from the inertial reference frame require Direction Cosine Matrices (DCM) and application of the transport theorem to maintain the dynamics.

When modeling aircraft dynamics and measuring forces and moments, three primary aircraft coordinate systems need to be understood: body-fixed coordinate system, stability-axes coordinate system, and wind-axes coordinate system. Figure 6 shows the difference between the axes systems and demonstrates that the two angles needed for DCM rotations are the equilibrium angle of attack (α_e) and the sideslip angle (β) [21].

The aircraft aerodynamic forces are typically converted from the wind-axes to the body-axes through the measurements of the aerodynamic angles α_e and β. The combination of aerodynamic angles and Euler angles is needed to define the aircraft

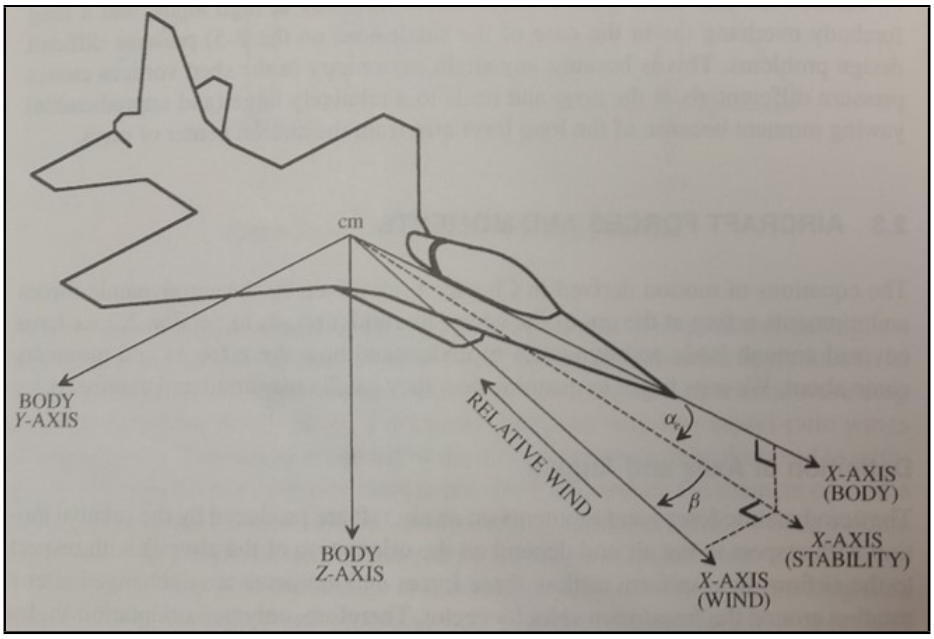

Figure 6. Aircraft Body and Wind axes Reference Frame [21]

rate of climb ($\dot{h}$), which can be calculated as the following:

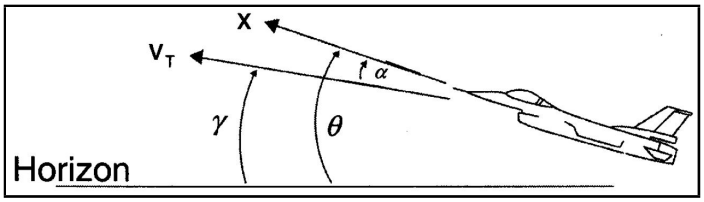

Figure 7. Aircraft Body and Wind axes Reference Frame [21]

$$\dot{h} = V_t \sin\gamma \tag{20}$$

$$\gamma = \sin^{-1}(\cos\alpha\cos\beta\sin\theta - (\sin\phi\sin\beta + \cos\phi\sin\alpha\cos\beta)\cos\theta) \tag{21}$$

Where V_t is the body velocity vector and γ is the flight path angle. The rate of climb can be a useful autopilot command for predetermined aircraft path trajectory.

In order to translate aircraft body velocity to inertial position velocities, a transformation between the body-fixed and the inertial reference frames must be conducted through the Body 3-2-1 orientation rotation as in Equation (22) below. For stability

and control applications, this is the standard orientation rotation through the roll, pitch, then yaw angles; the Direction Cosine Matrix (DCM) is provided below from Kunz [22] where a "C" and "S" represents "cos" and "sin" functions respectively:

$$\begin{bmatrix} \dot{x} \\ \dot{y} \\ \dot{z} \end{bmatrix}_{inertial} = \begin{bmatrix} C_\theta C_\psi & S_\phi S_\theta C_\psi - C_\phi S_\psi & C_\phi S_\theta C_\psi + S_\phi S_\psi \\ C_\theta S_\psi & S_\phi S_\theta S_\psi + C_\phi C_\psi & C_\phi S_\theta S_\psi - S_\phi C_\psi \\ -S_\theta & S_\phi C_\theta & C_\phi C_\theta \end{bmatrix} \begin{bmatrix} u \\ v \\ w \end{bmatrix}_{body} \tag{22}$$

2.5 Digital Elevation Model - Terrain Elevation

A 3-D mapping of terrain surface is referred to as a Digital Elevation Model (DEM). The DEM is actually a 2-D representation because it is a grid of terrain surface elevation for a given latitude and longitude, and can not represent caves, tunnels, or cliffs with overhangs [23]. A DEM can be sub-categorized further, but two important distinctions are a Digital Surface Model (DSM) and Digital Ground Model (DGM). The DSM provides terrain surface elevation including vegetation, buildings, etc, and the DGM provides terrain surface elevation without any vegetation or buildings [23]. This distinction is important because for operational Auto-GCAS, more than the DGM model needs to be added into the DEM used for collision avoidance, otherwise man-made obstacles or vegetation will not be factored in. The DoD standard DEM is produced by the NGA and referred to as Digital Terrain Elevation Data (DTED) [24]. Included in current DTED is information collected through the Shuttle Radar Topography Mission (SRTM), where two radar sensors on the space shuttle used interferometry to map over 80% of the Earth's surface between 60° N and 57° S [23, 24]. The DEM directly relates to how accurate the Auto-GCAS terrain collision prediction will be based on the fidelity of the model. Table 1 outlines the different DTED levels and accuracy.

The file size of DTED, especially SRTM DTED, can be excessively large for stor-

Table 1. Digital Terrain Elevation Data (DTED) Accuracy [24, 12]

DTED-Level	**Post Spacing (arc-seconds)**	**Post Spacing (ground dist)**	**Cells per Degree**	**Matrix Size** (1° x 1° grid)
DTED-0	30 arc-sec	~900 m	120	121 x 121
DTED-1/SRTM-1	3 arc-sec	~90 m	1,200	1201 x 1201
DTED-2/SRTM-2	1 arc-sec	~30 m	3,600	3601 x 3601
DTED-3	$\frac{1}{3}$ arc-sec	~10 m	10,800	10,801 x 10,801

age and also computationally expensive to interpolate with increasing cell matrix sizes. NASA developed a DEM compression algorithm called Global Elevation Data Adaptive Compression System (GEDACS). GEDACS used two numerical methods, "tip-tilt" and "semi-regular tree networks", to reduce the DEM file size from 400 GB to 170 MB while still maintaining accuracy of typical DEM data [25]. Figure 8 represents the tip-tilt DEM vs. the typical thinned DEM data.

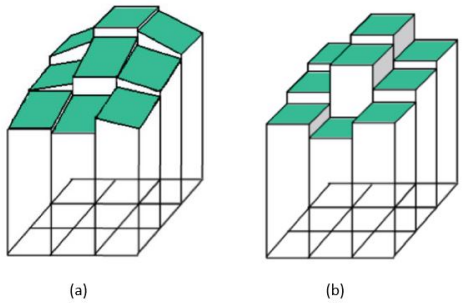

Figure 8. (a) Tip-Tilt DEM Data and (b) Typical Thinned DEM Data [25]

Tip-tilt DEM is able to better match the slope of the terrain surface [25] as seen in the center tiles of Figure 8. Tip-tilt has potential use for use in Auto-GCAS because a terrain safety buffer is best applied perpendicular to the terrain surface, as opposed to purely vertical posts in the typical DEM data. Additionally, the tip-tilt DEM can be used to measure the aircraft's relative angle to terrain by taking the dot product of the aircraft body velocity vector and gradient of the terrain, a useful measurement in a collision avoidance algorithm. The second GEDACS method was semi-regular

tree networks [25], which significantly reduced the number of elements of a matrix to approximate larger areas of similar terrain as the same terrain altitude. For example, a large area of flat land that has the same terrain altitude over multiple latitude and longitude values, can be approximated by a larger cell of terrain altitude. Figure 9 shows the GEDACS compression output DEM using both tip-tilt and semi-regular tree networks numerical methods.

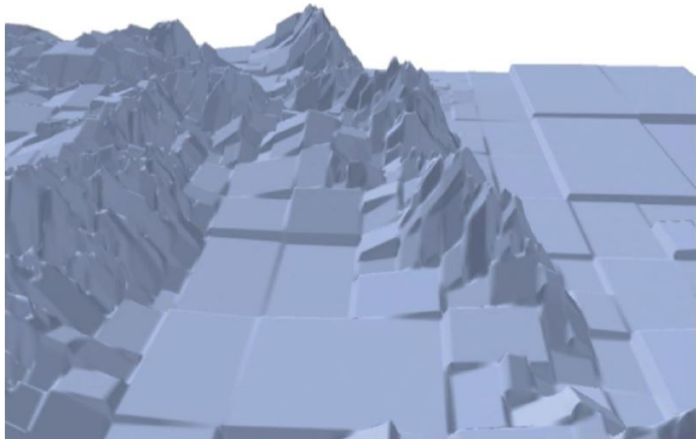

Figure 9. Output of NASA GEDACS compression algorithm for DEM data [25]

2.6 Auto-GCAS Research and Implementation

With the previous background on CDR systems, 3-DOF vs. 6-DOF models, and DTED, a comprehensive review of research specific to Auto-GCAS will be outlined. This includes a review of work done by AFRL on the F-16 platform and also joint research conducted by AFIT and the U.S. Air Force Test Pilot School (TPS). The goal was to transition lessons learned from the F-16 program to the heavy Auto-GCAS problem for performance limited aircraft.

2.6.1 F-16 Auto-GCAS System.

The F-16 Auto-GCAS program began in 2007 as part of the Fighter Risk Reduction Program (FRRP) to address the 2005 goal of reducing CFIT mishaps by 75%

established by the Defense Safety Oversight Council (DSOC) [26]. Within the CDR model, the F-16 Auto-GCAS uses a nominal state propagation method by generating a scan shape ahead of the aircraft. The 6-DOF F-16 model predicts a future flight path for the single escape-maneuver: roll-to-wings-level, 5-g pull-up maneuver once aircraft is past 90° of bank [8]. Referencing Figure 10, the conflict detection method first collects a terrain elevation vs. range profile from DTED Level 1 data, then adds a 70-ft safety buffer to the terrain elevation, and finally compares height above terrain for the escape-maneuver with an added 0.25 to 0.8 seconds time delay [26, 15, 25]. Once a prediction collision is calculated, the system is activated to resolve the

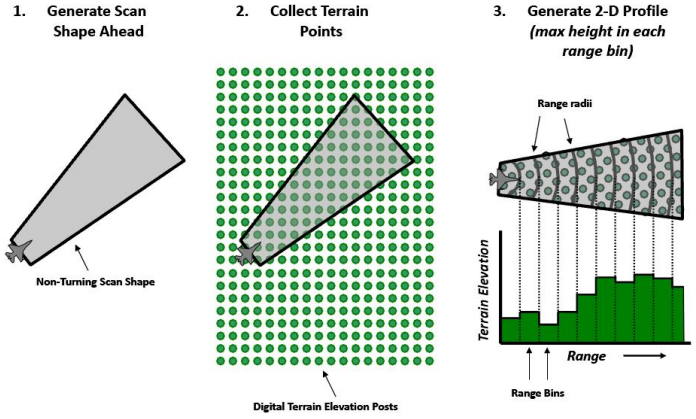

Figure 10. F-16 Auto-GCAS Terrain Scanning and Binning Process[12]

conflict and hands back control to the pilot once an escape angle away from terrain has been reached [27]. The single escape-maneuver for the F-16 system works for all terrain due to the high performance climb rate of the aircraft and because high aircraft speeds lend to large kinetic energy transformation to altitude [25].

To reduce nuisances during Auto-GCAS activation, AFRL conducted flight tests in 1995 using a Pilot Activated Recovery System (PARS) which was developed to assist pilots in spatial disorientation [27]. It was determined that time available until impact is the determining factor that a pilot uses to determine when to initiate an escape-maneuver [27]. Figure 11 shows the results that determined a 1.5 second time available

nuisance boundary that Auto-GCAS designers could use during development. No such

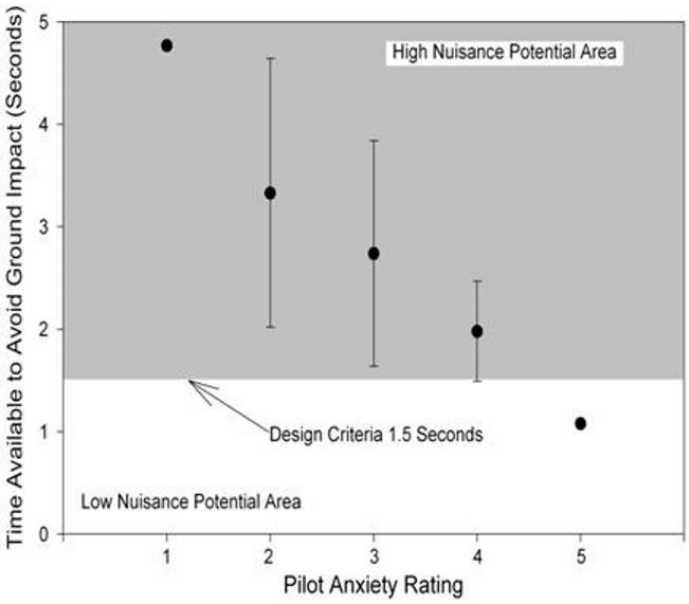

Figure 11. Nuisance Determination: Time Available vs. Pilot Anxiety Rating [26]

flight testing to determine a nuisance boundary has been done for heavy military aircraft [12].

2.6.2 NASA Small Unmanned Aerial Vehicle Auto-GCAS System.

NASA extended the F-16 Auto-GCAS project to a Small Unmanned Aerial Vehicle (SUAV) to demonstrate multiple escape-maneuvers, terrain scanning, compressed DEM data, and operation on low-cost commercially available devices [25]. The SUAV project was broken into three main modules: (1) Predict Avoidance Trajectories, (2) Identify Collision Threats, and (3) Determine Need to Avoid.

The Predict Avoidance Trajectories module determined that the single escape-maneuver implemented by the F-16 Auto-GCAS system, would not apply to medium to large Unmanned Aerial Vehicles (UAVs) and therefore lateral escape-maneuvers were needed to avoid nuisances and reduce needed forward-look-ahead time [25]. The three escape-maneuvers chosen are shown in Figure 12 as left and right lateral turns

(40° bank, 800 fpm climb, 60 KIAS) and a straight climb (bank to wings-level, 1000 fpm climb, 60 KIAS) [25]. Since the SUAV is a propeller aircraft at low speeds, the escape-maneuvers included the asymmetric propeller blade effect (P-factor) to account for varying radius turns, show in Figure 13. The autopilot escape-maneuver

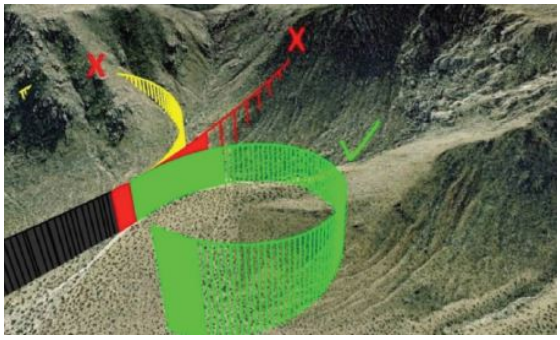

Figure 12. SUAV Escape-Maneuvers and Selection [25]

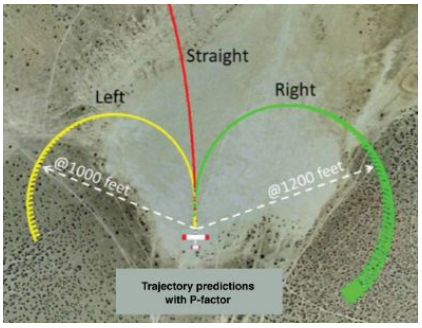

Figure 13. SUAV Top-view of Escape-Maneuvers with P-factor [25]

target values vary depend on the given aircraft in use, but the basic principles of targeting climb rate, bank angle, roll rate, and airspeed can be modified to other aircraft performance levels.

The Identify Collision Threats module determined the terrain scanning and collision prediction methods. A similar approach to the F-16 Auto-GCAS system was implemented where each escape-maneuver path had a scanning area to capture DTED elevation posts. Figure 14 shows the scanning zone overlaying DTED posts (green diamonds), where uncertainties are added to the width of the scanning zone for positional and prediction errors [25]. The scanning zone increased in search area as the escape-maneuver got farther away from the aircraft, which can be seen by the increasing circle diameter in Figure 15.

An important difference between the F-16 terrain scan and SUAV is that SUAV's terrain scan allowed inclusion of DTED posts near to the scan area (purple line in Figure 14) whereas the F-16 system would only include the DTED post if it was within the scan area [25]. The length of the turns were sufficient to allow at least a

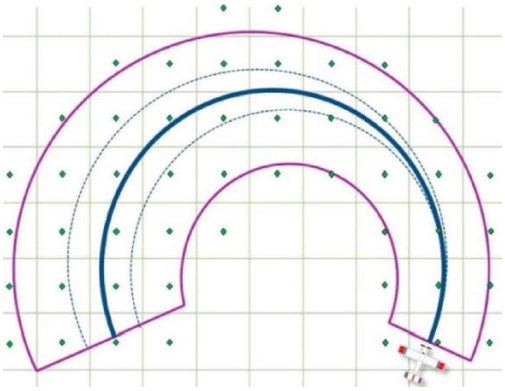

Figure 14. SUAV Scan Zone Overlaying DTED Posts [25]

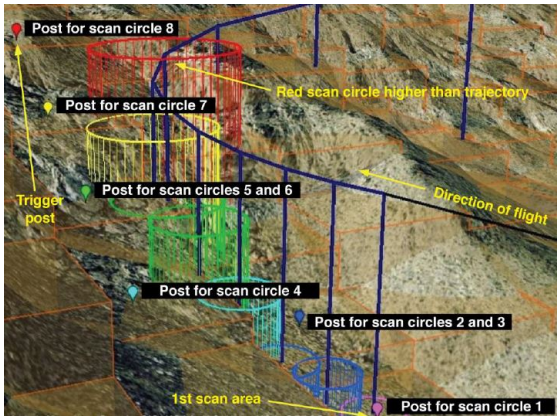

Figure 15. SUAV Post Scanning Technique to search DTED height [25]

225° heading change, enabling the aircraft to complete a full turn and return on the same heading [25].

The Determine Need to Avoid module determined a trigger activation of the Auto-GCAS escape-maneuver. The escape-maneuver becomes unavailable if any DTED post for the scanned area is higher than the projected escape-maneuver altitude, as seen in Figure 15 by the red circle being a higher maximum altitude than the aircraft trajectory in purple. Since SUAV had three escape-maneuvers, the autopilot would only trigger when all three projected escape-maneuvers became unavailable [25]. The escape-maneuver selected was the last available, as illustrated for a right turn in Figure 12.

2.7 AFIT Auto-GCAS Academic and Flight Test Research

AFIT in partnership with AFRL and TPS has continued expanding the research of Auto-GCAS towards performance limited "heavy" aircraft.

Suplisson's dissertation was an optimal control solution for aircraft with a lower climb performance. A different terrain scanning method, gridded DTED interpolation, was used from previous F-16 Auto-GCAS and NASA SUAV designs in order to

meet the continuous function requirements for nonlinear problem solvers in optimal control [12]. The cost performances of minimum control (with aggressive trigger) and maximum distance (with timely trigger) were used to calculate the escape-maneuver using a pseudospectral method on a 3-DOF point mass model [12]. Suplisson demonstrated that minimum control and maximum distance optimal control were equivalent at the trigger point of automatic recovery [12]. The optimal results were compared to a predetermined five multi-trajectory algorithms. On comparison, the optimal escape-maneuver was trigger later and required less control input than the multi-trajectory algorithm [12]. However, the optimal solution providing real-time optimal control (RTOC) was able to be calculated but is not practical yet for implementation due to speed of operation (~2 Hz) and convergence criteria needing additional work [12]. A different system has to bridge the gap until aircraft control computer processing speeds are able to handle RTOC, but the optimal solution proves useful as a comparison of performance.

Bridging the gap between Suplisson's optimal solution for Auto-GCAS was a series of AFIT/TPS flight tests conducted by Trombetta and Gahan using the LJ-25D model to show implementation on an aircraft. Trombetta had three main objectives, (1) use a 3-DOF point-mass model to compare three and five path algorithms against Suplisson's optimal Auto-GCAS, (2) perform a terrain analysis and maneuver determination to identify forward-look-ahead time required for performance limited aircraft, and (3) implement Auto-GCAS algorithm on a LJ-25D model for flight testing [13]. For the collision detection method, Trombetta used a safety bubble surrounding the aircraft in order to identify DTED posts in the predicted aircraft trajectory [13]. Upon comparison to optimal control, Trombetta's three and five escape-maneuver's were similar to optimal control only during the straight ahead climbs [13]. As a result of the terrain analysis, the longest look-ahead time required was 45 seconds for

low speed aircraft in high sloped terrain (more than 500 ft per $\frac{1}{2}$ nautical mile) [13]. Trombetta successfully implemented the algorithm to control the LJ-25D at USAF TPS, however his Auto-GCAS algorithm required steady level flight upon activation and did not allow for continuous terrain scanning after a path selection. To improve upon this design, Gahan used a 6-DOF LJ-25D model to allow for continuous terrain scanning during flight that was compatible with all initial conditions of the aircraft for trajectory prediction. The same model is used in this current research and is explained more directly in section 3.1. Gahan's current research is pending publication, but initial flight test results from TPS technical information memorandum USAFTPS-TIM-19A-02 [28] concluded that at least 12.5 Hz was the required refresh rate to maintain clearance of terrain with varying initial conditions, and the forward-look-ahead time for higher refresh rates (above 6.25 Hz) only required 20 seconds or less for both 220 and 270 Knots Indicated Air Speed (KIAS).

2.8 Existing Display and Warning Settings for Terrain Avoidance

The F-16 Auto-GCAS program never intended to have displays in operational use to notify the pilot of activation, however during developmental testing the operational pilots witnessed the visual and aural cues, and wanted the same capability in operational aircraft. It is important to have communication between the Auto-GCAS system and human operator. The operator must understand the process of the Auto-GCAS algorithm in order to develop trust and confidence, while the Auto-GCAS algorithm needs to communicate its calculations to the human operator so the pilot, if able, can react and decide an escape-maneuver given information from the Auto-GCAS algorithm. With new information being provided to the operator about terrain avoidance, it is important to clarify that an Auto-GCAS system should never be used by an operator as a terrain following technique [12].

The F-16 Auto-GCAS operational display consists of converging chevrons in the Heads Up Display (HUD) that indicate an impending collision course, shown in Figure 16 [15]. Once Auto-GCAS triggers, indicating the pilot no longer has control of the aircraft, the HUD depicts a flashing break "X" in the center with a directional cue above it saying "FLYUP" [29]. The HUD activation is depicted in Figure 17. Current

Figure 16. Auto-GCAS Chevrons Closing to Warn Impending Activation [29]

Figure 17. Auto-GCAS Activated with Break "X" and "FLYUP" on HUD [29]

heavy Auto-GCAS has not looked into the display options desired by a pilot, and the systems in use for F-16 Auto-GCAS can not be directly translated over to a heavy platform because of different nuisance levels between pilot types and also the single escape trajectory vs. a multi-escape trajectory system.

A starting point for displays used by heavy pilots is TAWS data provided through EGPWS-Mode 3 described earlier in section 2.2.2. During low-level flights, current cargo pilots have a dedicated Primary Flight Display (PFD) as a Heads-Down Display (HDD) in the aircraft with TAWS data being shown. Specific to the C-17 community, the operators typically fly with the non-peaks display (birds eye view) that displays a graphical approach to terrain height, where the aircraft flight path is overlaid. In addition, there is a path prediction value that overlays on the TAWS screen a projected 2-D representation of the aircraft's future position 60 seconds in advance. This is to help with projecting if the current flight path will intersect with terrain.

The TAWS information with corresponding color legends are displayed in Figures 18 and 19.

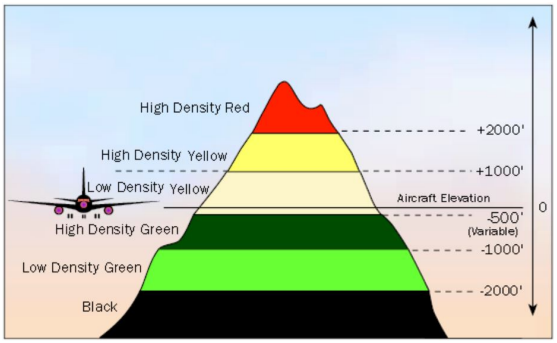

Figure 18. Enhanced Ground Proximity Warning System - Peaks Color Code [17]

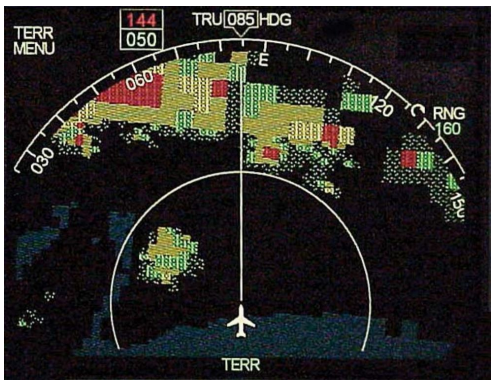

Figure 19. Enhanced Ground Proximity Warning System - Peaks Heads-Down Display [17]

There are HUD warnings that EGPWS provides to warn and caution pilots of impending terrain collision. A cautionary terrain conflict will repeat a visual warning on the HUD and an aural message of "Caution Terrain, Caution Terrain", where as a warning terrain conflict will repeat "Terrain, Terrain, Pull Up" [17]. The EGPWS does not provide a recommend escape-maneuver to avoid terrain, just the presence of terrain. Any future heavy auto-GCAS designs need to work around and supplement the current digital displays in the aircraft. Additionally, a similar study on the best symbology in the HUD should be conducted to increase situational awareness to the pilot [30] [31].

2.9 Flight Path Prediction: Selected Numerical Integration Methods

At the root of the Auto-GCAS collision detection algorithm is prediction of the aircraft's future flight path in order to compare it with terrain elevation along the predicted flight path. The aircraft's nonlinear ordinary differential equations of motion have to be propagated at discrete time steps over the look-ahead distance defined

by the Auto-GCAS algorithm [32]. Kuchar and Yang stressed this point in their review of CDR methods by stating, "Because conflict detection and resolution can only be as reliable as the ability of the model to predict the future, the most concrete difference between modeling approaches involves the method by which the current states are projected into the future " [11]. The flight path prediction for Auto-GCAS is different than a trajectory flight path prediction used for air traffic management (ATM), the reader is encouraged to look into ATM trajectory prediction in references [33, 34]. Auto-GCAS flight path prediction is an initial value problem (IVP) solving a system of ordinary differential equations (ODE) over a forward look-ahead time with no way-points known along the path prediction. There are numerous integration methods used to predict the aircraft future flight path but only those relevant to this research will be discussed.

2.9.1 Building Blocks of a Numerical Integration.

The basic data requirements for aircraft trajectory conditions require an (1) initial condition, (2) intent information, (3) environmental information, and (4) aircraft-specific information [14]. The initial condition are the aircraft state variables from Equation (7) at time = 0 for the trajectory integration. The intent information is the autopilot planned path or escape-maneuver, which for sub-optimal control will be a predetermined maneuver. The environmental information includes current altitude density, temperature, winds, etc. The aircraft-specific information is the model based requirements and include control deflection rates, weight, moments of inertia, configuration, etc. All the numerical integration methods require some form of these inputs in order to predict the future aircraft path.

2.9.2 Classification of Numerical Integration.

There are a plethora of numerical integration methods and classes. The classes discussed here will be (1) explicit vs. implicit, (2) single-step vs. multi-step, and (3) fixed vs. adaptive time step. Each class and method has an associated global truncation error, which comes from the combination of local truncation (error in a single step) and propagated truncation (error accumulated from previous steps) [35]. Round-off errors will be the same between methods due to the computer machine precision using double values (8 bytes of information).

An explicit method uses an *explicit* formula where the unknown variable (y_{i+1}) can be solved for only in terms of a function of known values (x_i,x_{i+1},y_i), as represented in Equation (23) [35].

$$y_{i+1} = F(x_i, x_{i+1}, y_i) \tag{23}$$

Whereas an implicit method uses an iterative approach to converge to a solution of the unknown variable (y_{i+1}) because the equation can not be solved for only in terms of a function of known values (x_i,x_{i+1},y_i), as represented in Equation (24) where the unknown variable is on both sides of the equation [35].

$$y_{i+1} = F(x_i, x_{i+1}, y_i, y_{i+1}) \tag{24}$$

Typically an implicit method is more accurate than explicit methods, but take longer to find a solution because implicit equations are solved multiple times at each time step [36].

Single-step methods calculate the solution at the next time step (y_{i+1}) based on the information known at the current time step (y_i). A single-step explicit method has the generic form:

$$y_{i+1} = y_i + Slope \cdot h \tag{25}$$

$$h = x_{i+1} - x_i \tag{26}$$

where h is the time step of the numerical integration and *Slope* is calculated by different methods such as Euler, Mid-Point, Modified-Euler, or Runge-Kutta.

A multi-step explicit method calculates the solution at the next time step (y_{i+1}) based on the information known at the current time step (y_i) and any number of previous time steps (y_{i-1}, y_{i-2}, y_{i-3}, y_{i-4}, etc.) [35].

$$y_{i+1} = F(x_{i+1},\ x_i,\ y_i,\ x_{i-1},\ y_{i-1},\ x_{i-2},\ y_{i-2}) \tag{27}$$

Since multi-step methods require previous solutions to factor into the equation, an initial step needs to be taken with another method in order to begin factoring in the multi-steps [37]. For example, the first step can be an Euler explicit method followed by a multi-step method with two previous points, followed by a multi-step method factoring in three previous points, etc.

Fixed vs. adaptive numerical integration methods deal with the time steps taken during the integration. The solution is being evaluated at discrete time steps, and therefore this value can be changed in order to increase the level of accuracy [38]. A fixed integration method uses a constant time step to evaluate the function over the forward look-ahead time. Decreasing the time step typically results in higher accuracy approximations, however this subsequently increases the number evaluations over the forward-look-ahead time, resulting in a more computationally expensive integration. An adaptive integration method changes the time step based on approximation errors as the integration progresses in order to achieve a preset acceptable error tolerance. Although there are different ways to control the adaptive time step selection, Dahlquist [36] explains adaptive time steps controlled by a tolerance value (tol) through Runge's second-order method. This method calculates a delta value (δ)

based off of the worst case delta value (δ_i) for the i^{th} state in the state vector (y_i). This insures that the step size taken passes the tolerance value for all states.

$$\delta = \max_i(\delta_i) \tag{28}$$

$$\delta_i = \frac{|k_{2,i} - k_{1,i}|}{3y_i} \tag{29}$$

Where $k_{2,i}$ and $k_{1,i}$ are the slopes at the step-size (h) and midpoint ($\frac{h}{2}$) respectively [36].

$$k_{1,i} = h \cdot f(x_i, y_i) \tag{30}$$

$$k_{2,i} = h \cdot f(x_i + \frac{h}{2}, y_i + \frac{k_{1,i}}{2}) \tag{31}$$

A step size is accepted if the delta (δ) is less than the tolerance (tol). If the step is accepted, then the next step size (h_{next}) is calculated based on the delta (δ) value [36]:

$$h_{next} = h \cdot min\{1.5, \sqrt{tol/(1.2\delta)}\} \tag{32}$$

A step size is rejected if the delta (δ) is greater than the tolerance (tol). If the step is rejected, a new step h_{new} has to be recomputed and is calculated based on the delta (δ) value [36]:

$$h_{new} = h \cdot max\{0.1, \sqrt{tol/(1.2\delta)}\} \tag{33}$$

This process continues and allows the step size to grow and shrink over the course of the integration based on the relation to the relative error of the worst case state component (δ_i) [36].

2.9.3 Euler Explicit (Forward Euler) Method.

Euler's method is the most basic explicit single-step solver for first-order ODE initial value problems. The solution is approximated by multiplying the time step (h) by the slope of the function at the current step [35], as illustrated in Figure 20.

$$x_{i+1} = x_i + h \tag{34}$$

$$y_{i+1} = y_i + h \cdot \frac{dy_i}{dx_i} \tag{35}$$

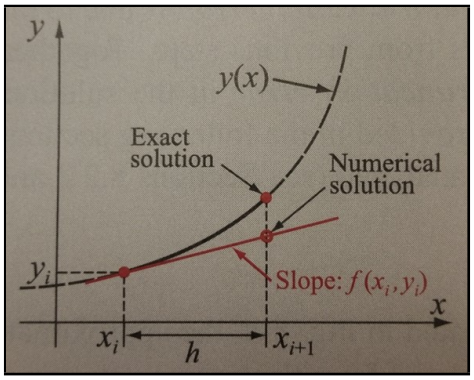

Figure 20. Euler Explicit Method for solving ODE initial value problems [35]

2.9.4 Runge-Kutta Method.

The Runge-Kutta methods are an explicit single-step solver for first-order ODE initial value problems. The method order factors in the multiple different slopes calculated at various sub-interval values, points between the time-step. Reference Figure 21 for the fourth-order method factoring in four slopes at sub-interval values. The Runge-Kutta methods are broken into order of accuracy (2^{nd}, 3^{rd}, 4^{th}, 5^{th} order Runge-Kutta) based on the global truncation error [35].

The equations used for second-order Runge-Kutta Methods are the following [35].

$$y_{i+1} = y_i + (c_1 K_1 + c_2 K_2) \cdot h \tag{36}$$

$$K_1 = f(x_i, y_i) \tag{37}$$

$$K_2 = f(x_i + a_2 h, y_i + b_{21} K_1 h) \tag{38}$$

where the $f(\ )$ designates the slope of the function at the x and y values inside the parenthesis; the constants c_1, c_2, a_2, and b_{21} come from a Butcher's tableau describing the method constants. For example, Huen's 2^{nd} Order Runge-Kutta method has the following constants [35]:

$$c_1 = \frac{1}{4}, \quad c_2 = \frac{3}{4}, \quad a_2 = \frac{2}{3}, \quad b_{21} = \frac{2}{3} \tag{39}$$

The equations used for third-order Runge-Kutta Methods are the following [35].

$$y_{i+1} = y_i + (c_1 K_1 + c_2 K_2 + c_3 K_3) \cdot h \tag{40}$$

$$K_1 = f(x_i, y_i) \tag{41}$$

$$K_2 = f(x_i + a_2 h, y_i + b_{21} K_1 h) \tag{42}$$

$$K_3 = f(x_i + a_3 h, y_i + b_{31} K_1 h + b_{32} K_2 h) \tag{43}$$

where the $f(\ )$ designates the slope of the function at the x and y values inside the parenthesis; the constants c_1, c_2, c_3, a_2, a_3, b_{21}, b_{31}, and b_{32} come from a Butcher's tableau [37] describing the method constants. Table 2 lists constants for various methods.

The equations used for fourth-order Runge-Kutta Methods are the following and the application is graphically represented in Figure 21 (a) - (d) for the stages of calculations required to evaluate one step in Equation (44) [35].

$$y_{i+1} = y_i + (c_1 K_1 + c_2 K_2 + c_3 K_3 + c_4 K_4) \cdot h \tag{44}$$

Table 2. Constants of third-order Runge-Kutta methods [35] [39]

Method	c_1	c_2	c_3	a_2	b_{21}	a_3	b_{31}	c_{31}
Classical	$\frac{1}{6}$	$\frac{4}{6}$	$\frac{1}{6}$	$\frac{1}{2}$	$\frac{1}{2}$	1	-1	2
Nystrom's	$\frac{2}{8}$	$\frac{3}{8}$	$\frac{3}{8}$	$\frac{2}{3}$	$\frac{2}{3}$	$\frac{2}{3}$	0	$\frac{2}{3}$
Nearly Optimal	$\frac{2}{9}$	$\frac{3}{9}$	$\frac{4}{9}$	$\frac{1}{2}$	$\frac{1}{2}$	$\frac{3}{4}$	0	$\frac{3}{4}$
Heun's Third	$\frac{1}{4}$	0	$\frac{3}{4}$	$\frac{1}{3}$	$\frac{1}{3}$	$\frac{2}{3}$	0	$\frac{2}{3}$
Bogacki-Shampine	$\frac{2}{9}$	$\frac{1}{3}$	$\frac{4}{9}$	$\frac{1}{2}$	$\frac{1}{2}$	$\frac{3}{4}$	0	$\frac{3}{4}$

$$K_1 = f(x_i, y_i) \tag{45}$$

$$K_2 = f(x_i + a_2 h, y_i + b_{21} K_1 h) \tag{46}$$

$$K_3 = f(x_i + a_3 h, y_i + b_{31} K_1 h + b_{32} K_2 h) \tag{47}$$

$$K_4 = f(x_i + a_4 h, y_i + b_{41} K_1 h + b_{42} K_2 h + b_{43} K_3 h) \tag{48}$$

where the $f(\ )$ designates the slope of the function at the x and y values inside the parenthesis; the constants are defined as the following for the *Classical* method [35]:

$$\begin{gathered} c_1 = c_4 = \frac{1}{6}, \quad c_2 = c_3 = \frac{2}{6}, \quad a_2 = a_3 = b_{21} = b_{32} = \frac{1}{2} \\ a_4 = b_{43} = 1, \quad b_{31} = b_{41} = b_{43} = 0 \end{gathered} \tag{49}$$

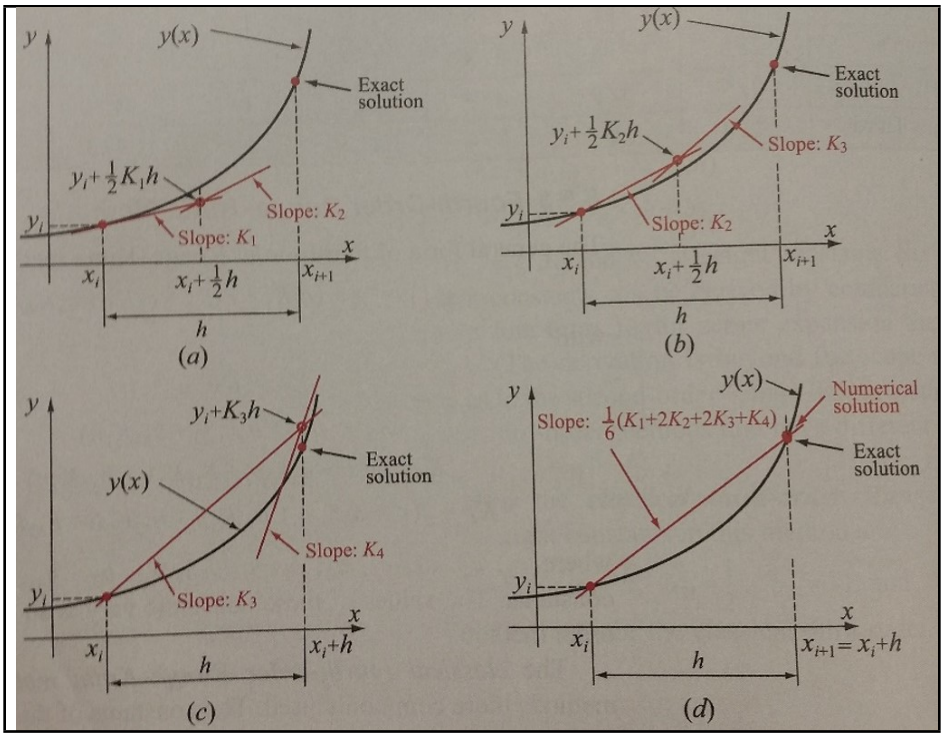

Figure 21. 4^{th} Order Runge-Kutta Explicit Method for solving ODE initial value problems [35]

2.9.5 Adams-Bashforth Method.

The Adams-Bashforth method is an explicit multi-step method for solving first-order ODE initial value problems [35]. Similar to Runge-Kutta schemes, there are higher order methods (2^{nd}, 3^{rd}, 4^{th} order Adams-Bashforth). The formulas factor in previous time steps slope evaluations instead of multiple sub-interval evaluations such as the Runge-Kutta schemes. Given a set of ODE to solve, the formulas are derived by integrating the respective ODE over the interval [x_i,x_{i+1}]:

$$y_{i+1} = y_i + \int_{x_i}^{x_{i+1}} f(x,y)\ dx \tag{50}$$

The value of the slope f(x,y) is approximated with a polynomial interpolation [36] factoring in previous evaluations of $f(x_{i-1}, y_{i-1})$,$f(x_{i-2}, y_{i-2})$, etc. The order and

corresponding equation for a given step size h are provided below [35]:

$$2^{nd}\ Order: \qquad y_{i+1} = y_i + \frac{h}{2}\left[3f(x_i, y_i) - f(x_{i-1}, y_{i-1})\right] \quad (51)$$

$$3^{rd}: \qquad y_{i+1} = y_i + \frac{h}{12}\left[23f(x_i, y_i) - 16f(x_{i-1}, y_{i-1}) + 5f(x_{i-2}, y_{i-2})\right] \quad (52)$$

$$4^{th}: y_{i+1} = y_i + \frac{h}{24}\left[55f(x_i, y_i) - 59f(x_{i-1}, y_{i-1}) + 37f(x_{i-2}, y_{i-2}) - 9f(x_{i-3}, y_{i-3})\right] \quad (53)$$

2.10 Chapter II Summary

This chapter reviewed the relevant aircraft avoidance models by describing Kuchar and Yang's review of CDR methods. A fundamental background of aircraft and Earth navigational reference frames was conducted. The existing TAWS systems applicable to performance limited aircraft was reviewed with the corresponding system displays and design limits. A review of the existing Auto-GCAS research from the implemented F-16 system to the NASA SUAV and AFIT's research based on Calspan's LJ-25D aircraft were described and summarized. Finally, the numerical integration techniques used in trajectory prediction algorithms was reviewed. This in depth review is critical for understanding the methodology of Auto-GCAS research.

III. Simulation Methodology

Chapter Overview

This chapter provides an outline of the methodology used to develop the Auto-GCAS algorithm for the 6-DOF Learjet-25D model, the terrain tools used to test the different performance metrics of the Auto-GCAS algorithm, and the performance metrics used for comparison. These sections will refer to existing references and background information from Chapter II to further explain the detail of the developed Auto-GCAS algorithm. Ultimately, Chapter III prepares the reader to understand the algorithm test results analyzed in Chapter IV.

3.1 Learjet 6-DOF System Model

The aircraft model used in this research is a Learjet Model 25D (LJ-25D) developed through USAF TPS, Textron Aviation, and the US Army Aviation Development Directorate [40]. This models the same aircraft Gahan flew for flight testing of his Auto-GCAS algorithm [28], which is a specifically modified Calspan Variable Stability Learjet-25D. The LJ-25D model is a quasi-Linear-Parameter-Varying (quasi-LPV) model which is a linearized state-space representation of a nonlinear system, where the state-space matrices are time-varying based on a scheduling parameter $\rho(t)$ [40]. For this LJ-25D model, the aircraft is stitched based on the following scheduling parameter vector:

$$\begin{bmatrix} \rho \end{bmatrix} = \begin{bmatrix} U \\ \\ \delta_f \end{bmatrix} \tag{54}$$

Where U is the x-body axis velocity state and δ_f is the flap deflection [40].

Quasi comes from the discrete flight test points that were collected to "stitch" the model together into a Linear-Parameter-Varying (LPV) system. The typical LPV

system is represented in the following equations [40]:

$$\dot{X}(t) = f\ (X(t), U(t)) \tag{55}$$

$$Y(t) = h\ (X(t), U(t)) \tag{56}$$

Where X(t) are the time dependent states, U(t) are the time dependent control inputs, Y(t) are the time dependent system outputs, and f and h are nonlinear functions describing the system [40]. The LPV model updated with the time-varying scheduling parameter is as follows [40]:

$$\dot{X}(t) = A(\rho(t))\ (X(t) - X_0(\rho(t)) + B(\rho(t))\ (U(t) - U_0(\rho(t)) + \dot{X}_0(\rho(t)) \tag{57}$$

$$Y(t) = C(\rho(t))\ (X(t) - X_0(\rho(t)) + D(\rho(t))\ (U(t) - U_0(\rho(t)) + Y_0(\rho(t)) \tag{58}$$

Where A, B, C, and D are the typical linearized state-space matrices representing the nonlinear system described in Equations (55 and 56) about a trim condition; $\rho(t)$ is the scheduling parameter vector; X, U, and Y are the states, control inputs, and system outputs; X_0, U_0, and Y_0 are the *trimmed* states, control inputs, and system outputs; X(t) are the time dependent states, U(t) are the time dependent control inputs, Y(t) are the time dependent system outputs; and $\dot{X}_0 = 0$ so it can be eliminated from the equation [40]. The data needed to create the values in Equations (57 and 58) are a combination of point models and trim data at different scheduling parameters ρ_0, which means that each A, B, C, D, X_0, U_0, and Y_0 change passed on ρ_0 [40].

The quasi-LPV model is broken into longitudinal and lateral directional modes represented in the aircraft body axes frame. Referencing Equations (8 - 19) from the paragraph discussing 6-DOF equations of motion in section 2.3, the non linear

aircraft forces and moments are wrapped into the state space matrices. The LJ-25D longitudinal aircraft body axes model is the following [40]:

$$\begin{bmatrix} \dot{u} \\ \dot{w} \\ \dot{q} \\ \dot{\theta} \end{bmatrix} = \begin{bmatrix} X_u & X_w & X_q - W_0 & -g\cos\theta_0 \\ Z_u & Z_w & Z_q + U_0 & -g\sin\theta_0 \\ M_u & M_w & M_q & 0 \\ 0 & 0 & 1 & 0 \end{bmatrix} \begin{bmatrix} u \\ w \\ q \\ \theta \end{bmatrix} + \begin{bmatrix} X_{\delta_e} & X_{\delta_T} \\ Z_{\delta_e} & Z_{\delta_e} \\ M_{\delta_e} & M_{\delta_e} \\ 0 & 0 \end{bmatrix} \begin{bmatrix} \delta_e \\ \delta_T \end{bmatrix} \tag{59}$$

$$\begin{bmatrix} q \\ \alpha \\ a_x \\ a_z \\ \dot{u} \\ \dot{w} \end{bmatrix} = \begin{bmatrix} 0 & 0 & 1 & 0 \\ 0 & \frac{1}{U_0} & 0 & 0 \\ X_u & X_w & X_q & 0 \\ Z_u & Z_w & Z_q & 0 \\ X_u & X_w & X_q - W_0 & -g\cos\theta_0 \\ Z_u & Z_w & Z_q + U_0 & -g\sin\theta_0 \end{bmatrix} \begin{bmatrix} u \\ w \\ q \\ \theta \end{bmatrix} + \begin{bmatrix} 0 & 0 \\ 0 & 0 \\ X_{\delta_e} & X_{\delta_T} \\ Z_{\delta_e} & Z_{\delta_e} \\ X_{\delta_e} & X_{\delta_T} \\ Z_{\delta_e} & Z_{\delta_e} \end{bmatrix} \begin{bmatrix} \delta_e \\ \delta_T \end{bmatrix} \tag{60}$$

The LJ-25D lateral aircraft body axes model is the following [40]:

$$\begin{bmatrix} \dot{v} \\ \dot{p} \\ \dot{r} \\ \dot{\theta} \end{bmatrix} = \begin{bmatrix} Y_v & Y_p + W_0 & Y_r - U_0 & g\cos\theta_0 \\ L_v & L_p & L_r + 0 & \\ N_v & N_p & N_r & 0 \\ 0 & 1 & \tan\theta_0 & 0 \end{bmatrix} \begin{bmatrix} v \\ p \\ r \\ \phi \end{bmatrix} + \begin{bmatrix} Y_{\delta_a} & Y_{\delta_r} \\ L_{\delta_a} & L_{\delta_r} \\ N_{\delta_a} & N_{\delta_r} \\ 0 & 0 \end{bmatrix} \begin{bmatrix} \delta_a \\ \delta_r \end{bmatrix} \tag{61}$$

$$\begin{bmatrix} p \\ r \\ a_y \\ \beta \\ \dot{v} \end{bmatrix} = \begin{bmatrix} 0 & 1 & 0 & 0 \\ 0 & 0 & 1 & 0 \\ Y_v & Y_p & Y_r & 0 \\ \frac{1}{V_{tot}} & 0 & 0 & 0 \\ Y_v & Y_p + W_0 & Y_r - U_0 & g\cos\theta_0 \end{bmatrix} \begin{bmatrix} v \\ p \\ r \\ \phi \end{bmatrix} + \begin{bmatrix} 0 & 0 \\ 0 & 0 \\ Y_{\delta_a} & Y_{\delta_r} \\ 0 & 0 \\ Y_{\delta_a} & Y_{\delta_r} \end{bmatrix} \begin{bmatrix} \delta_a \\ \delta_r \end{bmatrix} \tag{62}$$

The stitched LJ-25D has the longitudinal and lateral state-space matrices in tab-

ular form depending on the time varying scheduling parameter vector. Therefore, in order to be able to determine the longitudinal and lateral outputs from the tabulated stitched data, the following parameters are required as inputs into the LJ-25D model:

State Inputs: u, v, w, p, q, r

Control Inputs: δ_e, δ_a, δ_r, δ_T

Scheduling Parameters: U, δ_f

The state parameters and outputs of the LJ-25D model can then be used in the escape-maneuver trajectory prediction. Control actuators are modeled to provide positional output based on a time step (dt), current position, and rate limiting / saturation. The LJ-25D model was developed purely in Simulink, however Gahan converted portions of the model to MATLAB code for ease of manipulation and coding [10]. Gahan's converted code was compared to the same validation of the stitched LJ-25D model in section VIII of Berger et al. [40].

Lastly, to put the LJ-25D model into perspective, the following values represent some performance capabilities of the LJ-25D aircraft [40, 41]:

Maximum take-Off Weight: 15,000 lbs

Cruise Speed: 464 KTAS

maximum Range: 1,535 nm

Service Ceiling: 45,000 ft

maximum Climb Rate: 6,050 fpm

3.2 Implementation of LJ-25D Model in Auto-GCAS Algorithm

The implementation of the LJ-25D Auto-GCAS algorithm, representing performance limited aircraft, reflects the CDR model outlined in section 2.1.2. The state propagation, state dimensions, collision detection, collision resolution, collision resolution maneuvers, and multiple-conflicts will be further explained in their respective

details. The over-arching design architecture is represented in Figure 22.

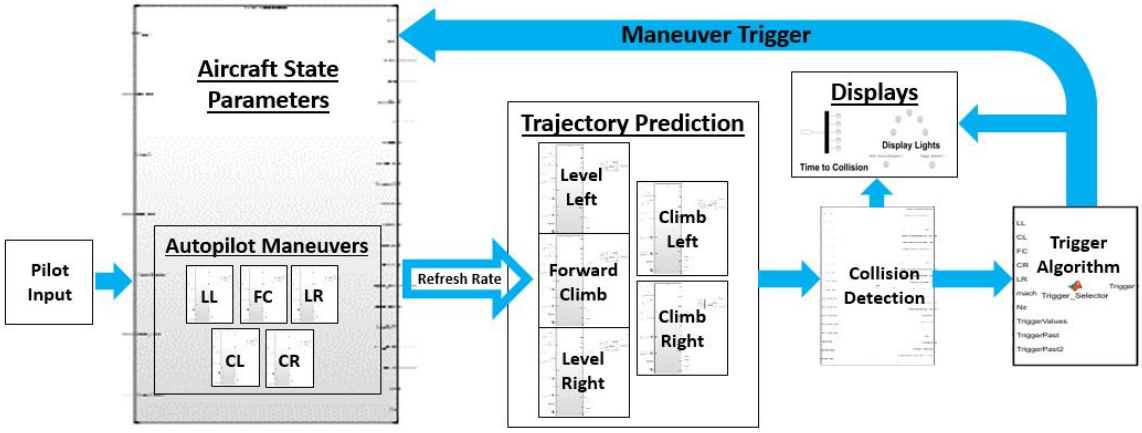

Figure 22. Auto-GCAS System Architecture [10]

3.2.1 LJ-25D State Propagation.

Referencing the state vector in Equation (7), the state parameters are provided as initial conditions from the LJ-25D aircraft model. Additional input values are the current latitude and longitude from the aircraft Embedded Global Positioning System/Inertial Navigation System (EGI), throttle position, initial trimmed horizontal stabilizer position, and vertical g-load on aircraft. This aircraft information is sent to the escape-maneuver prediction at a certain refresh rate, which defines the frequency of Auto-GCAS calculations. The escape-maneuver prediction is commonly referred to as Trajectory Prediction Algorithm (TPA) in similar research [28, 12, 13, 25]. The higher the refresh rate, the more collision calculations are performed, with an infinite refresh rate indicating continuous calculations. The refresh rate is depicted in Figure 23.

For the LJ-25D Auto-GCAS design, there are five escape-maneuvers consisting of a Level Left (LL), Climbing Left (CL), Forward Climb (FC), Climbing Right (CR), and Level Right (LR) escape-maneuver. The escape-maneuvers are targeted by the Auto-GCAS autopilots to attain the following values:

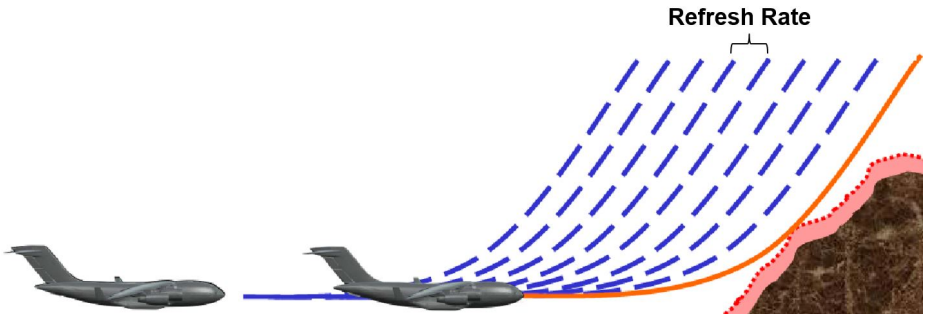

Figure 23. Auto-GCAS Refresh Rate [12]

Table 3. LJ-25D Auto-GCAS TPA Escape-Maneuvers [10]

Path Number	Maneuver Term	Description
Path 1	Level Left (LL)	60° bank, 0° climb angle, max throttle
Path 2	Climbing Left (CL)	15° bank, 12° AoA, max throttle
Path 3	Forward Climb (FC)	Roll to wings level, when under 10° bank begin climb 12° AoA (not to exceed 2-g vertical load), max throttle
Path 4	Climbing Right (CR)	15° bank, 12° AoA, max throttle
Path 5	Level Right (LR)	60° bank, 0° climb angle, max throttle

How far into the future each individual escape-maneuvers is projected is referred to as the forward look-ahead time. Different levels of forward look-ahead times were tested in this algorithm, however the basic determination came from Trombetta's terrain analysis [13], where ranges are defined in Table 4.

Overall, the forward look-ahead time affects the computational speed of running the algorithm. Additionally, the look-ahead time can affect the operator nuisance level depending on the collision detection and escape-maneuver trigger design.

Table 4. Proposed Escape-Maneuvers Propagation Times [13]

Aircraft Class (Kts GS)	Lowland*	Midland†	Upland‡
Low Speed (210)	17.25 s	29.19 s	44.54 s
Med Speed (310)	17.20 s	21.14 s	30.72 s
High Speed (540)	28.25 s	28.25 s	28.25 s

* Terrain $<$ 250 ft per $\frac{1}{2}$ nm
† Terrain between 250 ft per $\frac{1}{2}$ nm and 500 ft per $\frac{1}{2}$ nm
‡ Terrain $>$ 500 ft per $\frac{1}{2}$ nm

3.2.2 LJ-25D State Dimensions.

The LJ-25D Auto-GCAS terrain scanning method used a 3-D spatial projection of the aircraft future flight path from the state propagation method. Therefore a combination of horizontal and vertical data is utilized similar to EGPWS. The forward projection of the aircraft flight path can be compared to sloping terrain at the determined look-ahead time. For the LJ-25D Auto-GCAS, the forward look-ahead times were varied between 30 s for all paths, 45 s for all paths, 90 s for all paths, 30 s for all paths except the forward climb at 45 s, and an adaptive path where times on the lateral turns were added to the forward look ahead time if certain parameters were met at low speed conditions (full 180 ° turn or stall condition).

3.2.3 LJ-25D Collision Detection.

The collision detection method used was a gridded interpolation of DTED data utilized by Suplisson [12]. This method means that a continuous DTED grid is generated through interpolation between DTED posts within the height terrain matrix. Figure 24 is a representation of DTED height terrain information based on a "nearest" approximation as opposed to discrete data posts.

The flight path outputted by the TPA is then converted between East-North-UP

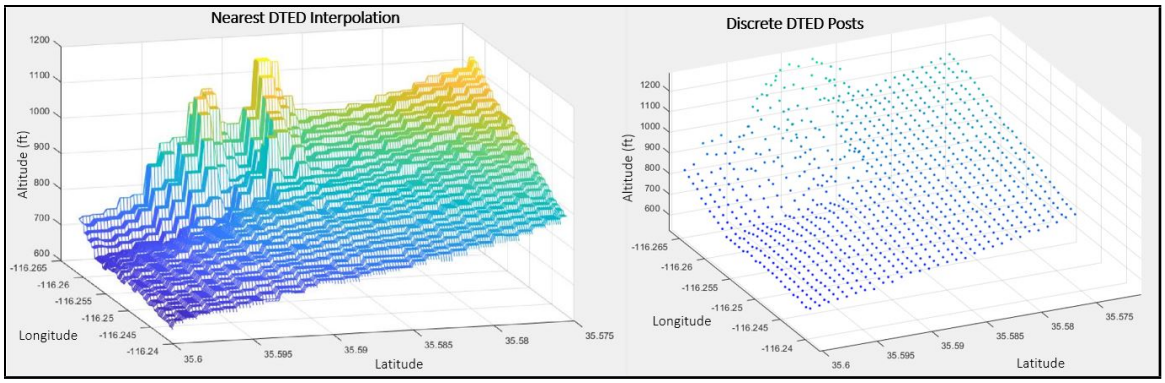

Figure 24. DTED Nearest Interpolation (Continuous Grid) vs. DTED Post Terrain (Discrete Grid)

(ENU) and Geodetic reference frames as outlined in section 2.4. All five escape-maneuver altitudes correspond to interpolated DTED at the calculated escape-maneuver's latitude and longitude values. This differential height represents Height Above Terrain (HAT) of the aircraft for every point along the escape path. If HAT is less than zero (including a safety buffer), the escape path is closed due to a predicted collision.

3.2.4 LJ-25D Collision Resolution and Maneuvers.

This HAT trigger information is sent to the collision resolution portion. A trigger number is assigned to each corresponding autopilot path (LL, CL, FC, CR, LR) when the respective autopilot path projected escape-maneuver is closed. A last man standing approach is taken similar to NASA SUAV multi-trajectory algorithm [25], where the Auto-GCAS activates based on when the last available open path closes. The last available path's associated trigger number is then sent back to the aircraft state parameters to take control away from the pilot and hand control to the Command Augmentation System (CAS) to execute the escape-maneuver. In the forward-open trigger algorithm, Auto-GCAS continues executing escape-maneuvers until the forward climb path is open, at which point the control is handed back to the pilot. The forward path is required to be open to avoid early hand back of the controls to the

pilot. Despite a previous Auto-GCAS activation, early hand back indicates the aircraft energy is still headed towards terrain and the Auto-GCAS system will activate again on the same terrain feature. At any point during Auto-GCAS, the pilot has the option to override the system.

3.2.5 LJ-25D Multiple-Conflicts.

Although this section is more pertinent to an Automatic Integrated Collision Avoidance System (Auto-ICAS) where conflicts between projected air and ground collisions have to be deconflicted, a multi-trajectory Auto-GCAS algorithm still has to decide a single path in the instance multiple paths close at the exact same time. The default trigger set for the LJ-25D Auto-GCAS is LR $\rightarrow$ CR $\rightarrow$ FC $\rightarrow$ CL $\rightarrow$ LL.

Additional conflicts considered in the trigger algorithm include preference to vertical g-load and Mach number. Despite all paths being closed off, the LJ-25D trigger algorithm will hand back control to the pilot if the vertical g-load exceeds 2.3 g's. The trigger algorithm will also override a selected escape-maneuver if the Mach number decreases below M = 0.25, and automatically enter a forward climb.

3.3 Numerical Integration Methods Used for Comparison

The solution to the aircraft trajectory initial value problem (IVP) will be discussed and the specific numerical integration methods compared in this research will be detailed. The following initial conditions are required for state propagation of the aircraft trajectory:

$$y = [x_0,\ u,\ v,\ w,\ p,\ q,\ r,\ \phi,\ \theta,\ \psi,\ x_i,\ y_i,\ z_i] \tag{63}$$

where x_0 represents the initial trimmed control surface state (remains 0 throughout integration); and x_i, y_i, and z_i are the inertial horizontal, lateral, and vertical positions

of the aircraft in geodetic coordinates. The rest are variables described in the 6-DOF equations of motion in section 2.3.

The first step is assigning an initial time step value for evaluating the numerical integration. This time step can then be carried through as a fixed time step solver or become an adaptive time step solver as discussed in section 3.3. The aircraft mass is considered constant for the aircraft trajectory projection because of the relatively short forward look-ahead time. The following steps are used to calculate the escape-maneuver state variables:

1. Calculate initial autopilot elevator position based on stick position input and time step.

2. Convert body axes to stability axes for roll, pitch, and yaw in order to obtain accurate control surface deflections.

3. Factor in desired escape-maneuver trajectory (LL, CL, FC, CR, LR) in order to calculate control surface command inputs ($\delta_{e_{com}}$, $\delta_{a_{com}}$, $\delta_{r_{com}}$).

4. Calculate control surface deflections (δ_e, δ_a, δ_r, δ_h) based on desired commands.

The LJ-25D has both a fully deflectable horizontal stabilator and elevator that work in conjunction to provide pitch control. The horizontal stabilator position is then biased into the position of the elevator control, leaving the three primary control surfaces (δ_e, δ_a, δ_r) as the control vector inputs to LJ-25D model in Equations (59 - 62).

5. Calculate engine control parameters for both left and right engines (δ_T value) in Equations (59 - 62) based on power setting required (0 to 1, 1 being maximum power). The escape-maneuvers assume maximum throttle control so power setting is set to 1.

6. Calculate thrust loads based on engine position (allows for asymmetric loading

if either engine is at a different power setting).

7. Calculate gravity force based on the aircraft mass and respective Euler angle positioning relative to the inertial reference frame.

8. Account for initial wind condition (considered constant magnitude and heading through the maneuver).

9. Account for turbulence using Dryden turbulence model (ignored for this current research).

10. Calculate in density altitude of aircraft at current altitude.

The LJ-25D model does not have altitude as a scheduling parameter since the stitched model was conducted only at 15,000 ft AGL at Edwards AFB [40]. Therefore density altitude is factored into input of stitched model to correct for altitude variation from test points.

11. Determine body axes u, v, w, p, q, and r based on center of gravity (CG) offset values in body axes x, y, and z directions.

12. Look up tabulated data from Stitched LJ-25D model based on scheduling parameter vector (U-velocity and flap deflection). Regarding the U-velocity, caution must be taken in choosing time step value because if the time step is too large, the U-velocity change between initial condition and desired time step exceeds the tabulated data. The aircraft configuration in simulations was with zero flaps as defined in the trim condition, so only the U-velocity was factored into the quasi-LPV model.

13. Calculate the forces and moments on the aircraft using the linearized state-space matrices.

14. Solve the nonlinear rigid body dynamic equations: $\dot{u}$, $\dot{v}$, and $\dot{w}$ are calculated from Equations (8 - 10).

15. Solve the nonlinear kinematic equations: $\dot{p}$, $\dot{q}$, and $\dot{r}$ are calculated from Equations (11 - 13).

16. Calculate the change in navigational position through the body 3-2-1 DCM in Equation (22). These coordinates will later be translated to latitude and longitude values for the collision detection.

17. Integrate the state variable derivatives ($\dot{y}$) over the time step (dt) to calculate the future state variables (y).

The integrating methods discussed in the following sections focus specifically on step 17 above. However, it is very important to note the calculations in steps 1-16 that are dependent on the time step (dt) and filter throughout the calculations. The initial pilot input through the control stick ($elev_{x0}$), the autopilot target commands for feedback control (N_{zg} and $\delta_{e_{com}}$, $\delta_{a_{com}}$, $\delta_{r_{com}}$), and the control surface deflections are all dependent on the time step chosen.

3.3.1 Euler Solver.

The first integration technique used was the fixed step Euler Explicit solver in section 2.9.3. The following equations were integrated over the forward look-ahead time at each incremental time step (dt):

$$\begin{bmatrix} u \\ v \\ w \end{bmatrix}_{y_{i+1}} = \begin{bmatrix} u \\ v \\ w \end{bmatrix}_{y_i} + dt \cdot \begin{bmatrix} \dot{u} \\ \dot{v} \\ \dot{w} \end{bmatrix}_{y_i} \tag{64}$$

$$\begin{bmatrix} p \\ q \\ r \end{bmatrix}_{y_{i+1}} = \begin{bmatrix} p \\ q \\ r \end{bmatrix}_{y_i} + dt \cdot \begin{bmatrix} \dot{p} \\ \dot{q} \\ \dot{r} \end{bmatrix}_{y_i} \tag{65}$$

$$\begin{bmatrix} x \\ y \\ z \end{bmatrix}_{I_{y_{i+1}}} = \begin{bmatrix} x \\ y \\ z \end{bmatrix}_{I_{y_i}} + dt \cdot \begin{bmatrix} C_\theta C_\psi & S_\phi S_\theta C_\psi - C_\phi S_\psi & C_\phi S_\theta C_\psi + S_\phi S_\psi \\ C_\theta S_\psi & S_\phi S_\theta S_\psi + C_\phi C_\psi & C_\phi S_\theta S_\psi - S_\phi C_\psi \\ -S_\theta & S_\phi C_\theta & C_\phi C_\theta \end{bmatrix} \begin{bmatrix} \dot{p} \\ \dot{q} \\ \dot{r} \end{bmatrix}_{B_{y_i}} \tag{66}$$

where I represents the inertial axes frame of reference and B represents the body axes frame of reference. This method is also the baseline integration technique used by Gahan for LJ-25D flight testing at TPS [10] [28].

3.3.2 Adams-Bashforth Solver.

The multi-step solver used was the explicit Adams-Bashforth method described in section 2.9.5. The initial time step uses the Explicit Euler integration described in 3.3.1. On the second time step, the 2^{nd} order Adams-Bashforth is used as described in Equation (51). On the third time step, the 3^{rd} order Adams-Bashforth is used as described in Equation (52). Finally, all steps after the fourth step will use a 4^{th} order Adams-Bashforth as described in Equation (53). As an example, only the u, v, w equation will be shown for the 4^{th} order Adams-Bashforth:

$$\begin{bmatrix} u \\ v \\ w \end{bmatrix}_{y_{i+1}} = \begin{bmatrix} u \\ v \\ w \end{bmatrix}_{y_i} + \frac{h}{24}(55 \begin{bmatrix} \dot{u} \\ \dot{v} \\ \dot{w} \end{bmatrix}_{y_i} - 59 \begin{bmatrix} \dot{u} \\ \dot{v} \\ \dot{w} \end{bmatrix}_{y_{i-1}} + 37 \begin{bmatrix} \dot{u} \\ \dot{v} \\ \dot{w} \end{bmatrix}_{y_{i-2}} - 9 \begin{bmatrix} \dot{u} \\ \dot{v} \\ \dot{w} \end{bmatrix}_{y_{i-3}}) \tag{67}$$

It is important to notice here that the integration method only depends on the current and previously calculated slopes at a given time step, and not directly dependent on the x_i and y_i states evaluated between the time step as seen in the following Runge-Kutta solvers.

3.3.3 MATLAB ode2 Solver.

MATLAB has a 2^{nd} order explicit fixed time step solver using Huen's midpoint method that is referred to as ode2 [42]. This solver is a Runge-Kutta method as described in section 2.9.4, Equations (36 - 38). The initial time step uses the Explicit Euler integration described in 3.3.1. As an example, only the u, v, w equation will be shown for Huen's midpoint method:

$$\begin{bmatrix} u \\ v \\ w \end{bmatrix}_{y_{i+1}} = \begin{bmatrix} u \\ v \\ w \end{bmatrix}_{y_i} + \left(\begin{bmatrix} \dot{u} \\ \dot{v} \\ \dot{w} \end{bmatrix}_{y_i} + K_2 \right) \cdot dt \tag{68}$$

$$K_2 = f(x_i + \frac{1}{2}\, dt, \begin{bmatrix} u \\ v \\ w \end{bmatrix}_{y_i} + \frac{1}{2} \begin{bmatrix} \dot{u} \\ \dot{v} \\ \dot{w} \end{bmatrix}_{y_i} dt) \tag{69}$$

where the $f(\ )$ designates the slope of the function at the x and y values inside the parenthesis; the x values are the dependent states on dt required to calculate state variables (reference section 3.3).

3.3.4 MATLAB ode3 Solver.

MATLAB has a 3^{rd} order explicit fixed time step solver using Bogacki-Shampine's method that is referred to as ode3 [42]. This solver is a Runge-Kutta method as described in section 2.9.4 equations (40 - 43) and the constants of integration in Table 2. The initial time step uses the Explicit Euler integration described in 3.3.1. As an

example, only the u, v, w equation will be shown for Bogacki-Shampine's method:

$$\begin{bmatrix} u \\ v \\ w \end{bmatrix}_{y_{i+1}} = \begin{bmatrix} u \\ v \\ w \end{bmatrix}_{y_i} + \frac{1}{2}(2 \begin{bmatrix} \dot{u} \\ \dot{v} \\ \dot{w} \end{bmatrix}_{y_i} + 3 \cdot K_2 + 4 \cdot K_3) \tag{70}$$

$$K_2 = f(x_i + \frac{1}{2}\ dt, \begin{bmatrix} u \\ v \\ w \end{bmatrix}_{y_i} + \frac{1}{2} \begin{bmatrix} \dot{u} \\ \dot{v} \\ \dot{w} \end{bmatrix}_{y_i} dt) \tag{71}$$

$$K_3 = f(x_i + \frac{3}{4}\ dt, \begin{bmatrix} u \\ v \\ w \end{bmatrix}_{y_i} + \frac{3}{4}\ K_2\ dt) \tag{72}$$

where the $f(\ )$ designates the slope of the function at the x and y values inside the parenthesis; the x values are the dependent states on dt required to calculate state variables (reference section 3.3).

3.3.5 MATLAB ode4 Solver.

MATLAB has a 4^{th} order explicit fixed time step solver using the classical Runge-Kutta method that is referred to as ode4 [42]. This solver is a Runge-Kutta method as described in section 2.9.4 Equations (44 - 48) and the constants of integration in Equation (49). The initial time step uses the Explicit Euler integration described in section 3.3.1. As an example, only the u, v, w equation will be shown for the classical

Runge-Kutta method:

$$\begin{bmatrix} u \\ v \\ w \end{bmatrix}_{y_{i+1}} = \begin{bmatrix} u \\ v \\ w \end{bmatrix}_{y_i} + \frac{1}{6}(\begin{bmatrix} \dot{u} \\ \dot{v} \\ \dot{w} \end{bmatrix}_{y_i} + 2 \cdot K_2 + 2 \cdot K_3 + K_4) \tag{73}$$

$$K_2 = f(x_i + \frac{1}{2}\ dt, \begin{bmatrix} u \\ v \\ w \end{bmatrix}_{y_i} + \frac{1}{2} \begin{bmatrix} \dot{u} \\ \dot{v} \\ \dot{w} \end{bmatrix}_{y_i} dt) \tag{74}$$

$$K_3 = f(x_i + \frac{1}{2}\ dt, \begin{bmatrix} u \\ v \\ w \end{bmatrix}_{y_i} + \frac{1}{2}\ K_2\ dt) \tag{75}$$

$$K_4 = f(x_{i+1}, \begin{bmatrix} u \\ v \\ w \end{bmatrix}_{y_i} + K_3\ dt) \tag{76}$$

where the $f(\ )$ designates the slope of the function at the x and y values inside the parenthesis; the x values are the dependent states on dt required to calculate state variables (reference section 3.3).

3.3.6 MATLAB ode5 Solver.

MATLAB has a 5^{th} order explicit fixed time step solver using the Dormand-Prince that is referred to as ode5 [42]. This solver is a Runge-Kutta method as described in section 2.9.4. The initial time step uses the Explicit Euler integration described in 3.3.1. As an example, only the u, v, w equation will be shown for the Dormand-Prince method. The Butcher's Tableau helps simplify the constants of integration:

Table 5. Butchers Tableau for Dormand-Prince 5th Order Runge-Kutta [42]

$\frac{1}{5}$	$\frac{1}{5}$					
$\frac{3}{10}$	$\frac{3}{40}$	$\frac{9}{40}$				
$\frac{4}{5}$	$\frac{44}{45}$	$\frac{-56}{15}$	$\frac{32}{9}$			
$\frac{8}{9}$	$\frac{19372}{6561}$	$\frac{-25360}{2187}$	$\frac{64448}{6561}$	$\frac{-212}{729}$		
1	$\frac{9017}{3168}$	$\frac{-355}{33}$	$\frac{46732}{5247}$	$\frac{49}{176}$	$\frac{-5103}{18656}$	
	$\frac{35}{384}$	0	$\frac{500}{1113}$	$\frac{125}{192}$	$\frac{-2187}{6784}$	$\frac{11}{84}$

where the Butchers Tableau is used to calculate the slopes at multiple points between the current time step and desired time step (dt) similar to previous Runge-Kutta methods. The final state solution only for the u, v, w equation will be shown not defining the individual K values. The reader is encouraged to review Dormand-Prince's paper on 4^{th} and 5^{th} order Runge-Kutta [43].

$$\begin{bmatrix} u \\ v \\ w \end{bmatrix}_{y_{i+1}} = \begin{bmatrix} u \\ v \\ w \end{bmatrix}_{y_i} + (\frac{35}{384} \begin{bmatrix} \dot{u} \\ \dot{v} \\ \dot{w} \end{bmatrix}_{y_i} + \frac{500}{1113}K_3 + \frac{125}{192}K_4 + \frac{-2187}{6784}K_5 + \frac{11}{84}K_6) \quad (77)$$

3.3.7 MATLAB ode45 Solver.

MATLAB ode45 uses an adaptive time step solver developed from the Dormand-Prince embedded Runge-Kutta of 4^{th} and 5^{th} orders [42, 43]. For this research, ode45 was used as the truth source for state propagation of the aircraft trajectory where all other methods were compared to. The Butcher's Tableau helps simplify the constants of integration [43]: Dormand-Prince's solver uses a 4^{th} and 5^{th} order Runge-Kutta solver to calculate the solution to the differential equation at each time step. The Butcher's Tableau therefore has two rows under the bottom line, indicating the constants for the 4^{th} order estimation and the 5^{th} order solution. For efficiency, the

Table 6. Butchers Tableau for Dormand-Prince ode45 Solver [42]

0							
$\frac{1}{5}$	$\frac{1}{5}$						
$\frac{3}{10}$	$\frac{3}{40}$	$\frac{9}{40}$					
$\frac{4}{5}$	$\frac{44}{45}$	$\frac{-56}{15}$	$\frac{32}{9}$				
$\frac{8}{9}$	$\frac{19372}{6561}$	$\frac{-25360}{2187}$	$\frac{65558}{6561}$	$\frac{-212}{729}$			
1	$\frac{9017}{3168}$	$\frac{-355}{33}$	$\frac{46732}{5247}$	$\frac{49}{176}$	$\frac{-5103}{18656}$		
1	$\frac{35}{384}$	0	$\frac{500}{1113}$	$\frac{125}{192}$	$\frac{-2187}{6784}$	$\frac{11}{84}$	
Order $O(h^4)$	$\frac{35}{384}$	0	$\frac{500}{1113}$	$\frac{125}{192}$	$\frac{-2187}{6784}$	$\frac{11}{84}$	0
Order $O(h^5)$	$\frac{5179}{57600}$	0	$\frac{7571}{16695}$	$\frac{393}{640}$	$\frac{-92097}{339200}$	$\frac{187}{2100}$	$\frac{1}{40}$

4^{th} order is an embedded estimate within the 5^{th} order calculation to avoid calculating the solution two separate times [43]. The estimated local error is calculated from the difference in the 5^{th} order solution and the 4^{th} order estimate. The error term for each state is required to meet the following requirement in order to continue propagating forward [42]:

$$local\ error = y_{i+1_{RK5}} - \widehat{y}_{i+1_{RK4}} \ \leq \ max\ (\ rtol \cdot |y_{i+1}|,\ atol) \tag{78}$$

where MATLAB has a default relative tolerance ($rtol$) of $1e^{-3}$ and a default absolute tolerance ($atol$) of $1e^{-6}$. If the local error is greater than the acceptable error for any one state, the solver reduces the step size and tries again. The step size is recalculated based on an interpolated estimation of what step size *would* have meet the relative tolerance level, and then MATLAB takes 0.8 this step size value to be the new smaller step [42]. If the error term meets the requirement, the step size is increased based on the error and relative tolerance to speed up operation. Additionally, ode45 stretches the step size by 1.1 if the time is within 10% of t_{final}-t_{step}.

3.4 System Under Test and Measures of Performance

3.4.1 Description of LJ-25D Auto-GCAS algorithm.

This section describes the comparison techniques of different LJ-25D Auto-GCAS algorithms. The differences between different Auto-GCAS algorithms were differences in forward look-ahead time, predicted aircraft trajectory integration method, integration time-step, and trigger activation. The different algorithms are described in Table 7.

The *AB Varying* algorithm varies the forward look-ahead time for each of the five escape-maneuvers. The total sum look-ahead time between all five escape-maneuvers does not change, just the allocation of the time. This is accomplished by allocating time to the forward climb portions from trimming down the lateral maneuvers. The maneuver length for the level turns (LT) is the minimum value between 180° turn and 30s. The maneuver length for the climbing turns CT is a $\theta < 0°$ after 15 seconds into the path, which allows ample time for an aircraft to recover from steep initial pitch angles.

$$LT_{min} = min(\ 180°\ Turn\ ,\ 30s\ ) \tag{79}$$

$$CT_{max} = max(\ \theta < 0°\ ,\ 30s\ ) \tag{80}$$

This particularly helps at lower speeds, where the look-ahead time is recommended to be 45s from Table 4. The algorithm extends the forward climb to exceed 45s at low speeds while only trimming *non-utilized* look-ahead times for the lateral paths (i.e. stall conditions for climbing turns and turning back into itself on level turns). Graphically the *AB Varying* algorithm looks like Figure 25. The flight conditions here are 200 KIAS, $\gamma = 3°$, $= 5°$, and $\phi = 5°$.

For Figure 25, the *AB30* algorithm's lateral maneuvers, displayed in red lines,

Table 7. LJ-25D Auto-GCAS Algorithm Differences

Algorithm Name	**Forward Look-Ahead Time**	**Integration Method**	**Time Step**	**Trigger Activation**	**Trigger Handback**
Euler30*	30s All Paths	Euler Explicit	0.01s	Last Man Standing	First-Open†
Euler45	45s All Paths	Euler Explicit	0.01s	Last Man Standing	First-Open†
Euler90	90s All Paths	Euler Explicit	0.01s	Last Man Standing	First-Open†
AB30	30s All Paths	4^{th}Order Adams-Bashforth	0.01s	Last Man Standing	First-Open†
AB45	45s All Paths	4^{th}Order Adams-Bashforth	0.01s	Last Man Standing	First-Open†
Euler30 45FC	30s LL/CL 45s FC 30s CR/LR	Euler Explicit	0.01s	Last Man Standing	Forward-Open††
AB30 45FC	30s LL/CL 45s FC 30s CR/LR	4^{th}Order Adams-Bashforth	0.01s	Last Man Standing	Forward-Open††
AB Varying‡	[LT_{min},30]s LL/LR [30,50]s FC [15,CT_{max}]s CL/CR	4^{th}Order Adams-Bashforth	0.015s	Last Man Standing	Forward-Open††

* Baseline LJ-25D Auto-GCAS algorithm from Gahan [10]
† Last man standing trigger, first path open disengages Auto-GCAS
†† Last man standing trigger, forward path open disengages Auto-GCAS
‡ [min,max] defines the range of possible Forward Look-Ahead Times since the escape-maneuver length varies, see Equations (79,80)

were all 30s (total time of 150s). The trimmed lateral escape-maneuvers are shown in black lines, which stop trajectory prediction when the aircraft is stalled or turning

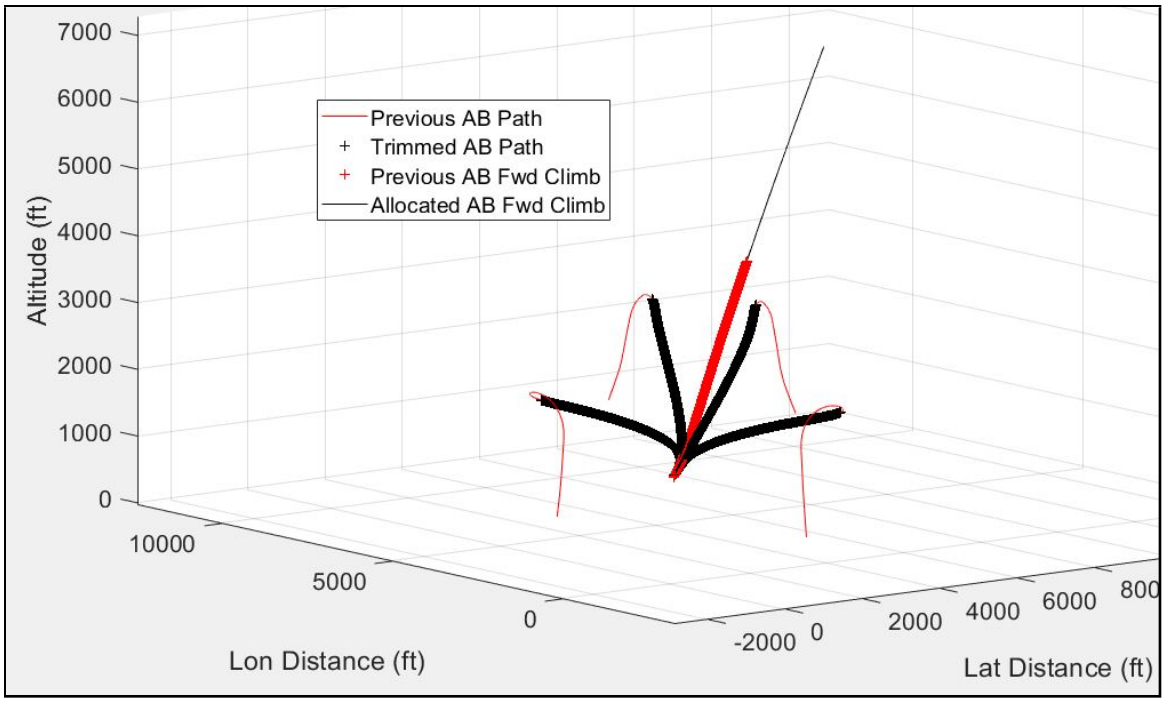

Figure 25. Auto-GCAS Algorithm Varying Path Lengths Based on Escape-Maneuver Performance

back into itself. Based on trimming the lateral maneuvers, the forward climb became 80s while the other lateral maneuvers became LL = 16.51s, CL = 18.39s, CR = 18.57s, and LR = 16.3s (still 150s total allocated time). Varying path method helps the aircraft predict terrain farther in advance when it has the least amount of kinetic energy, without increasing the computational cost of the algorithm.

3.4.2 Down Selection of Integration Methods.

All integration methods explained in section 3.3 were compared to ode45 for varying fixed time step values. Additionally, the time required to compute the path was measured to develop a speed vs. accuracy chart. Speed was defined as the MATLAB clock time to compute the numerical integration over the forward look-ahead time. Since speed was used as a comparison between integration methods, the clock time was normalized ode45's clock time run on the same computer. Accuracy was defined

as the Root-Sum-Square (RSS) error of each integration method compared to the ode45 flight path. RSS error was calculated from the latitudinal, longitudinal, and vertical deviations at each time step (i) per Equation (81).

$$RSS_{max} = max(\sqrt{(X_{ode45_i} - X_{method_i})^2 + (Y_{ode45_i} - Y_{method_i})^2 + (Z_{ode45_i} - Z_{method_i})^2}) \tag{81}$$

The comparison between all integration methods was first compared at initial conditions for steady level flight, listed below as the following trim conditions:

Airspeed: 300 KTAS	Altitude: 1,563 ft	Heading: 35
Gamma: 0°	Beta: 0°	Phi: 0°
Fuel Total: 4580.3 lbs	Fuel Wing Tip: 1919.4 lbs	

The feasible integration methods were selected by a design region in the speed vs. accuracy chart. Integration methods that were faster than ode45 and within 100 ft maximum RSS error were selected as possible candidates to implement into the Auto-GCAS algorithm. 100 ft maximum RSS error was chosen because low-level flying by C-130 and C-17 is around 300 ft AGL. However, if pilots perform modified contour flying, the AGL limit can be even lower because instead of terrain following, small terrain bumps are neglected to avoid abrupt deviations in flight path. Additionally, there are other compounding errors to factor into the Auto-GCAS algorithm that come from the safety buffer level, refresh rate, turbulence, wind, etc.

This speed vs. accuracy at a steady-level flight down selected the integration methods to Euler Explicit and Adams-Bashforth. These two methods were then additionally compared to ode45 at three different off-nominal conditions to determine the time step that diverges from the acceptable RSS. It was determined that the Adams-Bashforth with a time step of 0.015 s was the fastest time and still within the acceptable error bounds for off-nominal initial conditions. This is therefore the best

integration method analyzed to improve computational speed performance from the baseline Euler Explicit initially used by Gahan [10].

3.4.3 Measure of Performance (MOP): Comparison of LJ-25D Auto-GCAS Models.

3.4.3.1 Modified Test Box of DTED Terrain.

In order to evaluate how the Auto-GCAS algorithm would react to cliff walls and also increase frequency of different activations, superimposed terrain was created over existing DTED terrain to create a modified test box. The terrain test DTED is represented in Figure 26. The superimposed terrain consisted of vertical cliff walls

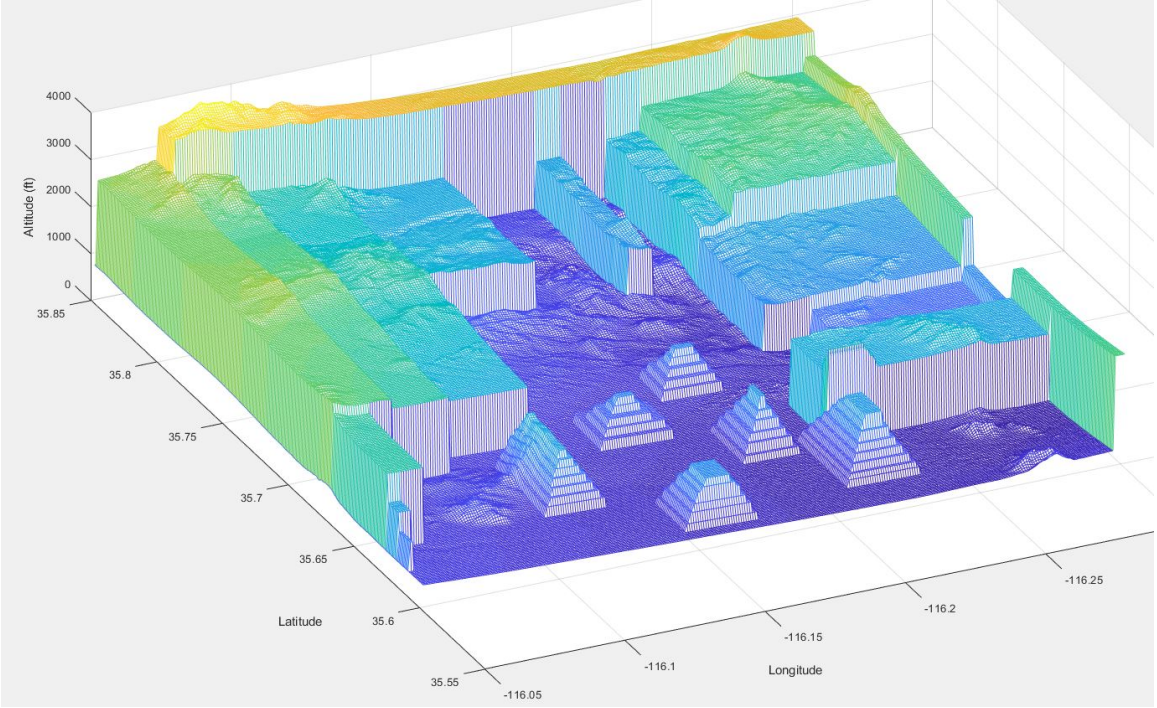

Figure 26. Modified DTED Terrain for Simulation Comparison (Front Wall Not Shown)

between 1,800 and 9,000 ft to simulate a boxed canyon and act as fencing to contain the aircraft within the terrain boundaries. Pyramids were added that classify as upland terrain (Table 4) with maximum heights ranging from 1,200 to 3,000 ft. The

selection of Auto-GCAS algorithms from Table 7 were compared to each other in this terrain test box to ascertain any differences in performance between methods. An example of a simulation is shown in Figure 27, where the line indicated the flight path and the color represented the selected escape-maneuver activated by the Auto-GCAS algorithm.

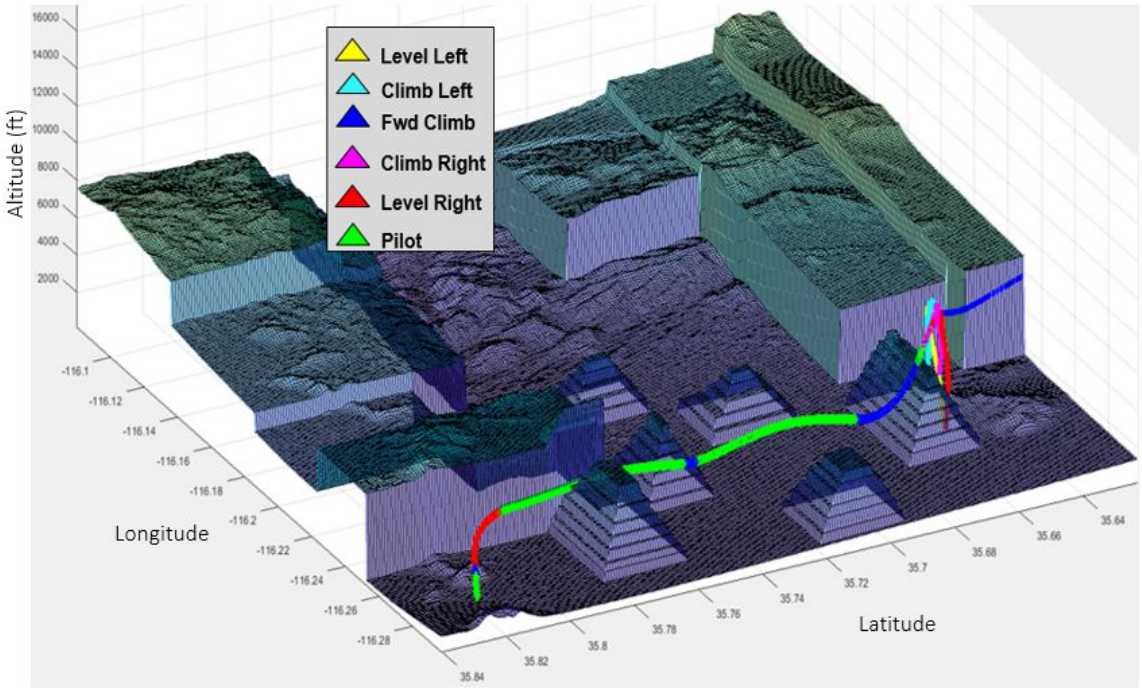

Figure 27. Modified DTED Terrain Simulation Example Run

3.4.3.2 MOP1: Computational Speed.

To measure computation time, two different methods were used. First, when comparing the integration methods escape-maneuver trajectory prediction algorithm in MATLAB, clock time was used to measure the time required to run the algorithm over the same forward look-ahead time and at the same fixed time step. These values were normalized against the time taken to run ode45.

Second, to measure the computation time when running the Auto-GCAS algo-

rithm in Simulink, Equation (82) was used to measure the computational rate (*Comp Rate*) running the Auto-GCAS algorithm. A higher value of *Comp Rate* indicates a higher performing Auto-GCAS algorithm:

$$CompRate\ (Hz) = \frac{Simulation\ Time}{Refresh\ Rate\ Time} \cdot \frac{1}{(Clock\ Time - Compile\ Time)} \tag{82}$$

where *Simulation Time* is the inputted simulation runtime; *Refresh Rate Time* is the time step to achieve the inputted refresh rate; *Clock Time* is the time required by Simulink to run the inputted simulation time; and *Compile Time* is the amount of time required by Simulink to build the model before a simulation. The values attained for *Comp Hz* will change based on computer performance, but since only a comparison is being done between algorithm speed on the same computer this variation is not a concern.

3.4.3.3 MOP2: Height Above Terrain.

The Height above Terrain (HaT) was graphed for each simulation. Providing the safety buffer and refresh rate was equivalent between LJ-25D Auto-GCAS algorithms, the minimum distance above terrain measures how effective the algorithm was at identifying terrain features and evading it. However, if the aircraft crashed (i.e. HaT below zero), it is also important to know the maximum distance below terrain to determine a proper safety buffer.

3.4.3.4 MOP3: Over-G.

Since the LJ-25D algorithm includes a fail safe to terminate the escape-maneuver if over 2.3 vertical g's are exceeded, the g-load was tracked for each simulation. This indicates if the escape-maneuver was able to be completed based on the autopilot commands.

3.5 Chapter III Summary

This chapter outlined the methodology and analytical procedures preceding the simulations of the LJ-25D Auto-GCAS and piloted study. An explanation of how the different numerical integrations were propagated was conducted for six different methods, with ode45 being considered as the truth source for data comparison. The fundamental LJ-25D Auto-GCAS algorithm was explained in terms of the CDR method and the differences between tested methods was explained in Table 7. Measures of performance were outlined to facilitate results comparison and performance between algorithm designs. The next chapter presents the aircraft escape-maneuver trajectory integration comparison and simulation results of different LJ-25D Auto-GCAS algorithms in the modified test terrain box.

IV. Simulation Results

Chapter Overview

This chapter outlines the data, results, and analysis of the escape-maneuver trajectory integration results. Additional results from simulations comparing different LJ-25D Auto-GCAS algorithms are discussed.

4.1 Predicted Aircraft Trajectory Integration Comparison

The different trajectory prediction integrations described in section 3.3 were compared for computational speed vs. accuracy for a trim condition of steady-level flight described in section 3.4.2. Six different time steps ranging from 0.005 to 0.02 seconds for each integration method were calculated over 30 s forward look-ahead time. Larger time steps than ~0.15 s could not be computed due to the fidelity of the LJ-25D stitched model U-velocity scheduling parameter being used for interpolation. The full results of the integration comparison with methods, speed, and accuracy are tabulated in Appendix A.

Since this was at steady-level flight, the results for left lateral turns are only shown due to symmetry with the right lateral turns. Figures 28, 29, and 30 display *Clock Speed* on the y-axis normalized to the ode45 clock speed, represented as the dashed horizontal line. *Max RSS* on the x-axis was compared to the ode45 path as the truth source which is represented as the dashed vertical line. The graphs are zoomed into the desired design region with a clock speed below ode45 and a maximum RSS under 100 ft.

Figures 28 and 29 show only the Euler and Adams-Bashforth methods being quicker than ode45 and with RSS values within 100 ft. The higher-order methods of ode2 - ode5 having to calculate multiple intermediate steps between time steps slowed

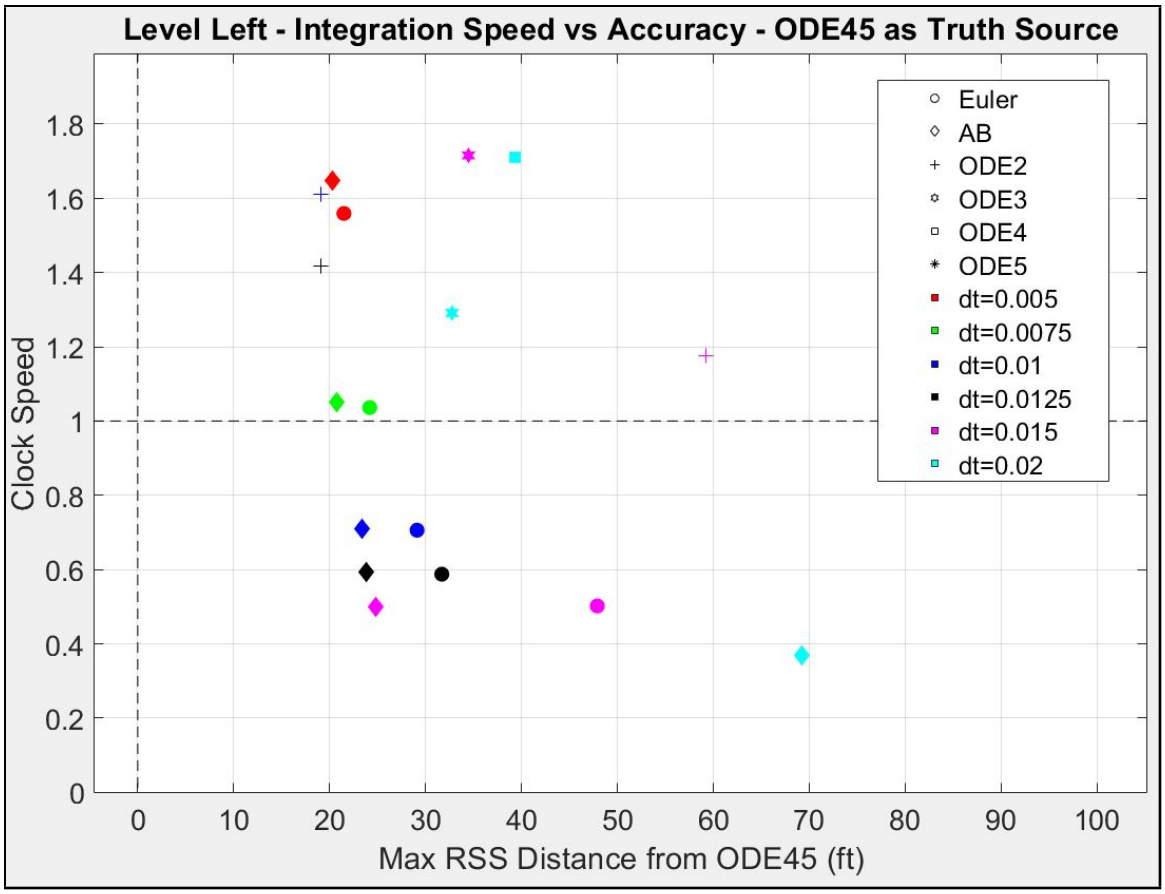

Figure 28. Level Left Accuracy vs. Speed Integration Comparison for Steady-Level Flight

the computation speed and did not provide any significantly lower RSS values as they were within 40 ft maximum RSS of the Euler and Adams-Bashforth approximations. When comparing the larger fixed time steps, specifically at 0.015 s, the higher-order systems had worse RSS errors than the multi-step Adams-Bashforth method as seen in Table 8. Notice the time at which the maximum RSS occurs as well, ideally it would be at the maximum forward look-ahead time (listed as *Path Length* in the figure).

When comparing the Climbing Left escape-maneuver at the larger fixed time steps, specifically at 0.015 s, the higher-order systems had worse RSS errors than both the Euler and multi-step Adams-Bashforth methods as seen in Table 9. The results of

Table 8. Level Left Integration Comparison with 0.015s time step

Path	Integration Method	Path Length (s)	Step Size	Clock Time (s)	Lat max (ft)	Time @ Max (s)	Lon max (ft)	Time @ Max (s)	Alt max (ft)	Time @ Max (s)	RSS - Distance max (ft)	Time @ Max (s)
LL	Euler	30	0.015	2.4921	36.5643	30	-29.7498	30	21.5824	13.965	47.9023	30
LL	AB	30	0.015	2.485	-19.2534	30	-16.5002	15.345	15.1557	30	24.8398	30
LL	ODE2	30	0.015	5.8347	55.907	30	-15.5889	30	19.3478	13.23	59.2010	30
LL	ODE3	30	0.015	8.5176	-24.0821	30	-24.0946	17.625	20.8781	30	34.4775	29.7
LL	ODE4	30	0.015	11.2909	-25.5422	30	-25.2528	17.61	22.021	30	36.3771	29.715
LL	ODE5	30	0.015	17.0462	-42.9416	21.135	-44.8986	15.78	55.5396	19.56	80.0480	19.005
LL	ODE45	30	Adaptive	4.9651	-	-	-	-	-	-	-	-

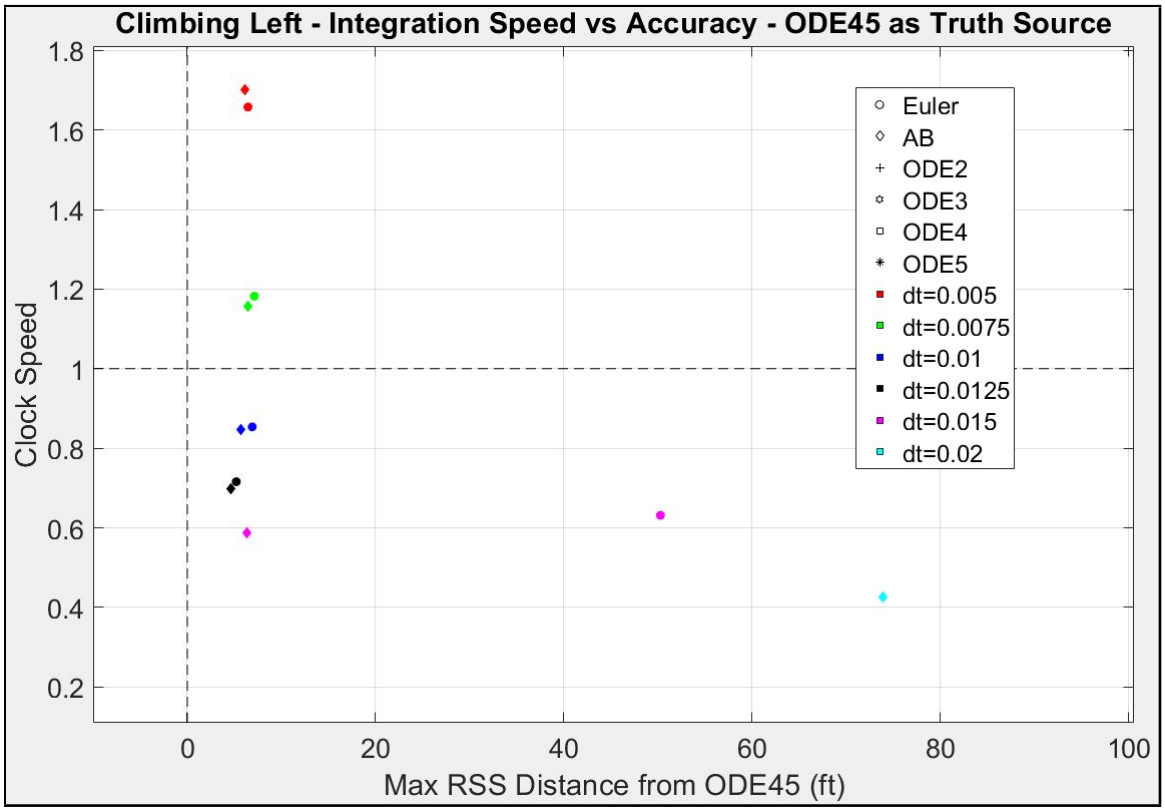

Figure 29. Climbing Left Accuracy vs. Speed Integration Comparison for Steady-Level Flight

a climbing turn starkly contrast from the level left maneuver, where the errors for ode2 - ode5 diverged to above 2,000 ft for an integration step of 0.015 s. Additionally, the Euler integration has the maximum error 24.6 s into the forward look-ahead time with a higher error than the Adams-Bashforth method.

For comparison on the Forward Climb escape-maneuver, Figure 30 also repeats

Table 9. Climbing Left Integration Comparison with 0.015s time step

Path	Integration Method	Path Length (s)	Step Size	Clock Time (s)	Lat max (ft)	Time @ Max (s)	Lon max (ft)	Time @ Max (s)	Alt max (ft)	Time @ Max (s)	RSS - Distance max (ft)	Time @ Max (s)
CL	Euler	30	0.015	2.6191	25.0648	29.34	17.3	26.1	-43.7	23.4	50.3	24.6
CL	AB	30	0.015	2.4355	-4.6385	30	-4.2	30	-4.7	0.645	6.3	30
CL	ODE2	30	0.015	5.828	-1140.4	30	-967.2	30	1920.1	30	2433.7	30
CL	ODE3	30	0.015	8.5116	-1199.5	30	-1041.0	30	2085.3	30	2621.3	30
CL	ODE4	30	0.015	10.8491	-1199.5	30	-1041.3	30	2085.5	30	2621.5	30
CL	ODE5	30	0.015	15.9724	-1107.4	30	-923.1	30	1799.1	30	2305.5	30
CL	ODE45	30	Adaptive	4.1473	-	-	-	-	-	-	-	-

the trend that the Euler and Adams-Bashforth's methods were the only combination that provided the speed and accuracy combination. However, ode2 and ode5 had lower RSS values than the Euler and Adams-Bashforth methods until the 0.015 s time step. Specifically at the 0.015 s time step in Table 10, the forward climb showed the Euler method with improved accuracy over the Adams-Bashforth, different from the lateral maneuvers.

Table 10. Forward Climb Integration Comparison with 0.015s time step

Path	Integration Method	Path Length (s)	Step Size	Clock Time (s)	Lat max (ft)	Time @ Max (s)	Lon max (ft)	Time @ Max (s)	Alt max (ft)	Time @ Max (s)	RSS - Distance max (ft)	Time @ Max (s)
FC	Euler	30	0.015	2.5284	14.2	29.7	9.95	29.685	-29.8	23.6	31.4	24.1
FC	AB	30	0.015	2.512	67.6	29.6	47.36	29.64	-39.0	12.4	82.6	29.0
FC	ODE2	30	0.015	5.8439	-43.9	21.0	-30.76	21.045	39.0	12.7	59.1	13.0
FC	ODE3	30	0.015	8.5836	-261.4	30.0	-183.06	30	131.9	13.2	319.8	30.0
FC	ODE4	30	0.015	11.3244	-261.5	30.0	-183.12	30	132.0	13.2	319.9	30.0
FC	ODE5	30	0.015	16.6934	-65.5	21.2	-45.89	21.195	60.7	12.7	90.9	13.0
FC	ODE45	30	Adaptive	5.2038	-	-	-	-	-	-	-	-

From these results, the trend of a fixed-step integration being accurate and fast was achieved by the Euler and Adams-Bashforth methods. Additionally, the tabulated data showed that higher-order integration methods do not always yield higher accuracy results, and that a lower step size does not guarantee a more accurate result than a higher fix size. It depends on the model fidelity and complexity of escape-maneuver. When varying the time step length, the Adams-Bashforth showed that maximum RSS values under 100 ft can be achieved for steady-level fight conditions in lateral maneuvers up to 0.02 s and in forward climb up to 0.015 s. The Euler method

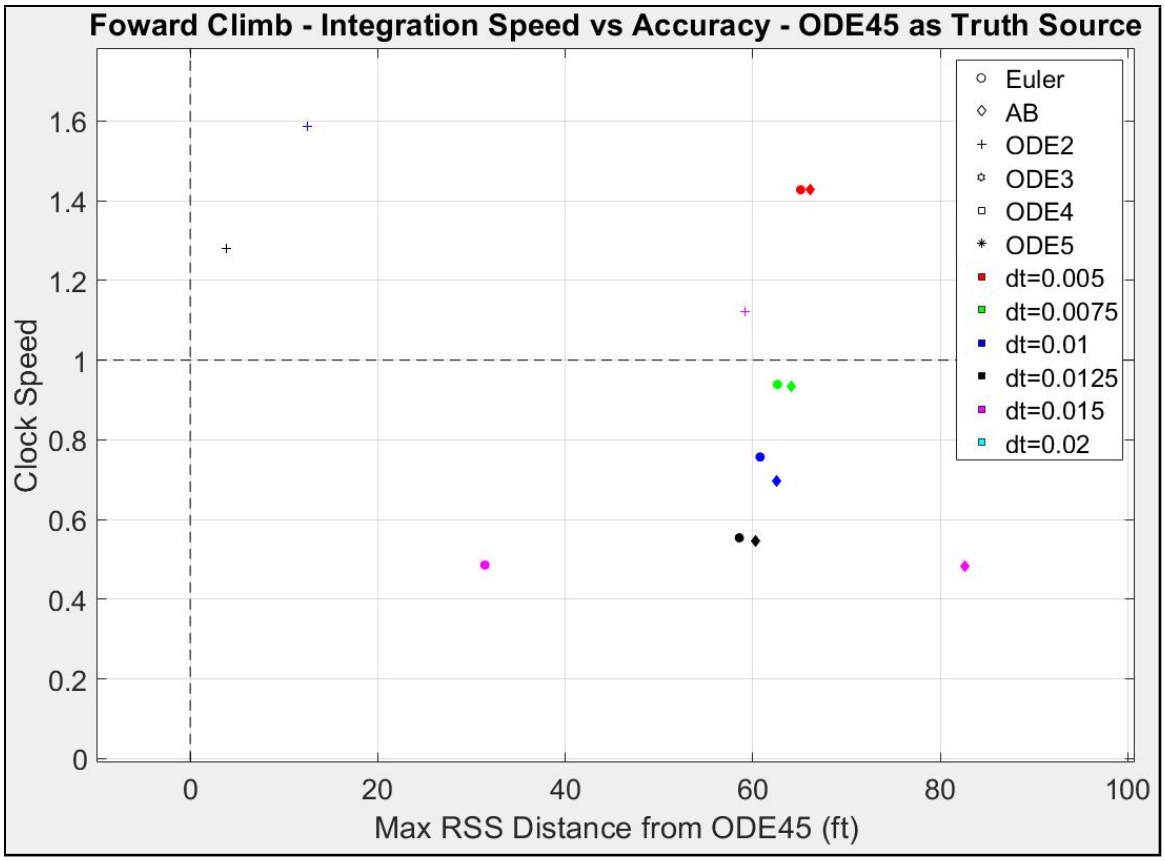

Figure 30. Forward Climb Accuracy vs. Speed Integration Comparison for Steady-Level Flight

showed maximum RSS values under 100 ft in lateral maneuvers and the forward climb up to 0.015 s. Even though the Adams-Bashforth had a larger RSS error on the forward climb, since it was within 100 ft and located 29.04 s into the escape-maneuver this is relatively a small 3% error of the final climbed. For the Forward Climb, 3,100 ft was climbed over a 30 s forward look-ahead time, where half of the altitude gained occurred in the last 10 s of the escape-maneuver.

Not all flight initial conditions are going to be steady-level flight, and therefore a comparison between just the Euler and Adams-Bashforth was done at off-nominal conditions to verify the results for the steady-level flight.

4.2 Euler and Adams-Bashforth Off-Nominal Integration Comparison

The Euler and Adams-Bashforth methods are compared for computational speed vs. accuracy for three different trim conditions. The first two mimic initial Euler angle conditions that were tested in Gahan's flight testing [28], while the third is an "extreme" case to test an atypical entry condition. The full results of the integration comparison with methods, speed, and accuracy are tabulated in Appendix C.

Trim Condition 1:

Airspeed: 300 KTAS	Altitude: 1,563 ft	Heading: 35
Gamma: -10°	Beta: 0°	Phi: 0°
Fuel Total: 4580.3 lbs	Fuel Wing Tip: 1919.4 lbs	

Trim Condition 2:

Airspeed: 300 KTAS	Altitude: 1,563 ft	Heading: 35
Gamma: 0°	Beta: 0°	Phi: 45°
Fuel Total: 4580.3 lbs	Fuel Wing Tip: 1919.4 lbs	

Trim Condition 3:

Airspeed: 425 KTAS	Altitude: 1,563 ft	Heading: 35
Gamma: 10°	Beta: -10°	Phi: -45°
Fuel Total: 4580.3 lbs	Fuel Wing Tip: 1919.4 lbs	

4.2.1 Trim Condition 1.

Since this initial condition only has a nose down flightpath angle, the results between lateral left and right escape-maneuvers were similar. The graphs of speed vs. accuracy for Adams-Bashforth methods are shown in Figures 31 - 33 with a more refined grid of time steps than in the previous steady-level flight comparison. Similar

to steady-level flight, the lateral maneuvers show the Adams-Bashforth method consisting of the same clock speed as Euler, but with higher accuracy and the ability to have a larger time step before divergence. For the forward climb, the Euler method was more accurate than the Adams-Bashforth (but within 30 ft) and diverged at a larger time step than the Adams-Bashforth. Adams-Bashforth exceeded the 100 ft RSS error at a time step of 0.016 seconds.

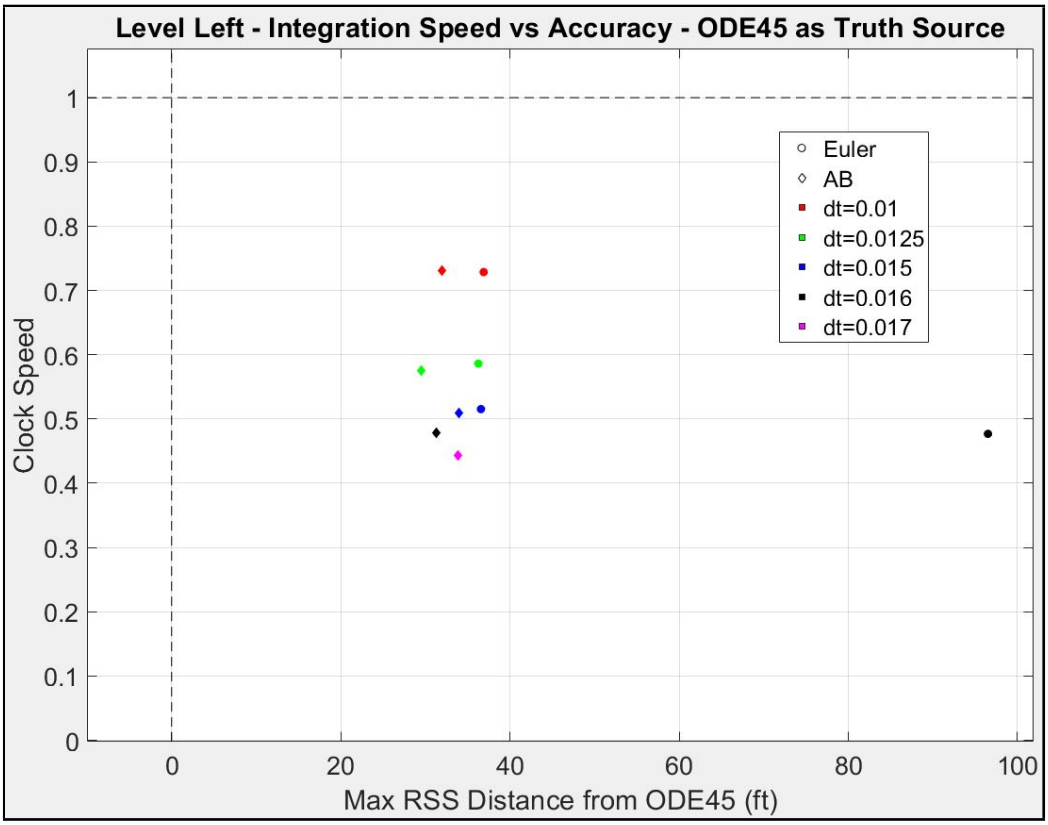

Figure 31. Level Left Accuracy vs. Speed Comparison for Trim Condition 1

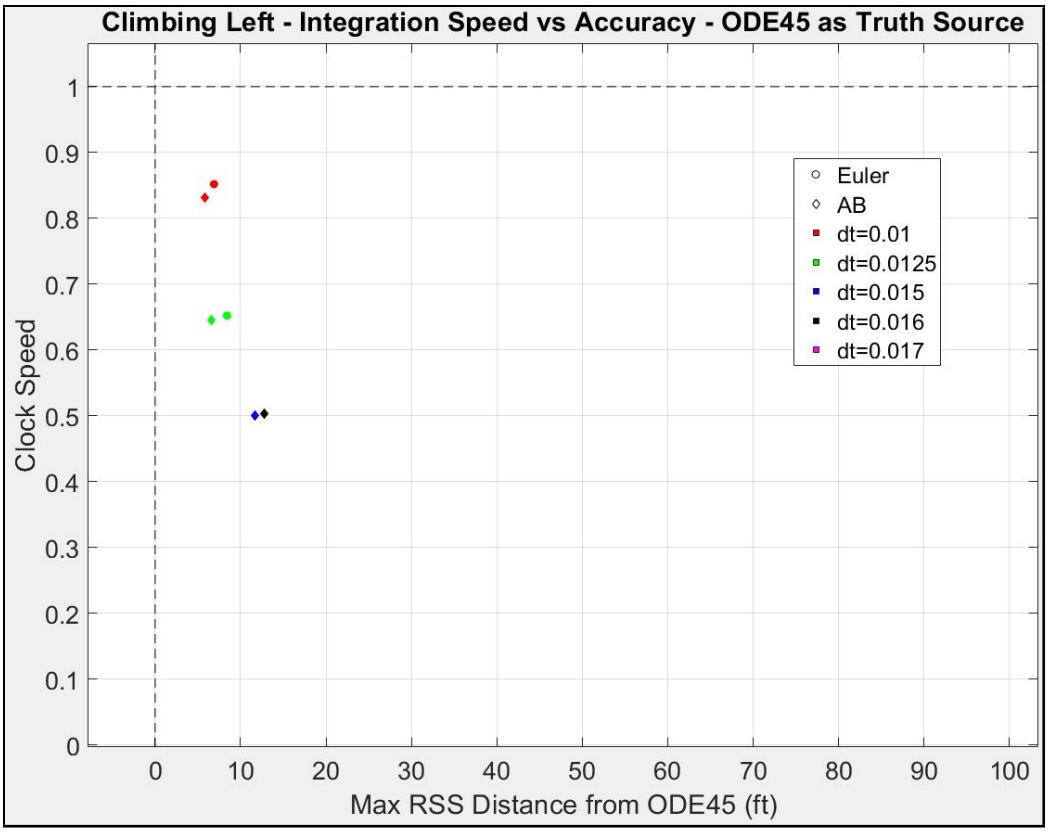

Figure 32. Climbing Left Accuracy vs. Speed Comparison for Trim Condition 1

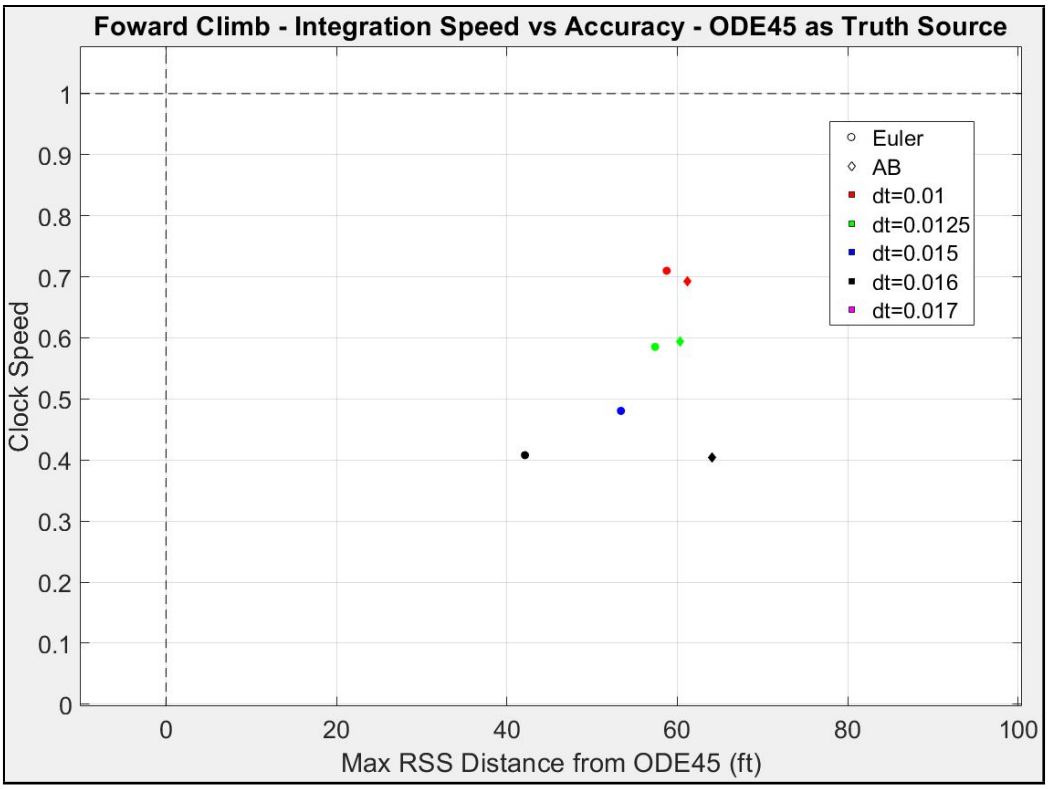

Figure 33. Forward Climb Accuracy vs. Speed Comparison for Trim Condition 1

4.2.2 Trim Condition 2.

Since this initial condition included a 45° right bank, the escape-maneuvers were not perfectly symmetrical because of the rolling motion to become straight and level required before initiating the left lateral escape-maneuvers. However, this means the left lateral maneuvers were tested more than the right, and therefore showed slightly worse maximum RSS errors (within 5 ft). The graphs of speed vs. accuracy for Adams-Bashforth methods are shown in Figures (34 - 36) for the lateral left and forward climb escape-maneuvers.

The trends in the results are similar to Trim Condition 1, where the Adams-Bashforth has less maximum RSS error in the lateral maneuvers compared to Euler and can be extended to a larger time step before error divergence. In the forward climb escape-maneuver, the Euler integration is more accurate and diverges after the

Adams-Bashforth, which diverges from the 100 ft maximum RSS error range at a time step of 0.016 s.

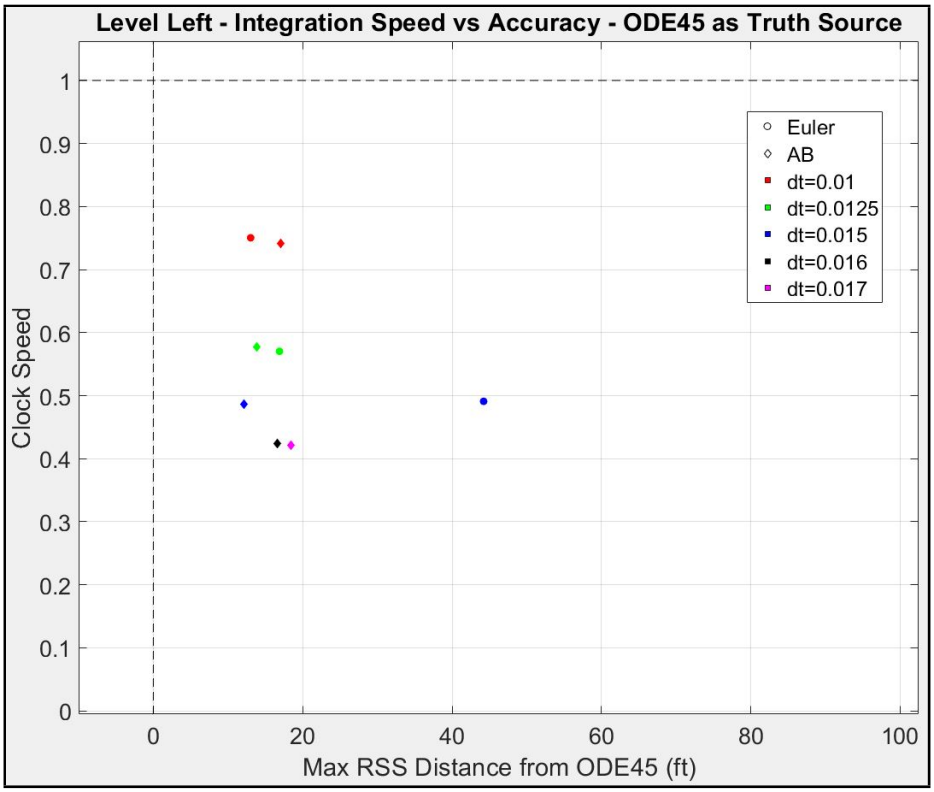

Figure 34. Level Left Accuracy vs. Speed Comparison for Trim Condition 2

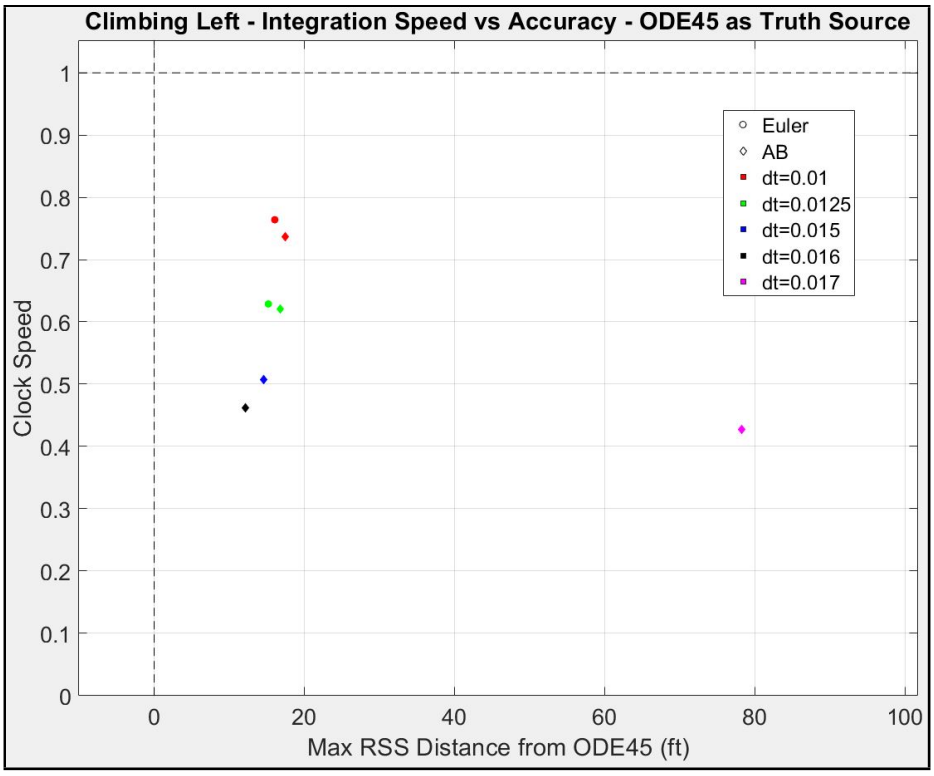

Figure 35. Climbing Left Accuracy vs. Speed Comparison for Trim Condition 2

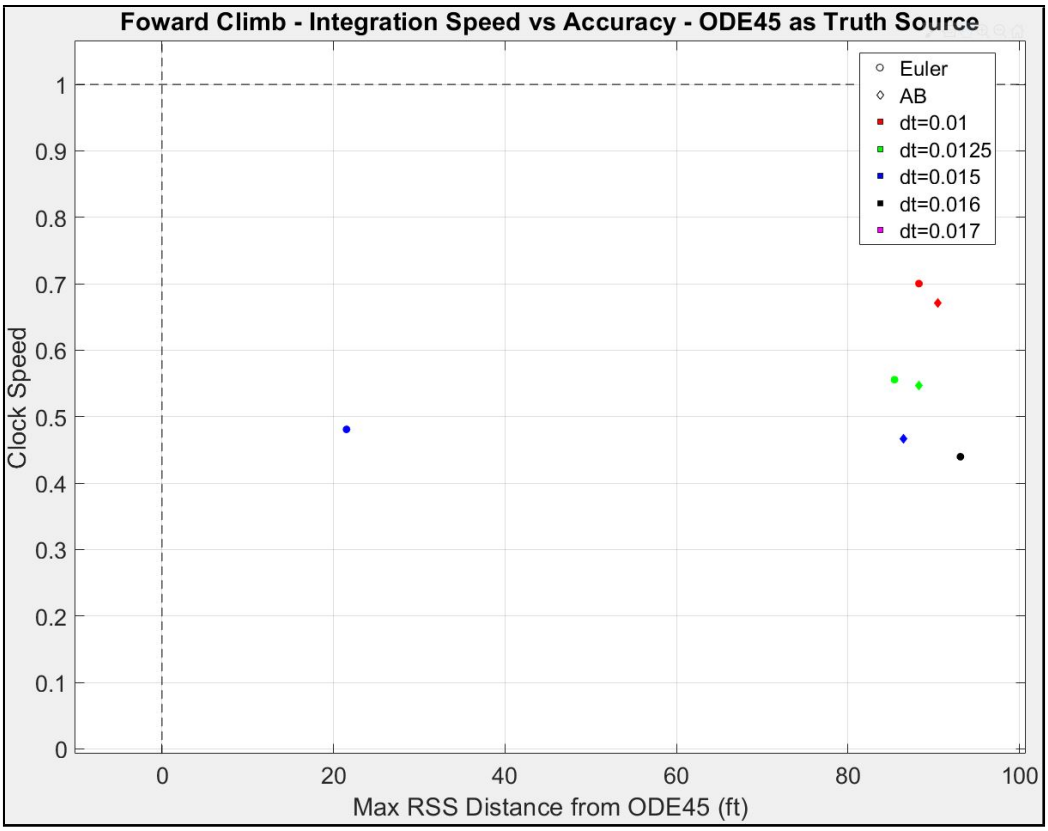

Figure 36. Forward Climb Accuracy vs. Speed Comparison for Trim Condition 2

4.2.3 Trim Condition 3.

Since this initial condition included a combination of 10° climbing angle, 10° left sideslip, and a 45° left bank, the escape-maneuvers differed from the previous symmetrical pattern of left and right maneuvers. All five escape-maneuvers varied in accuracy with the time step and also with different left vs. right lateral maneuvers. The Euler method overall performed better than the Adams-Bashforth in Trim Condition 3, but there was no consistent trend in time step value or path that clearly labeled Euler the preferred method. Nor were there consistent trends in the time step increasing accuracy with smaller time steps. The lowest RSS error regardless of clock speed is in Table 11 for both Euler and Adams-Bashforth methods.

One interesting part of the data showed that for certain maneuvers, larger time

Table 11. Trim Condition 3: Best Approximations for Trajectory Prediction

Maneuver Term	Method	Time Step (s)	Maximum RSSerror (ft)
Level Left (LL)	Euler	0.016	242.17
	Adams-Bashforth	0.015	1229.44
Climbing Left (CL)	Euler	0.01	23.99
	Adams-Bashforth	0.01	6.75
Forward Climb (FC)	Euler	0.016	140.61
	Adams-Bashforth	0.015	833.31
Climbing Right (CR)	Euler	0.015	117.13
	Adams-Bashforth	0.01	1024.33
Level Right (LR)	Euler	0.0125	33.62
	Adams-Bashforth	0.0125	41.80

steps had more accurate results than smaller time steps. For example, the RSS error has turbulent growth in the beginning of the forward look-ahead time path (reference Figure 37), which indicates the integration is receiving conflicting slope values at the fixed time step points. The local truncation error is not being monitored so the global truncation error in the integration continues to grow.

As a result from the Euler vs. Adams-Bashforth comparison at three different trim objects, the Adams-Bashforth time step of 0.015 s was the fastest integration method able to maintain a 100 ft buffer for Trim Conditions 1 and 2. Neither fixed time-step method was able to maintain accurate RSS values for all escape-maneuvers for the "extreme" Trim Condition 3 and therefore indicates the need for an adaptive time-step method to monitor local truncation error.

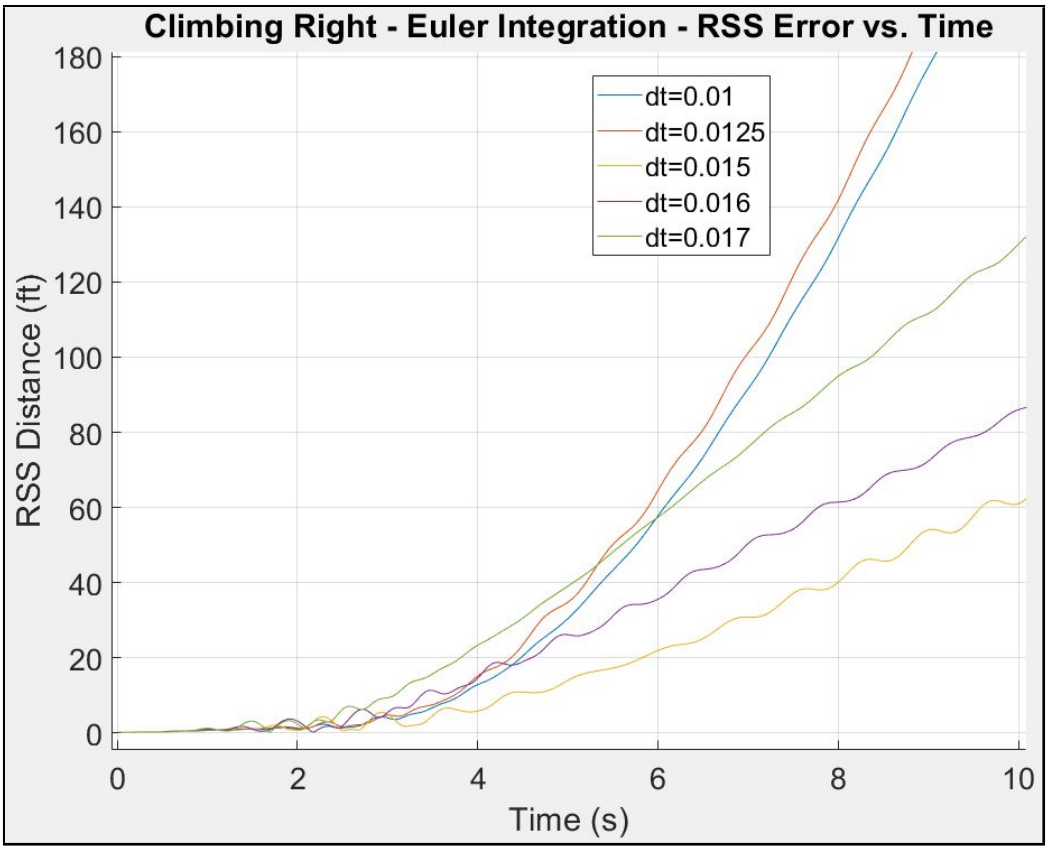

Figure 37. Climbing Right Euler Integration at Trim Condition 3 - Maximum RSS Error vs. Time

4.3 Comparison of Extending Forward Look-Ahead Time

The amount of forward look-ahead time was compared between methods in order to determine the advantage to extended the collision prediction range. Full tabulated data is listed in Appendix C. The results of a 200 s long simulation in the test box terrain described in section 3.4.3 for different methods are listed in Table 12. The test box represented extreme terrain with vertical cliff walls, so collision with terrain was expected. The algorithm refresh rate was set at 7.15 Hz (time step of 0.14 s) and the state parameters were calculated every 0.005 s. In addition to the overall comparison, a breakdown of the effect different airspeed and terrain safety buffer had on the height above ground and over-g is included. A collision means the height above

terrain went below zero at any point during the simulation.

Table 12. Overall LJ-25D Auto-GCAS Extending Forward Look-Ahead Time

Algorithm Name	**Comp Rate (HZ)**	**Number of Collisions (% total runs)†**	**Number of Over-G (% total runs)†**
Euler30*	10.49	60%	10%
Euler45	7.045	55%	0%
Euler90	3.682	55%	15%
AB30	10.42	60%	7.5%
AB45	7.039	55%	0%
AB30 45FC	6.24	37.5%	7.5%

* Baseline LJ-25D Auto-GCAS algorithm from Gahan [10]

† Percentages based on 40 total runs for each algorithm

The number of collisions decreased from 60% to 55% when extending the forward look-ahead time from 30 s to a higher value greater than 45 s. However, over 45 s did not improve the number of terrain features avoided. The results between the Euler and Adams-Bashforth methods were similar, indicating no noticeable difference between the integration paths. However, with the different trigger activation in the *AB30 45FC* algorithm, the number of collisions decreased 17.5% for a small computational cost in *Comp HZ*.

Results varying the terrain safety buffer are presented in Table 13. As expected, the number of collisions decreased with increasing terrain safety buffer. Additionally, the *AB30 45FC* algorithm showed improved collision prevention for each safety buffer

height.

Table 13. Varying Safety Buffer: LJ-25D Auto-GCAS Extending Forward Look-Ahead Time

Buffer Height (ft)	Algorithm Name	Number of Collisions (% total runs)	Number of Over-G (% total runs)
50†	Euler30*	87%	6.7%
	Euler45	87%	0%
	Euler90	87%	20%
	AB30	87%	0%
	AB45	87%	0%
	AB30 45FC	73%	6.7%
250†	Euler30*	40%	13%
	Euler45	40%	0%
	Euler90	40%	13%
	AB30	40%	13%
	AB45	40%	0%
	AB30 45FC	30%	0%
500‡	Euler30*	55%	11%
	Euler45	33%	0%
	Euler90	33%	11%
	AB30	55%	11%
	AB45	33%	0%
	AB30 45FC	22%	22%

* Baseline LJ-25D Auto-GCAS algorithm from Gahan [10]
† Percentages based on 15 total runs for each algorithm
‡ Percentages based on 9 total runs for each algorithm

Results varying the aircraft initial airspeed are presented in Table 14. This small sample size showed that the lower the airspeed, the longer the required look-ahead time is to prevent collisions.

Table 14. Varying Initial Airspeed: LJ-25D Auto-GCAS Extending Forward Look-Ahead Time

Initial Airspeed (KTAS)	Buffer Height (ft)	Number of Collisions (% total runs)†	Number of Over-G (% total runs)†
200	Euler30*	100%	25%
	Euler45	75%	0%
	Euler90	62.5%	75%
	AB30	100%	0%
	AB45	75%	0%
	AB30 45FC	37.5%	25%
250	Euler30*	75%	0%
	Euler45	50%	0%
	Euler90	62.5%	0%
	AB30	62.5%	0%
	AB45	50%	0%
	AB30 45FC	62.5%	0%
300	Euler30*	25%	25%
	Euler45	62.5%	0%
	Euler90	62.5%	0%
	AB30	25%	0%
	AB45	62.5%	0%
	AB30 45FC	12.5%	0%
350	Euler30*	50%	0%
	Euler45	37.5%	0%
	Euler90	37.5%	0%
	AB30	50%	0%
	AB45	37.5%	0%
	AB30 45FC	37.5%	0%
400	Euler30*	50%	0%
	Euler45	50%	0%
	Euler90	50%	37.5%
	AB30	50%	0%
	AB45	50%	0%
	AB30 45FC	37.5%	12.5%

* Baseline LJ-25D Auto-GCAS algorithm from Gahan [10]
† Percentages based on 8 total runs for each algorithm

Although, when looking at overall reduced collision numbers, the different trigger

criteria (forward path open) used in the *AB30 45FC* algorithm had a larger impact than purely extending the look-ahead time to 45 s or greater. One explanation can be found when examining the control exchanges between the pilot and Auto-GCAS when the algorithm is engaged and disengaged (i.e. Auto-GCAS activation and handback). Control chattering was observed between pilot control and Auto-GCAS control in the first-open trigger activation code. Therefore the *AB30 45FC* algorithm was compared between the two different trigger activation designs. The first-open trigger activation shown in Figure 38 hands back control to the pilot for 2.8 s between the forward climb and level left activations. The result is a collision into the terrain if the pilot did not react within that time window.

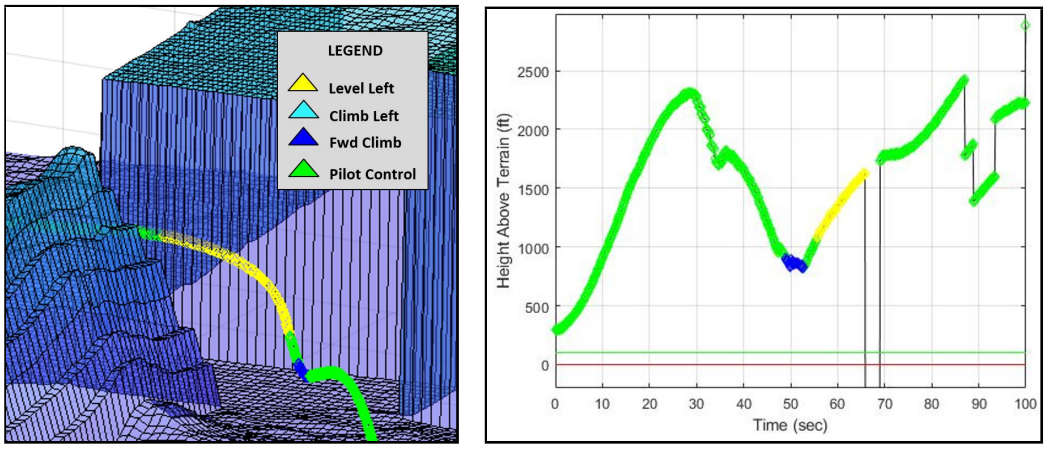

(a) (b)

Figure 38. Simulation of First-Open Trigger Activation showing (a) Flightpath and (b) Height Above Terrain profiles

However, for the forward-open trigger activation shown in Figure 39, the control is seamlessly transferred between the forward climb and level left autopilot to avoid collision with the terrain.

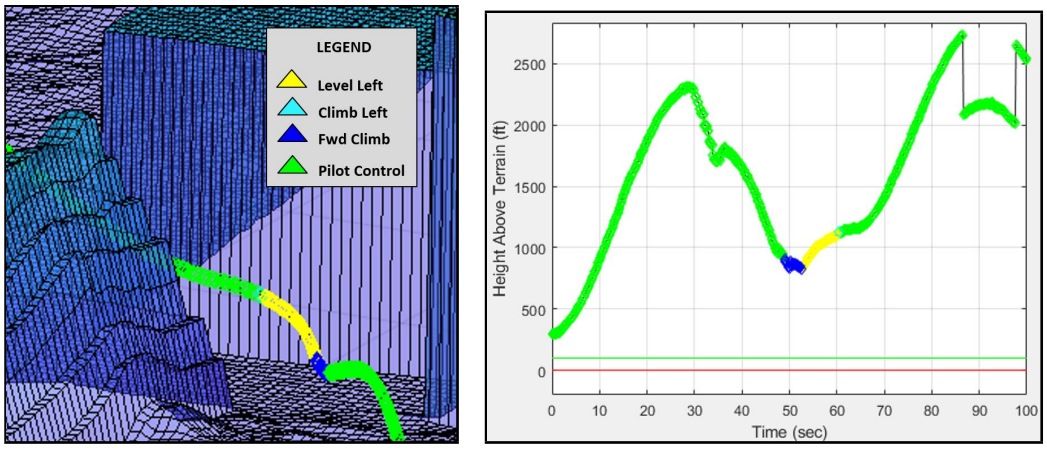

(a) (b)

Figure 39. Simulation of Forward-Open Trigger Activation showing (a) Flightpath and (b) Height Above Terrain profiles

4.4 Time Varying Paths

From the simulations in section 4.3 comparing extended forward look-ahead time, the observation of wasted computation time was discovered for lateral escape-maneuvers. The forward climb escape-maneuver did not enter a stall and therefore only needed to be defined by a maximum desired forward look-ahead time. Figure 40 shows the wasted trajectory prediction during simulated flight where the lateral escape-maneuvers stall.

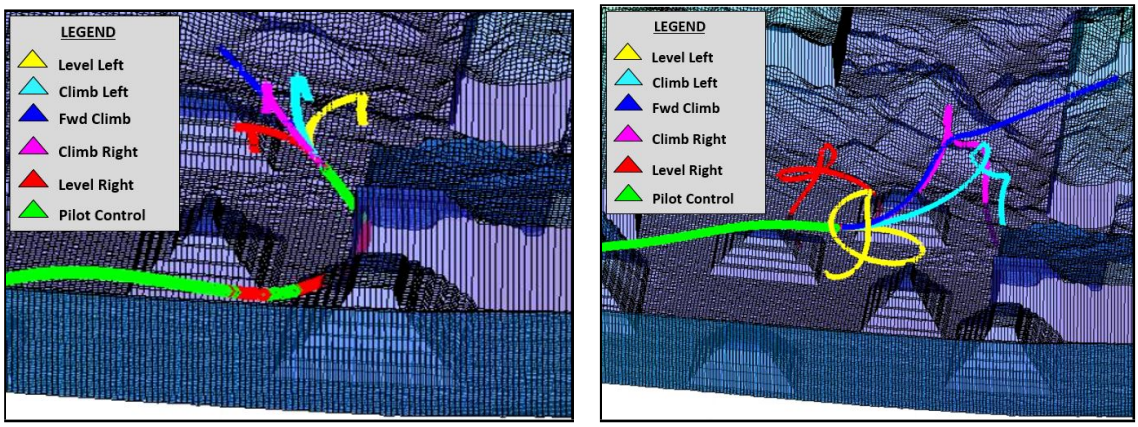

(a) *Euler30* Trajectory Lengths (b) *Euler90* Trajectory Lengths

Figure 40. Wasted Computation Time for Trajectory Prediction - Stalled Flight Conditions

Since computation effort was being expended on projected stalled aircraft states, a performance based Auto-GCAS algorithm with time varying lateral escape-maneuver was designed per section 3.4.1, Figure 25. To test the computational speed and observe any differences in terrain avoidance, a scenario where the aircraft was flying into a box canyon was recreated with a vertical cliff wall in front of the aircraft that was impossible to climb away from (9,000 ft). For the boxed canyon comparison, the terrain safety buffer was set at 200 ft and the aircraft initial conditions were 250 KTAS, 500 ft AGL, Heading: 0, $\gamma = 0°$, $= 0°$, $\phi = 0°$.

Table 15. Boxed Canyon Simulation Comparison

Algorithm Name (ft)	**Comp HZ**	**Time to Collision Activation Path(s)**	**Collision (Y/N)**
Euler 30*	8.6245	15.76	Y
AB30 45FC †	8.5431	11.49	Y
AB Varying †	8.4643	29.985	N

* Baseline LJ-25D Auto-GCAS algorithm from Gahan [10]

† Time step is 0.015 s instead of 0.01 s as described in Table 7

The *Comp HZ* values in Table 15 between all three methods are very similar, yet the Adams-Bashforth with varying length escape-maneuvers activated at a farther look-ahead time than the other algorithms. This was due to a combination of the forward-open trigger activation and the longer look-ahead time provided by the varying length escape-maneuvers. The combination resulted in the Auto-GCAS algorithm to take a different path and climb out of the canyon, shown in Figure 41.

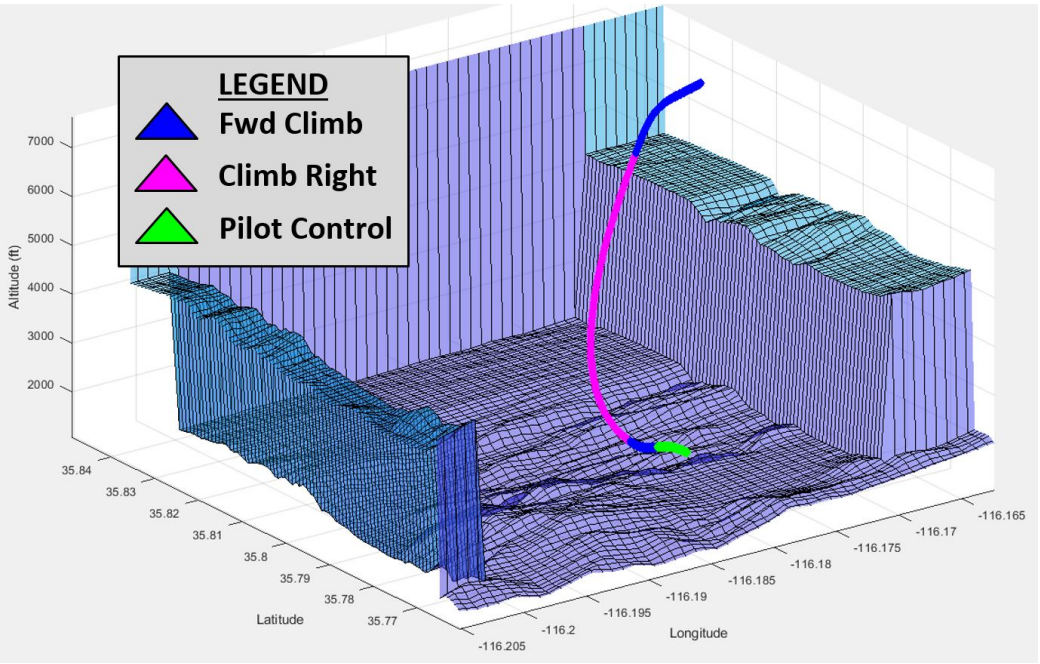

Figure 41. ***AB Varying*** **Auto-GCAS Algorithm Flying Towards Boxed Canyon**

One caveat to this scenario is the terrain safety buffer. Since we are dealing with vertical terrain in a boxed canyon, the terrain safety buffer does not factor into the collision prediction with the side of the wall because it is only added to the vertical height. This is why the *Euler 30* and *Euler30 45FC* collided with the terrain during the simulation shown in Figure 42.

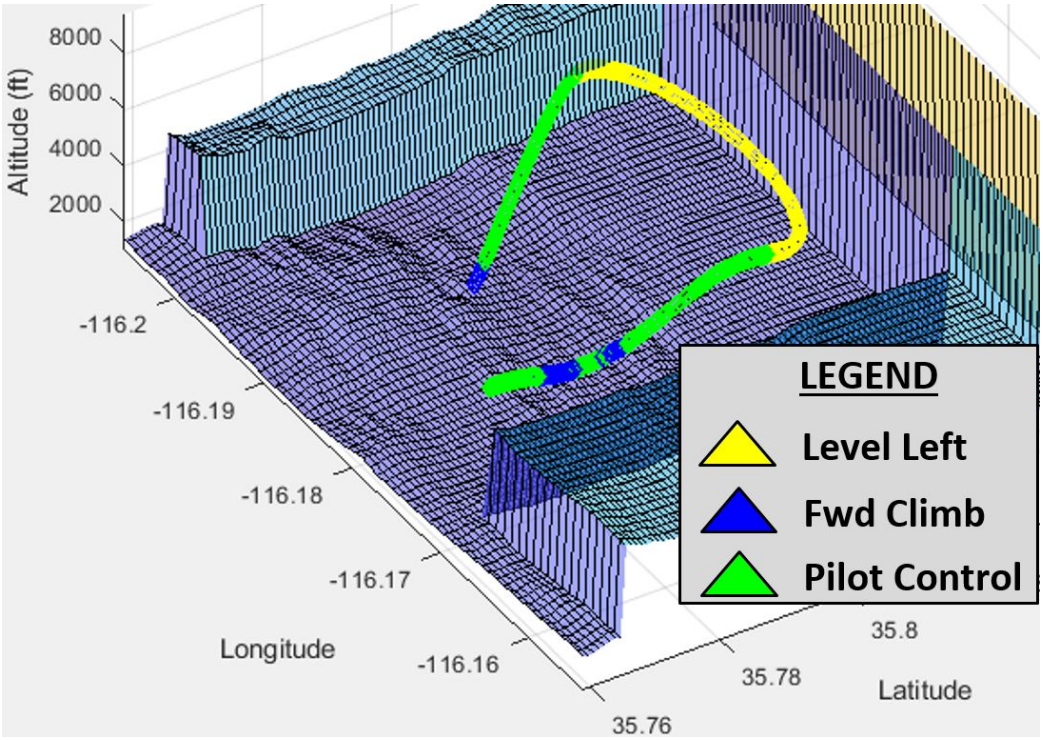

Figure 42. ***AB30 45FC*** **Auto-GCAS Algorithm Flying Towards Boxed Canyon**

Although the vertical walls are an extreme terrain case, Figure 42 demonstrated a different terrain safety buffer mapping to the DTED terrain was required for high sloping terrain. The boxed canyon comparison also showed that for lower flight velocity, an increased forward look-ahead time can achieve the same computation cost if trimming the lateral escape maneuvers. Additionally it showed how combining different trigger algorithms and forward look-ahead lengths can change the outcome from the same initial condition.

4.5 Chapter IV Summary

This chapter analyzed the results of trajectory predication integration methods, simulations for the Euler and Adams-Bashforth LJ-25D Auto-GCAS algorithms at 30 s, 45 s, and 90 s. Highlighted was the difference in trigger activation and the ability for time varying escape-maneuvers to allocate time to the forward climb at

low speeds. The following chapter will detail the piloted simulator study using the LJ-25D Auto-GCAS algorithm and summarize the study results.

V. Piloted Simulator Study Methodology and Results

Chapter Overview

This chapter outlines the piloted simulator study. The specific test methodology and set-up are discussed. Time to collision results from the study are presented and pilot feedback on display concepts are consolidated.

5.1 Piloted Simulator Study - MCCS

The Multi-Crew Cockpit Simulator (MCCS) at AFRL/RQQ was used to host a piloted simulator study on the LJ-25D Auto-GCAS algorithm between 3-10 December, 2018. Figure 43 shows the MCCS representation of a heavy aircraft flight deck with an out-the-window visual scene spanning 200° horizontal, and 40° vertical field of view. A configurable HUD, joystick, and PFD allowed for integration of display concepts.

Figure 43. View of the Multi-Crew Cockpit Simulator (MCCS) [44]

The test plan used for the piloted simulator study is listed in Appendix D, and was approved through the AFRL Institutional Review Board under document number FWR20190014N. The *Euler30 45FC* Auto-GCAS algorithm described in Table 7 was

used in the simulator. The aircraft calculated state properties every 0.005 seconds. The refresh rate was set at 7.15 Hz (every 0.14 seconds).

There were two objectives of the simulator study: (1) develop a nuisance boundary for the LJ-25D aircraft that would be representative of a performance limited aircraft, and (2) preliminary pilot feedback on Auto-GCAS display designs and warnings. The nuisance boundary was based on similar testing done with the F-16 PARS system discussed in section 2.6.1.

5.1.1 Nuisance Boundary.

The data collected to determine the nuisance boundary derived from the following steps. Note the Auto-GCAS algorithm was turned off during this part of the test, so the pilots could have flown into the simulated terrain at any point.

1. Pilots were tasked to fly straight and level towards a preset terrain feature. Initial conditions of heading, airspeed, latitude and longitude location, altitude, and each of the five individual escape-maneuvers (LL, CL, FC, CR, LR).

2. For each escape-maneuver, the pilot would hold the initial condition course until they were uncomfortable with not clearing the terrain performing that specific escape-maneuver. This point is referred to as the anxiety point and was marked by the pilot by holding down the red recording button on the joystick (reference Figure 45). From this location, the data point of *Time Available* can be calculated by projecting the aircraft velocity forward in time along the heading angle until collision with terrain.

3. The pilot would then fly the specific escape-maneuver until they felt clear of the terrain feature. The pilot would then release the red recording button indicating termination of the escape-maneuver. Along the marked flight path, the data point of *Time Available Min Distance* can be calculated. This time value was calculated by

scanning the flight path along the initial anxiety point heading towards the terrain feature, as shown in Figure 44.

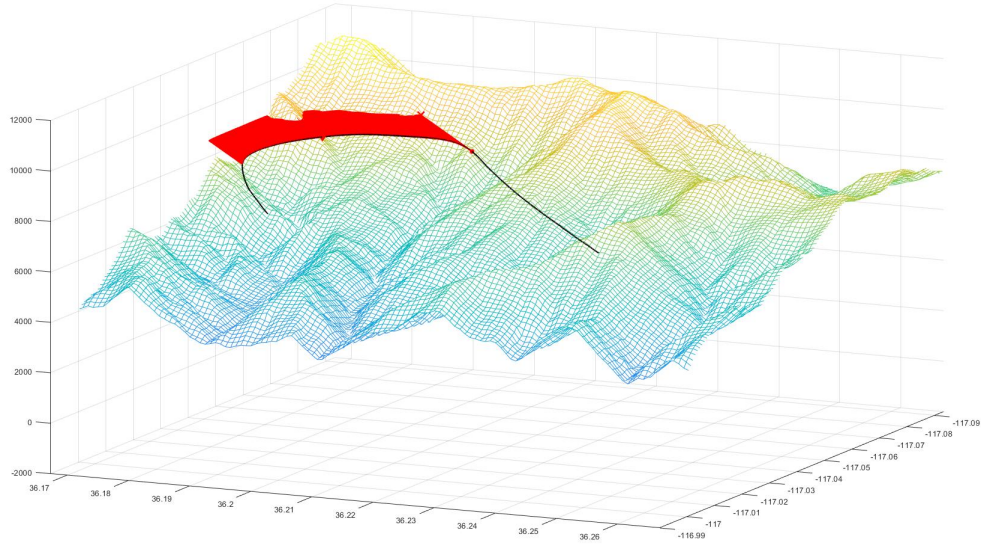

Figure 44. Collision Point Scan Area

The location of minimum distance to the terrain is used to calculate *Time Available Min Distance* by projecting the aircraft velocity at the anxiety point forward in time along the anxiety point's heading angle until collision with the terrain.

4. The pilot would than be asked the anxiety rating of collision with terrain as they flew the specific escape-maneuver. The rating scale is listed in Table 16, which is the same used in the F-16 PARS study [26].

5. Each specific escape-maneuver was flown three times by each pilot with the same initial conditions.

The following graph shows an example of one level left turn flown by a test subject. The anxiety point displays a longer line of time available than at the minimum distance point. Since the pilot's calculating terrain clearance along the entire escape-maneuver, the better indication of the *Time Available* until collision is the point at minimum distance flown by the pilot during the executed escape-maneuver.

Table 16. Anxiety Rating For Time Available Determination [26]

Value	Anxiety Rating
1	Was never more than casually aware of the ground
2	Would have felt comfortable with a recovery at a lower altitude
3	Recovery went as anticipated
4	Recovery went lower than personal comfort levels allow
5	Sensations of life threatening conditions

The pilot flown escape-maneuvers are then able to validate the design of the LJ-25D Auto-GCAS by the following logic: if the autopilot activates after the mean pilot response time, then it successfully mitigates a potential nuisance [26]. The only caveat is that the autopilot can not react too far beyond the nuisance boundary that it collides with the terrain, thus providing a design window for autopilot maneuvers. An additional benefit of the simulator data is that the predetermined escape-maneuvers can be fine tuned to lie just within the anxiety point for the pilots. This allows for less aggressive maneuvers that would more closely resemble pilot reaction to a terrain situation.

5.1.2 Pilot Displays and Warnings.

An automatic system on board an aircraft must communicate with the human operator. The F-16 Auto-GCAS displays referenced in section 2.8 were used as the basis for the display design study. Since the LJ-25D Auto-GCAS has more escape-maneuvers than F-16 Auto-GCAS and an underlying difference in escape-maneuver activation, the same HUD display system was not directly transferable. A combination of HUD and PFD images were created to communicate what the automatic system was calculating, and ultimately when it was in control of the aircraft. Some basic design principles were taken from standardized HUD symbology described by

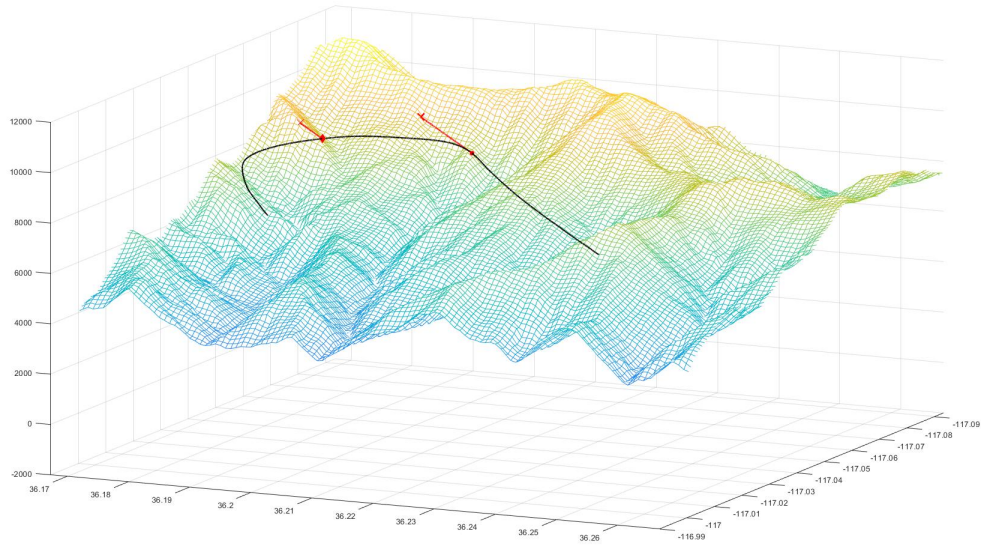

Figure 45. Level Left Turn: Time Available at Anxiety Point vs. Time Available at Min Distance Point

Bitton [31]. The information displayed between the HUD and the PFD should be consistent or completely separate to reduce cross-check between two displays [31]. Additionally, critical information needs to be displayed on both PFD and HUD screens in the case of an individual screen failure [31]. Lastly, any Auto-GCAS displays should not hinder critical flight data already displayed on the HUD, to include climb/dive angle, bank, altitude, heading, AoA, and airspeed [31]. The primary information to be communicated from LJ-25D Auto-GCAS was how long into each path was available to fly before collision with terrain, when Auto-GCAS was activated, and what path did Auto-GCAS choose. This information advised the pilot on when they did or did not have control, and also what escape-maneuver was the known safe direction to fly to safety.

The displays were broken into four different categories: no initiation, partial initiation, pre-initiation, and initiation. No initiation means that all escape-maneuvers are open. There is no HUD symbology displayed. The PFD has a page that can be

selected to show the path values, but it is at the discretion of the operator to choose to view it. Partial initiation indicates that one or more paths are closed off due to projected terrain collision. The HUD and PFD symbology is the same as No Initation, except that the coloring will show which paths are closed off. Pre-initiation means that one escape-maneuver is open. The HUD symbology will show two stationary chevrons with the name of the last escape-maneuver. This is to communicate to the operator of an impending Auto-GCAS override and to be more cautious of terrain (reference Figure 46).

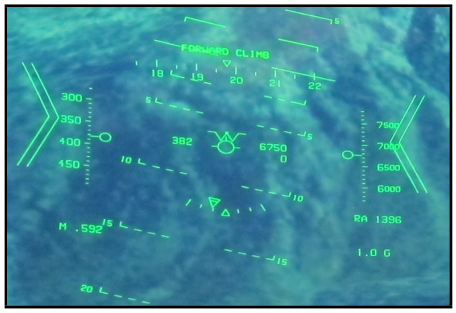

Figure 46. HUD Symbology for Pre-Initiation of Auto-GCAS Algorithm [44]

Figure 47. HUD Symbology for Initiation of Auto-GCAS Algorithm [44]

Initiation means that Auto-GCAS has activated and a green dot above the PFD turns on indicating Auto-GCAS is in control. If the operator disengages Auto-GCAS, the HUD and PFD symbology will still show up but this green dot will turn off, indicating the pilot has control. At initiation, the two chevrons on the HUD will move together to form a " X " in the center of the HUD (reference Figure 47). The escape-maneuver being executed by Auto-GCAS is repeated by an audio voice recording and is also displayed at the top of the screen. The PFD screen is automatically selected to the Auto-GCAS display to override any other PFD pages in use.

Four different display designs were selected for the PFD while the HUD symbology remained the same. Figure 48 depicts the four different displays, where the specific sequencing of the displays is shown in Appendix D.

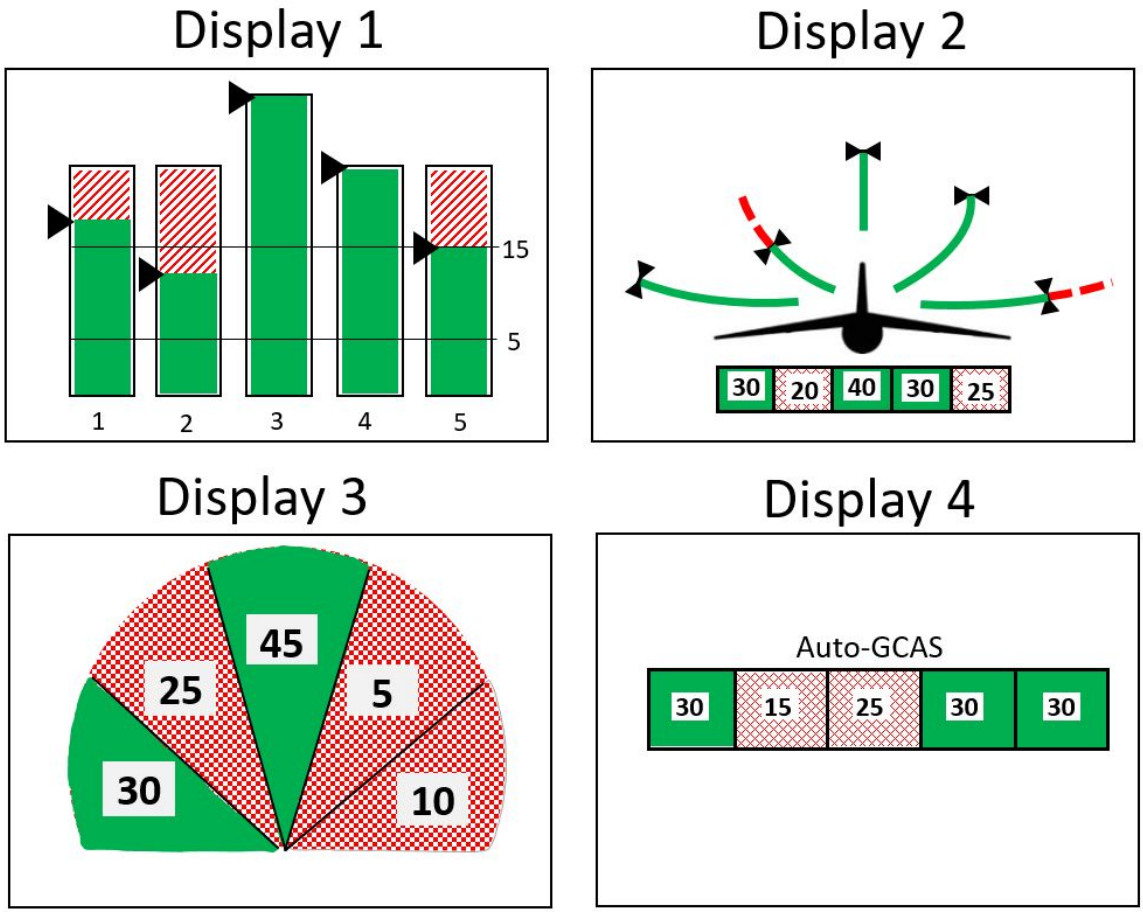

Figure 48. Four PFD Designs for Piloted Simulator Study

Display 1 is a time to collision based vertical bar, where the five escape-maneuvers are displayed left to right as Paths 1 to 5. This is similar to an engine-tape bar where a percentage of the escape-maneuver length can be quickly determined based on sliding bars and barber pole cross-hatching of closed off terrain. Display 2 provided a 3^{rd} person view of the aircraft cross-section with escape-maneuvers in the vertical and lateral plane. Bow tie icons helped delineate the closed and open portions of the escape-maneuver, while a bar reading underneath provided the time to collision for each path. Display 3 provided a birds eye sector view of the aircraft in the lateral and forward planes of motion, where each sector represented an escape-maneuver. Time to collision was overlaid on each sector. Display 4 was a pure time to collision

reading for each path displayed left to right as Paths 1 to 5. This design would easily be allowed to overlay on an existing PFD page and provide a time reading to the pilot. Although there are many other possible displays, the HUD symbology and PFD displays were selected as the most feasible starting point. Recommended changes to the Auto-GCAS displays are discussed in the pilot feedback comments at the end of the chapter.

5.2 Piloted Simulator Study Results

The study consisted of six test subjects, all previous or current C-130, C-21, C-160, or C-17 USAF pilots. The average number of cargo aircraft flight hours per test subject was 2,567 ± 542 hrs, with a maximum of 3000 and a min of 1800. The last time mountainous low-level flying was conducted by test subjects was an average of 6.9 ± 6 years, with a maximum of 16 years and a minimum of 3 months. One finding on integration of the Auto-GCAS algorithm into the MCCS was that the size of the DTED file directly affects the computational speed of the computer. This was because the interpolation function in the collision prediction had to search through the size of the inputted DTED file matrix size. Original MCCS integration with a 1°x1° DTED file (1201x1201) had no issues running the algorithm, however with a 3°x3° DTED file (3601x3601), the simulator lagged considerably in operation.

5.2.1 Time to Impact.

Time Available at the minimum distance to collision as described in section 5.1.1 is plotted against the pilot anxiety rating. Standard deviation error bands are plotted about the averages. An example of the data used to calculate the Anxiety vs. Time Available graphs are shown as graphical representations in Appendix D. Plots for each of the five escape-maneuvers was generated similar to the F-16 PARS study

completed, where expectations would see a decrease in time to collision with an increase in anxiety rating. Figures 49 - 53 show no definite nuisance boundary between all maneuvers because the anxiety ratings do not increase with a decreasing Time to Collision. The only maneuver that showed a similar trend to the F-16 PARS study was for the level left escape-maneuver, which had a 1.5 s time to collision between anxiety ratings of 4 and 5. A trend between methods was that lateral maneuvers had a larger time to collision than the forward climb, indicating that pilots were more cautious on turning maneuvers than on a straight ahead climb. Since the approach heading was changed between the lateral left, forward climb, and lateral right escape-maneuvers,

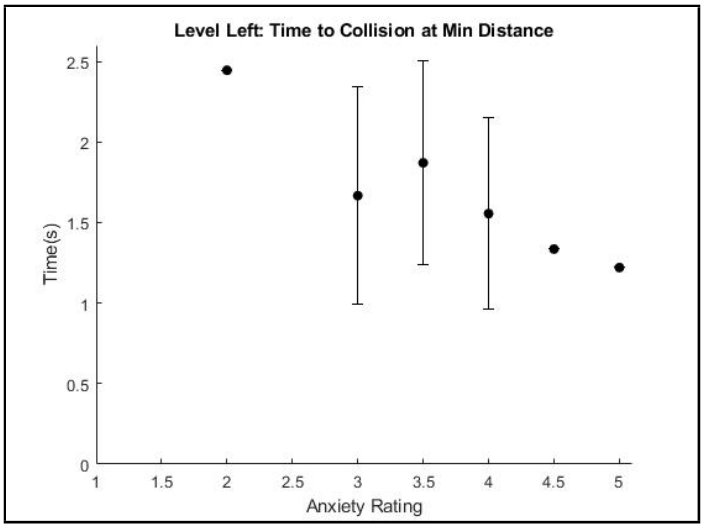

Figure 49. Level Left Minimum Distance Time to Collision at Anxiety Point

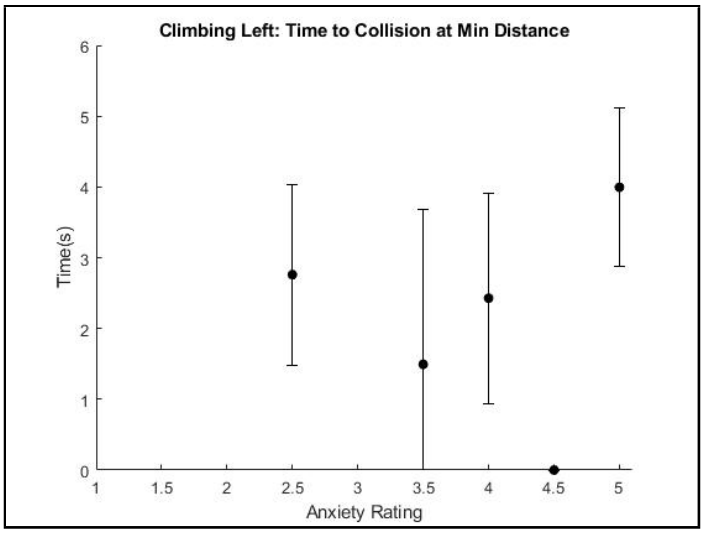

Figure 50. Climbing Left Minimum Distance Time to Collision at Anxiety Point

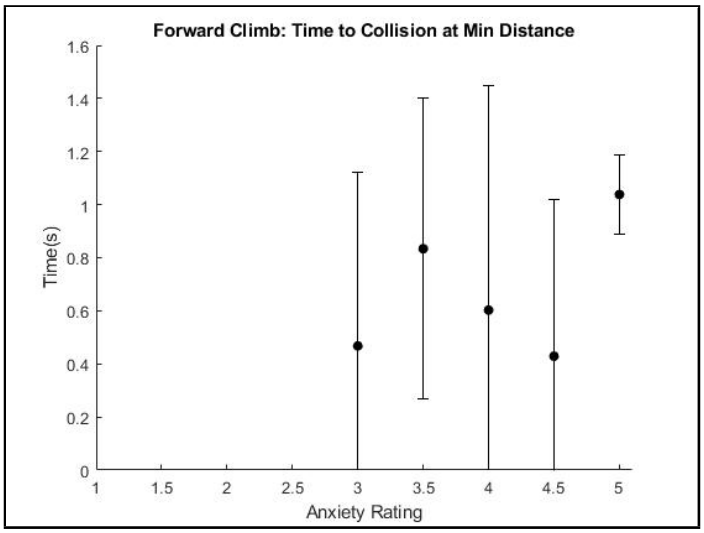

Figure 51. Forward Climb Minimum Distance Time to Collision at Anxiety Point

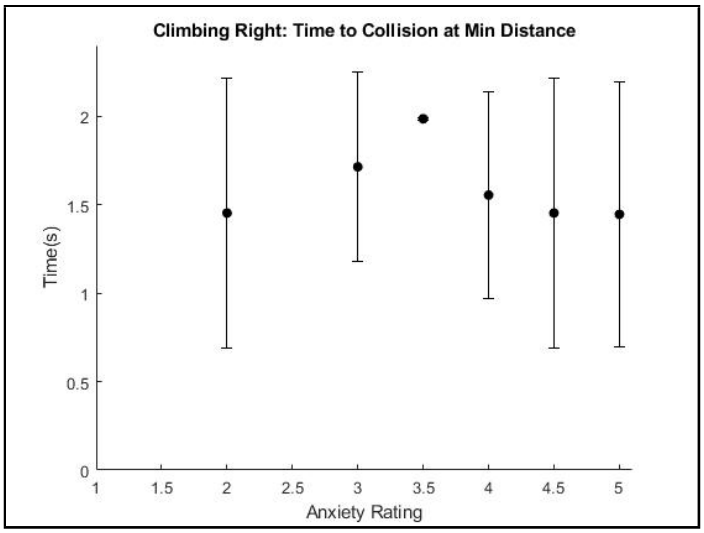

Figure 52. Climbing Right Minimum Distance Time to Collision at Anxiety Point

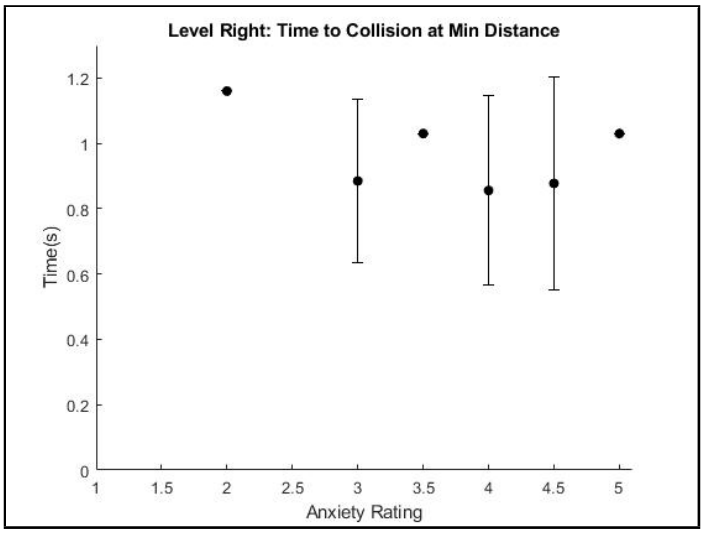

Figure 53. Level Right Minimum Distance Time to Collision at Anxiety Point

There were possible sources of error for the variation in Time to Collision results between escape-maneuvers. One finding during the data collection was that the DTED map used by the LJ-25D Auto-GCAS algorithm did not have the same terrain profile as the MCCS simulator DEM. The calculations for Time to Collision were based on DTED, whereas the test subject responded to an anxiety point based on the simulator visuals. Recommendations for future piloted simulator studies would be to

have consistent DTED terrain between the Auto-GCAS algorithm and the simulator visuals. Additionally, the choice of terrain severity and angle affects the different escape-maneuvers. Even though the terrain feature did not change, changing the approach heading altered the severity of escape area. Further research could determine the impact different initial flight angles have on the Time to Collision in order to establish a time range similar to the F-16 PARS study.

5.2.2 Feedback on System Operation.

The second part of the piloted simulator study was to get feedback on LJ-25D Auto-GCAS system operation and displays. Test subjects provided feedback on the Auto-GCAS prediction, activation, and handback phases of operation. Results were divided into three categories: (1) HUD display feedback, (2) PFD display feedback, and (3) overall system operation.

5.2.2.1 Piloted Simulator Study Feedback - HUD Display.

The following pilot comments about the HUD display were collected:

(1) Good information displayed through HUD, not going to confuse it with any other warnings provided by other systems.

(2) Warning location could mimic the "Wind Shear" advisory in EGPWS for C-17 HUD (one path remaining warning at bottom of HUD, and flash warning at center of HUD when activated).

(3) Did not like the 2 chevrons in break " X " as warning when Auto-GCAS activated. Instead do a chevron that tells the pilot where to go similar to a flight tracker, although, the chevrons are OK as a warning on pre-initiation when one path is remaining.

(4) Tie HUD symbology to TACTICAL Mode so it is not always displayed.

(5) Would prefer a target to fly the flightpath marker to on the HUD instead of telling the maneuver to fly, as it points the pilot in the direction quicker if they take over control.

(6) Missing flight director guidance on the HUD. Still like to have the words of the escape-maneuver to fly but prefer to have a target to put the flightpath marker on. Recommend double flight director size instead of single chevron size.

(7) Tie into alpha mode on C-17 (stick shaker limiting).

(8) Prefer arrows point in the direction rather than words.

5.2.2.2 Piloted Simulator Study Feedback - PFD Display.

Subject pilots rated each PFD display on a best to worst scale of 1 to 4. The rating was based on preference of situational awareness and clarity of information. The overall rating for each PFD display is listed in Table 17:

Table 17. Piloted Simulator Study - Overall Rating for PFD Displays

SubjectNumber	**Display 1 Ranking**	**Display 2 Ranking**	**Display 3 Ranking**	**Display 4 Ranking**
1	1	3	2	4
2	4	1	3	2
3	3	4	1	2
4	3	1	2	4
5	2	1	4	3
6	2	4	1	3
Average	2.5	2.3	2.2	3

The overall favorite displays were Display 2 and 3, which both feature a sectional plane view of the aircraft, 3^{rd} person tail-view, and birds-eye view respectively. Collected pilot comments about the PFD displays are the following:

(1) During simulator flying with Auto-GCAS on, the pilot could get away with just HUD initiation warnings and information, did not use the PFD display for primary information.

(2) PFD displays would have to fit into TAWS database, as that is the primary page on PFD during low-level flights.

(3) Do not like the time to collision numbers moving suddenly (ex: 45 s down to 10 s) as that does not help with situational awareness.

(4) Integrate Auto-GCAS information into path prediction (noodle) and TAWS display.

(5) Display 3 is the best representational view of aircraft escape-maneuvers, would

like it to have a scale though instead of just numbers.

(6) Did not like the box with numbers indicating time to collision for each path, too much information to interpret.

(7) Liked the sector map in Display 3, prefer it to have time length built into the size of the sector instead of just open / closed paths being different colors. This would mean that each of the five sectors can have multiple colors indicating open / closed corresponding to the forward look-ahead time. More representative of the TAWS displays.

5.2.2.3 Piloted Simulator Study Feedback - Overall System Operation.

Collected pilot comments about the overall Auto-GCAS algorithm are the following:

(1) Modified contour flying would require varying safety terrain buffer heights to be inputted by pilot (similar to F-16 with a low-level mode and a normal operation mode).

(2) OK with a paddle on / off switch on the joystick for pilot to disengage Auto-GCAS.

(3) Typically agree with a forward climb as better option than a lateral maneuver, although algorithm did climb in instances where a lateral maneuver was more practical.

(4) Have capability to predict path trajectory based on limited engine / limited aircraft performance capabilities.

(5) Do not recommend using a flight director as pilot notification of engaged escape-maneuver during a tactical environment.

(6) The level turn autopilot dropped the nose during Auto-GCAS activation, this should not happen.
(7) Preferred an understanding of altitude as the escape-maneuver, trading altitude and airspeed is the concerning factor for low-level flying. Therefore a flight director or tracker is preferred for HUD symbology as well.
(8) Display only available paths, do not indicate that a path is closed off. This keeps the information relevant and what is important to the pilot.
(9) Auto-GCAS handback to pilot feels sudden, and does not handback control when in a better spot to take over.
(10) Auto-GCAS paths are more conservative on ridge lines and makes more aggressive turns.

5.3 Chapter V Summary

A summary of the MCCS piloted study was conducted on the nuisance boundary determination and also feedback on initial displays. A nuisance boundary between maneuvers was inconclusive but implementable design feedback was collected on displays. The following chapter will synthesize the major results of both Chapters IV and V and provide recommendations for future Auto-GCAS designs.

VI. Conclusions and Recommendations

Controlled flight into terrain remains a significant contributor to aviation accidents among the DoD, commercial, and general aviation communities. The success of F-16 Auto-GCAS illustrates a viable solution to reducing terrain collision fatalities and emphasizes the need for a similar solution in performance limited aircraft. A literature review was conducted to review the design framework of an Auto-GCAS algorithm, the previous research conducted on Auto-GCAS, numerical integration methods, and pilot display designs. The methodology was discussed to answer the research goals outlined in Chapter I. The results presented in Chapters IV and V are summarized to identify specific contributions to the research goals. The results of the trajectory integration, extended forward look-ahead simulations, varying length TPA, and piloted simulator study are reiterated. Final recommendations for future work are presented to continue design refinement of an Auto-GCAS algorithm for performance limited aircraft.

6.1 Contributions to Research Goals

The research goals listed in Chapter I are summarized with specific their respective contributions.

(1) Expand previous 3-DOF aircraft point model to a 6-DOF aircraft model

The LJ-25D model using 6-DOF aircraft equations of motion was used during simulations. This model was also converted into the Multi-Crew Cockpit Simulator at AFRL for use in piloted simulator studies and to showcase the system. The trigger activation was updated to allow for transition between escape-maneuvers until the forward climb opened. This allowed for increasing the Auto-GCAS activation time

to the amount necessary to handback control to the pilot when the aircraft was on a safe trajectory.

(2) Implement path predictions longer than 30 seconds

The baseline LJ-25D Auto-GCAS algorithm from Gahan was test in simulated terrain with 30 s, 45 s, and 90 s forward look-ahead times. From simulated terrain testing, the *AB30 45FC* algorithm using a 0.015 s time step allowed for path predictions to have different fixed look-ahead times and kept the computational speed the same as the baseline *Euler30* algorithm.

(3) Examine different aircraft path integration methods to improve computation time while maintaining accuracy

Higher-order Runge-Kutta and Adams-Bashforth methods were integrated into the LJ-25D TPA to compare accuracy and computational speed against MATLAB's ode45. This numerical integration comparison expanded the allowable time step used for integration, resulting in a decreased computation time. The integration comparison also demonstrated that fixed step integration methods do not work for all aircraft initial conditions.

(4) Develop an algorithm with adaptive maneuvers to vary trajectory prediction lengths

Expanding on the *AB30 45FC* algorithm, the TPA was updated to allow for performance based criteria changing the forward look-ahead time. While keeping the computational cost the same, the forward climb was projected farther than 45 s by trimming lateral escape-maneuvers once a stalled or over 180° turn condition occurred.

(5) Evaluate initial display concepts that can be incorporated into future pilot system design

Initial HUD and PFD displays were designed and integrated into the MCCS.

Pilot feedback was collected through a piloted simulator study to understand what information the pilot needs from Auto-GCAS. This information is a starting point for implementation into an operational aircraft.

6.2 Predicted Aircraft Trajectory Integration Methods

The predicted aircraft trajectory (a.k.a TPA) is a solution to the numerical integration of the aircraft 6-DOF equations of motion. Six different fixed-step algorithms (Euler, Adams-Bashforth, ode1 - ode5) were compared to a truth source (ode45) to analyze accuracy vs. computation speed. The Euler Explicit and 4^{th} order Adams-Bashforth multi-step methods were the only two to have faster computational speed than ode45 while maintaining maximum RSS errors under 100 ft. The Adams-Bashforth multi-step method demonstrated accuracy for an extended time step compared to Euler, 0.015 s vs. 0.01 s for most initial conditions, however the values diverge for extreme aircraft initial conditions resulting in divergence of the integration model. Therefore an adaptive time step using the Adams-Bashforth method is recommended to monitor local truncation error between 3^{rd} and 4^{th} order methods. Additionally, with the LJ-25D model specifically, higher order Runge-Kutta integration methods did not deliver better accuracy for lateral maneuvers compared to the lower order Euler or Adams-Bashforth, most likely due to the fidelity of data points in the stitched aircraft model.

6.3 Simulation Results in Terrain Test Matrix

The Euler and Adams-Bashforth methods were then compared in simulated test terrain that included vertical cliff walls and high slope obstacles with the expectation of causing multiple Auto-GCAS activations and at random initial conditions. This simulated test terrain allowed for Auto-GCAS activations in a boxed canyon environ-

ment, and can be used for future benchmark testing of design improvements. The forward look-ahead times were compared between 30 s, 45 s, and 90 s to determine affect on collision prevention. Additionally, the handback trigger activation algorithm was changed between a first-open and forward-open to determine the affect on collision prevention. Purely extending all escape-maneuver forward look-ahead times did not reduce the number of collisions with terrain, and required more computational calculations. But the change in trigger activation to forward-open handback of the Auto-GCAS algorithm did reduce the number of collisions. This was attributed to a reduction in handback chatter, where the aircraft was handing control back over to the pilot while the aircraft energy was still on a collision heading with terrain.

6.4 Time Varying TPA

The final addition to the LJ-25D Auto-GCAS algorithm was to vary the forward look-ahead times of the escape maneuvers based on performance of level turn heading and climbing flight path angle.

The forward climb escape-maneuver was found to be the most important path for extending forward look-ahead time and therefore time varying escape-maneuvers were found to be a beneficial compromise between computation cost and extending forward look-ahead time. The final addition to the LJ-25D Auto-GCAS algorithm was varying the forward look-ahead times of the escape maneuvers based on performance of level turn heading and climbing flight path angle. This trimmed the lateral escape-maneuver integration time and allocated the trimmed time to the forward climb escape-maneuver. In turn this reduced unnecessary calculations for stalled flight and also for flight turning back into the direction of initial terrain conflict. The largest time reduction is at lower speeds which is where the forward look-ahead time benefits from being extended. This resulted in the same computation cost as existing methods

but with a longer look-ahead time, which enabled the Auto-GCAS algorithm to escape a boxed canyon where the previous algorithms were not able to.

6.5 Piloted Simulator Study

Regarding a nuisance boundary, the only maneuver that showed a similar trend to the F-16 PARS study was for the level left escape-maneuver, which had a 1.5 s time to collision between anxiety ratings of 4 and 5. However, due to the variability in other escape-maneuver results, the nuisance boundary for the LJ-25D or performance limited aircraft was not defined from the piloted simulator study. Further research would need to be conducted either in a simulator or through actual flight tests. Recommendations for future piloted study are to select a group of pilots with low-level flying within the last year, improvement to terrain feature initial heading which affected the perceived anxiety level between maneuvers, and lastly DTED terrain that matches the simulator visuals.

With respect to the Auto-GCAS displays, the pilot consensus was that all collision information and warnings could be displayed in the HUD, with minor integration to an existing TAWS display. Subjects were not concerned with knowing the time to collision for each escape-maneuver but rather a directional overview of open vs. closed escape-maneuvers. Recommendations for HUD displays are to include text for pre-initiation warning of the last escape-maneuver available, display the escape-maneuver selected during Auto-GCAS activation, and have an aural warning of the escape-maneuver selected.

6.6 Recommendations for Future Auto-GCAS Design

This current research brought up additional areas to further explore in order to develop the LJ-25D Auto-GCAS algorithm to be operationally implemented.

(1) Redesign implementation of terrain safety buffer

The terrain safety buffer could be further researched to provide coverage beyond a pure vertical addition to slope. The benefit of a vertical terrain buffer is reduced in high sloping terrain, and therefore a possible approach would be to add a terrain safety buffer perpendicular to terrain. The GEDACS algorithm for creating tip-tilt DTED can be used as a starting point.

(2) Decrease computational cost of interpolation with collision detection algorithm

Specific to a continuous interpolated DTED terrain map, the size of the interpolation matrix within the collision prediction algorithm can be trimmed to reduce computational cost. This is important when loading in a large DTED file to the aircraft flight computer. A DTED trimming algorithm can be written to select only the latitude and longitude values associated with the TPA latitude and longitude boundaries.

(3) Improve Auto-GCAS autopilot design

The Auto-GCAS steady-level flight autopilot is slower to stabilize and can be improved for simulation purposes. For an operational Auto-GCAS, the autopilot designs could target a rate of climb as opposed to a AoA value. This could help decrease the high pitch attitude observed in the MCCS on Auto-GCAS handback.

(4) Factor in limited performance to TPA

The current Auto-GCAS algorithm assumes maximum power and a fully operational aircraft. Level turns perform a tighter turn radius at less than maximum engine power. Additionally, if an aircraft suffers engine loss or reduced control surface authority, this degraded state could be factored into trajectory predictions.

(5) Define TPA integration method boundaries and implement adaptive Adams-Bashforth method

The off-nominal trim conditions showed decreasing accuracy for fixed-step numerical integrations at extreme initial flight angles. The boundaries of the integration methods could be examined to define when one method should be used over another, and what level of error in the TPA is expected for certain initial conditions. An adaptive Adams-Bashforth method could be implemented to monitor local truncation error while allowing for increased computational cost.

(6) Design different trigger activation algorithms

The affect of the trigger activation and handback criteria had a significant effect on the LJ-25D Auto-GCAS collision prevention. Other improvements could be expanded from the current forward-open design. The effect of the trigger activation on nuisance boundary would be interesting.

(7) Determine nuisance boundary for heavy limited performance aircraft Flight testing to determine the nuisance boundary for heavy limited performance aircraft

The piloted simulator study did not result in conclusive Time to Collision data for the LJ-25D. A different piloted simulator study could be conducted to see if the results differ, or flight testing similar to the F-16 PARS study could be conducted to determine the nuisance boundary. This nuisance boundary information would be helpful to factor into the design of the Auto-GCAS system before operational testing.

6.7 Conclusion

This research expanded the prospects of implementing current Auto-GCAS algorithms to performance limited aircraft by presenting design considerations and improvements to the LJ-25D model as a test bed for other "heavy" aircraft. This is an additional step towards flight testing performance limited aircraft at real terrain in order to implement an operational working system.

Appendix A. Path Integration Comparison for Steady-Level Flight

The initial conditions for steady level flight were at the following trim condition:

Airspeed: 300 KTAS	Altitude: 1,5663 ft	Heading: 35
Gamma: 0°	Beta: 0°	Phi: 0°
Fuel Total: 4580.3 lbs	Fuel Wing Tip: 1919.4 lbs	

The following tabulated data compare the RSS error over the forward look-ahead time for each trajectory integration method at different time steps. The results were used to select the best integration method balancing RSS error and computational speed.

Path	Integration Method	Path Length (s)	Step Size	Clock Time	Lat-distance max (ft)	Time @ Max (s)	Lon-distance max (ft)	Time @ Max (s)	Alt-distance max (ft)	Time @ Max (s)	RSS - Distance max (ft)	Time @ Max (s)
LL	Euler	30	0.005	7.0149	-11.61	24.30	-11.03	12.81	18.04	28.89	21.49	24.16
LL	AB	30	0.005	7.4123	-9.42	23.44	-8.48	11.52	17.92	28.89	20.30	29.56
LL	ODE2	30	0.005	16.7177	-5.10	19.48	8.89	30.00	17.09	28.90	19.24	30.00
LL	ODE3	30	0.005	25.2441	-18.82	30.00	-17.89	16.45	22.34	29.53	30.08	24.27
LL	ODE4	30	0.005	32.5548	-19.46	30.00	-18.42	16.46	22.90	29.54	30.93	25.00
LL	ODE5	30	0.005	47.8733	-5.36	20.00	8.85	30.00	17.37	28.90	19.51	30.00
LL	ODE45	30	Adaptive	4.4988	-	-	-	-	-	-	-	-
LL	Euler	30	0.0075	4.8438	-16.35	30.00	-15.21	14.80	17.54	29.12	24.19	27.20
LL	AB	30	0.0075	4.9134	-11.30	27.02	-10.93	13.37	17.36	29.12	20.70	29.78
LL	ODE2	30	0.0075	11.2212	-5.86	20.87	6.28	30.00	16.75	29.75	18.36	30.00
LL	ODE3	30	0.0075	16.5925	-21.73	30.00	-20.40	16.38	21.92	29.88	32.12	27.85
LL	ODE4	30	0.0075	21.6645	-22.63	30.00	-21.14	16.91	22.62	29.89	33.29	27.86
LL	ODE5	30	0.0075	34.0031	-6.34	23.12	6.19	30.00	17.16	29.75	18.89	30.00
LL	ODE45	30	Adaptive	4.6742	-	-	-	-	-	-	-	-
LL	Euler	30	0.01	3.5764	-20.79	30.00	-18.39	16.54	17.80	25.38	29.11	24.75
LL	AB	30	0.01	3.592	-14.36	25.43	-12.22	14.19	17.62	25.38	23.36	24.72
LL	ODE2	30	0.01	8.1653	-8.38	23.30	-5.74	12.08	17.17	24.80	19.09	24.76
LL	ODE3	30	0.01	12.0909	-23.20	30.00	-21.36	17.97	22.09	25.41	34.34	25.39
LL	ODE4	30	0.01	15.9305	-24.25	30.00	-22.23	17.97	22.86	25.42	35.69	25.39
LL	ODE5	30	0.01	24.3086	-9.09	23.97	-6.16	12.12	17.72	25.38	19.89	24.77
LL	ODE45	30	Adaptive	5.0656	-	-	-	-	-	-	-	-
LL	Euler	30	0.0125	2.8509	-24.60	30.00	-21.24	17.46	17.71	29.50	31.70	28.64
LL	AB	30	0.0125	2.8744	-15.82	29.60	-13.57	14.48	17.64	29.51	23.82	27.19
LL	ODE2	30	0.0125	6.8848	-8.09	26.50	-6.39	12.23	17.18	29.54	19.09	29.56
LL	ODE3	30	0.0125	10.2564	-25.07	30.00	-22.24	18.11	22.46	29.59	35.35	29.48
LL	ODE4	30	0.0125	13.3959	-26.26	30.00	-23.23	18.10	23.34	29.60	36.91	29.49
LL	ODE5	30	0.0125	20.437	-8.83	26.51	-6.70	12.98	17.86	29.54	20.06	29.58
LL	ODE45	30	Adaptive	4.8525	-	-	-	-	-	-	-	-
LL	Euler	30	0.015	2.4921	36.56	30.00	-29.75	30.00	21.58	13.97	47.90	30.00
LL	AB	30	0.015	2.485	-19.25	30.00	-16.50	15.35	15.16	30.00	24.84	30.00
LL	ODE2	30	0.015	5.8347	55.91	30.00	-15.59	30.00	19.35	13.23	59.20	30.00
LL	ODE3	30	0.015	8.5176	-24.08	30.00	-24.09	17.63	20.88	30.00	34.48	29.70
LL	ODE4	30	0.015	11.2909	-25.54	30.00	-25.25	17.61	22.02	30.00	36.38	29.72
LL	ODE5	30	0.015	17.0462	-42.94	21.14	-44.90	15.78	55.54	19.56	80.05	19.01
LL	ODE45	30	Adaptive	4.9651	-	-	-	-	-	-	-	-
LL	Euler	30	0.02	1.8039	-110.81	9.99	-137.68	7.55	139.61	8.73	216.67	8.65
LL	AB	30	0.02	1.8281	44.88	15.00	-47.84	6.07	46.16	7.07	69.27	6.81
LL	ODE2	30	0.02	4.3755	91.52	15.00	-113.09	6.98	130.43	8.16	186.01	7.89
LL	ODE3	30	0.02	6.396	-23.35	15.00	-20.98	9.00	19.57	12.39	32.77	12.70
LL	ODE4	30	0.02	8.4731	-28.62	15.00	-23.71	8.96	24.35	12.71	39.28	12.72
LL	ODE5	30	0.02	12.2525	99.19	15.00	-121.75	6.93	139.89	8.18	198.80	7.89
LL	ODE45	30	Adaptive	4.954	-	-	-	-	-	-	-	-

Path	Integration Method	Path Length (s)	Step Size	Clock Time	Lat-distance max (ft)	Time @ Max (s)	Lon-distance max (ft)	Time @ Max (s)	Alt-distance max (ft)	Time @ Max (s)	RSS - Distance max (ft)	Time @ Max (s)
CL	Euler	30	0.005	7.4944	-6.19	30.00	-0.95	30.00	-4.66	0.60	6.44	30.00
CL	AB	30	0.005	7.6929	-6.04	30.00	0.21	21.23	-4.66	0.63	6.17	30.00
CL	ODE2	30	0.005	16.7429	-1205.00	30.00	-1036.80	30.00	2082.90	30.00	2620.20	30.00
CL	ODE3	30	0.005	25.0774	-1203.10	30.00	-1039.40	30.00	2085.70	30.00	2622.60	30.00
CL	ODE4	30	0.005	32.2936	-1202.90	30.00	-1039.40	30.00	2085.40	30.00	2622.30	30.00
CL	ODE5	30	0.005	49.0268	-1205.00	30.00	-1037.00	30.00	2083.00	30.00	2620.30	30.00
CL	ODE45	30	Adaptive	4.5206	-	-	-	-	-	-	-	-
CL	Euler	30	0.0075	5.0242	-6.08	30.00	-2.62	30.00	-4.66	0.62	7.12	30.00
CL	AB	30	0.0075	4.911	-5.83	30.00	-1.31	30.00	-4.66	0.65	6.39	30.00
CL	ODE2	30	0.0075	11.1327	-1204.70	30.00	-1037.70	30.00	2083.70	30.00	2621.10	30.00
CL	ODE3	30	0.0075	16.3928	-1203.00	30.00	-1040.40	30.00	2086.60	30.00	2623.70	30.00
CL	ODE4	30	0.0075	22.0053	-1202.80	30.00	-1040.50	30.00	2086.40	30.00	2623.40	30.00
CL	ODE5	30	0.0075	32.8089	-1204.80	30.00	-1038.00	30.00	2083.80	30.00	2621.30	30.00
CL	ODE45	30	Adaptive	4.2491	-	-	-	-	-	-	-	-
CL	Euler	30	0.01	3.7877	-5.11	30.00	-3.70	30.00	-4.66	0.62	6.90	30.00
CL	AB	30	0.01	3.7574	-4.72	30.00	-2.01	30.00	-4.66	0.66	5.65	30.00
CL	ODE2	30	0.01	8.5785	-1203.50	30.00	-1038.00	30.00	2083.60	30.00	2620.60	30.00
CL	ODE3	30	0.01	12.9867	-1202.10	30.00	-1040.70	30.00	2086.50	30.00	2623.30	30.00
CL	ODE4	30	0.01	16.852	-1201.80	30.00	-1040.80	30.00	2086.40	30.00	2623.10	30.00
CL	ODE5	30	0.01	24.205	-1203.60	30.00	-1038.30	30.00	2083.70	30.00	2620.80	30.00
CL	ODE45	30	Adaptive	4.4365	-	-	-	-	-	-	-	-
CL	Euler	30	0.0125	3.0535	-3.32	30.00	-3.70	30.00	-4.66	0.64	5.20	30.00
CL	AB	30	0.0125	2.9758	-2.75	30.00	-1.65	30.00	-4.67	0.68	4.67	0.68
CL	ODE2	30	0.0125	6.9033	-1201.30	30.00	-1037.20	30.00	2082.00	30.00	2617.90	30.00
CL	ODE3	30	0.0125	10.0788	-1200.10	30.00	-1040.10	30.00	2085.10	30.00	2621.00	30.00
CL	ODE4	30	0.0125	13.0343	-1199.90	30.00	-1040.30	30.00	2085.00	30.00	2621.00	30.00
CL	ODE5	30	0.0125	19.5261	-1201.40	30.00	-1037.40	30.00	2082.00	30.00	2618.10	30.00
CL	ODE45	30	Adaptive	4.2657	-	-	-	-	-	-	-	-
CL	Euler	30	0.015	2.6191	25.06	29.34	17.32	26.10	-43.68	23.40	50.26	24.60
CL	AB	30	0.015	2.4355	-4.64	30.00	-4.25	30.00	-4.66	0.65	6.34	30.00

CL	ODE2	30	0.015	5.828	-1140.40	30.00	-967.24	30.00	1920.10	30.00	2433.70	30.00
CL	ODE3	30	0.015	8.5116	-1199.50	30.00	-1041.00	30.00	2085.30	30.00	2621.30	30.00
CL	ODE4	30	0.015	10.8491	-1199.50	30.00	-1041.30	30.00	2085.50	30.00	2621.50	30.00
CL	ODE5	30	0.015	15.9724	-1107.40	30.00	-923.06	30.00	1799.10	30.00	2305.50	30.00
CL	ODE45	30	Adaptive	4.1473	-	-	-	-	-	-	-	-
CL	Euler	30	0.02	1.8328	-271.62	30.00	-207.54	30.00	294.12	30.00	450.95	30.00
CL	AB	30	0.02	1.8099	-14.52	16.32	-12.26	12.22	-73.65	25.20	73.94	25.20
CL	ODE2	30	0.02	4.3239	-966.27	30.00	-751.14	30.00	1330.60	30.00	1807.80	30.00
CL	ODE3	30	0.02	6.3211	-1199.70	30.00	-1043.00	30.00	2086.70	30.00	2623.30	30.00
CL	ODE4	30	0.02	8.3355	-1199.70	30.00	-1043.30	30.00	2087.10	30.00	2623.60	30.00
CL	ODE5	30	0.02	12.7055	-1443.90	30.00	-1246.40	30.00	2379.60	30.00	3049.70	30.00
CL	ODE45	30	Adaptive	4.2353	-	-	-	-	-	-	-	-

Path	Integration Method	Path Length (s)	Step Size	Clock Time	Lat-distance max (ft)	Time @ Max (s)	Lon-distance max (ft)	Time @ Max (s)	Alt-distance max (ft)	Time @ Max (s)	RSS - Distance max (ft)	Time @ Max (s)
FC	Euler	30	0.005	7.5685	47.71	25.09	33.41	25.09	-46.52	12.37	65.10	12.64
FC	AB	30	0.005	7.5651	46.50	23.99	32.56	23.99	-47.15	12.35	66.14	12.61
FC	ODE2	30	0.005	16.6177	2.93	10.68	2.05	10.68	-4.70	8.72	5.75	9.48
FC	ODE3	30	0.005	25.1023	-240.06	30.00	-168.09	30.00	119.64	13.16	294.16	30.00
FC	ODE4	30	0.005	33.3847	-239.96	30.00	-168.02	30.00	119.67	13.16	294.04	30.00
FC	ODE5	30	0.005	49.638	2.98	10.71	2.08	10.71	-4.80	8.74	5.87	9.50
FC	ODE45	30	Adaptive	5.3022	-	-	-	-	-	-	-	-
FC	Euler	30	0.0075	5.0698	48.74	26.49	34.13	26.49	-44.64	12.39	62.63	12.67
FC	AB	30	0.0075	5.0467	46.51	24.59	32.57	24.59	-45.50	12.36	64.09	12.62
FC	ODE2	30	0.0075	11.4199	2.34	10.37	1.64	10.37	-3.54	8.52	4.44	9.34
FC	ODE3	30	0.0075	16.5905	-240.95	30.00	-168.71	30.00	122.98	13.15	295.32	30.00
FC	ODE4	30	0.0075	22.4296	-240.75	30.00	-168.57	30.00	123.03	13.15	295.08	30.00
FC	ODE5	30	0.0075	33.1499	2.33	10.40	1.63	10.40	-3.55	8.62	4.45	9.37
FC	ODE45	30	Adaptive	5.3989	-	-	-	-	-	-	-	-
FC	Euler	30	0.01	4.0526	39.85	22.02	27.90	22.02	-43.19	12.40	60.77	12.66
FC	AB	30	0.01	3.733	39.02	18.30	27.32	18.30	-44.19	12.36	62.57	12.61
FC	ODE2	30	0.01	8.4965	-9.39	30.00	-6.57	30.00	5.77	23.34	12.46	30.00
FC	ODE3	30	0.01	12.4097	-253.04	30.00	-177.18	30.00	126.01	13.17	309.75	30.00
FC	ODE4	30	0.01	16.4877	-252.72	30.00	-176.95	30.00	126.03	13.17	309.36	30.00
FC	ODE5	30	0.01	24.3713	-9.68	30.00	-6.78	30.00	5.86	23.37	12.79	30.00
FC	ODE45	30	Adaptive	5.3534	-	-	-	-	-	-	-	-
FC	Euler	30	0.0125	2.9463	47.65	27.29	33.37	27.29	-40.85	12.43	58.56	28.65
FC	AB	30	0.0125	2.9037	43.95	24.20	30.78	24.20	-42.16	12.36	60.26	12.64
FC	ODE2	30	0.0125	6.8046	-2.45	30.00	-1.72	30.00	2.43	30.00	3.86	30.00
FC	ODE3	30	0.0125	9.9821	-244.06	30.00	-170.89	30.00	129.29	13.14	299.16	30.00
FC	ODE4	30	0.0125	13.9358	-243.66	30.00	-170.61	30.00	129.32	13.14	298.69	30.00
FC	ODE5	30	0.0125	19.9013	-12.37	30.00	-8.67	30.00	9.22	12.79	15.16	30.00
FC	ODE45	30	Adaptive	5.3165	-	-	-	-	-	-	-	-
FC	Euler	30	0.015	2.5284	14.22	29.69	9.95	29.69	-29.77	23.58	31.42	24.11
FC	AB	30	0.015	2.512	67.64	29.64	47.36	29.64	-39.01	12.42	82.63	29.04
FC	ODE2	30	0.015	5.8439	-43.93	21.05	-30.76	21.05	39.03	12.71	59.14	13.02
FC	ODE3	30	0.015	8.5836	-261.45	30.00	-183.06	30.00	131.93	13.16	319.76	30.00
FC	ODE4	30	0.015	11.3244	-261.52	30.00	-183.12	30.00	132.01	13.16	319.86	30.00
FC	ODE5	30	0.015	16.6934	-65.54	21.20	-45.89	21.20	60.66	12.71	90.93	13.01
FC	ODE45	30	Adaptive	5.2038	-	-	-	-	-	-	-	-
FC	Euler	30	0.02	1.8994	-88.76	14.86	-62.14	14.86	-164.18	25.60	165.24	25.40
FC	AB	30	0.02	1.8319	209.73	30.00	146.86	30.00	-178.96	24.44	278.28	27.60
FC	ODE2	30	0.02	4.3486	-120.68	18.02	-84.50	18.02	105.89	12.86	168.97	13.24
FC	ODE3	30	0.02	6.333	-257.67	30.00	-180.41	30.00	134.86	13.14	315.37	30.00
FC	ODE4	30	0.02	8.2788	-254.83	30.00	-178.43	30.00	135.63	13.16	312.07	30.00
FC	ODE5	30	0.02	12.413	-160.78	30.00	-112.58	30.00	118.43	12.84	201.92	30.00
FC	ODE45	30	Adaptive	5.2162	-	-	-	-	-	-	-	-

Path	Integration Method	Path Length (s)	Step Size	Clock Time	Lat-distance max (ft)	Time @ Max (s)	Lon-distance max (ft)	Time @ Max (s)	Alt-distance max (ft)	Time @ Max (s)	RSS - Distance max (ft)	Time @ Max (s)
CR	Euler	30	0.005	7.4152	-2.59	30.00	-5.27	30.00	-4.66	0.61	6.00	30.00
CR	AB	30	0.005	7.4365	-1.69	30.00	-5.44	30.00	-4.66	0.64	5.77	30.00
CR	ODE2	30	0.005	16.9091	-1385.70	30.00	-777.13	30.00	2082.20	30.00	2619.10	30.00
CR	ODE3	30	0.005	24.7235	-1387.10	30.00	-773.94	30.00	2084.20	30.00	2620.50	30.00
CR	ODE4	30	0.005	32.771	-1387.30	30.00	-774.06	30.00	2084.50	30.00	2620.80	30.00
CR	ODE5	30	0.005	49.0798	-1386.00	30.00	-777.30	30.00	2082.60	30.00	2619.60	30.00
CR	ODE45	30	Adaptive	4.5727	-	-	-	-	-	-	-	-
CR	Euler	30	0.0075	4.9678	-3.38	30.00	-4.57	30.00	-4.66	0.59	5.87	30.00
CR	AB	30	0.0075	4.9186	-2.07	30.00	-4.78	30.00	-4.66	0.63	5.33	30.00
CR	ODE2	30	0.0075	11.068	-1385.70	30.00	-776.50	30.00	2082.00	30.00	2618.80	30.00
CR	ODE3	30	0.0075	16.6402	-1387.60	30.00	-773.85	30.00	2084.80	30.00	2621.10	30.00
CR	ODE4	30	0.0075	22.1386	-1387.80	30.00	-773.95	30.00	2085.10	30.00	2621.60	30.00
CR	ODE5	30	0.0075	32.4695	-1386.20	30.00	-776.79	30.00	2082.60	30.00	2619.60	30.00
CR	ODE45	30	Adaptive	4.2749	-	-	-	-	-	-	-	-
CR	Euler	30	0.01	3.8126	-4.08	30.00	-3.09	30.00	-4.66	0.61	5.28	30.00
CR	AB	30	0.01	3.7308	-2.36	30.00	-3.31	30.00	-4.66	0.65	4.66	0.65
CR	ODE2	30	0.01	8.5485	-1385.50	30.00	-775.01	30.00	2081.40	30.00	2617.80	30.00

CR	ODE3	30	0.01	12.4734	-1387.50	30.00	-772.55	30.00	2084.10	30.00	2620.20	30.00
CR	ODE4	30	0.01	16.3811	-1387.80	30.00	-772.67	30.00	2084.60	30.00	2620.80	30.00
CR	ODE5	30	0.01	24.9564	-1386.10	30.00	-775.43	30.00	2082.20	30.00	2618.80	30.00
CR	ODE45	30	Adaptive	4.4719	-	-	-	-	-	-	-	-
CR	Euler	30	0.0125	3.0099	-5.40	30.00	-2.31	30.00	-4.66	0.64	6.34	30.00
CR	AB	30	0.0125	3.0001	-3.28	30.00	-2.47	30.00	-4.67	0.68	4.67	0.68
CR	ODE2	30	0.0125	6.6425	-1385.80	30.00	-774.01	30.00	2082.00	30.00	2618.10	30.00
CR	ODE3	30	0.0125	9.826	-1388.20	30.00	-771.86	30.00	2085.10	30.00	2621.20	30.00
CR	ODE4	30	0.0125	12.9535	-1388.70	30.00	-772.09	30.00	2085.70	30.00	2622.00	30.00
CR	ODE5	30	0.0125	19.3899	-1386.50	30.00	-774.63	30.00	2082.90	30.00	2619.40	30.00
CR	ODE45	30	Adaptive	4.2514	-	-	-	-	-	-	-	-
CR	Euler	30	0.015	2.4879	25.57	27.56	18.98	30.00	-44.62	23.36	51.66	24.68
CR	AB	30	0.015	2.4646	-4.88	30.00	-2.66	30.00	-4.66	0.65	5.56	30.00
CR	ODE2	30	0.015	5.716	-1203.50	30.00	-703.88	30.00	1739.10	30.00	2228.90	30.00
CR	ODE3	30	0.015	8.5299	-1387.30	30.00	-770.30	30.00	2084.00	30.00	2619.40	30.00
CR	ODE4	30	0.015	11.0657	-1388.00	30.00	-770.63	30.00	2084.90	30.00	2620.50	30.00
CR	ODE5	30	0.015	16.3111	-1245.60	30.00	-724.77	30.00	1798.90	30.00	2304.90	30.00
CR	ODE45	30	Adaptive	4.336	-	-	-	-	-	-	-	-
CR	Euler	30	0.02	1.9097	-394.04	30.00	-257.29	30.00	413.87	30.00	626.70	30.00
CR	AB	30	0.02	1.8717	-50.10	30.00	-40.61	30.00	33.70	11.36	64.50	30.00
CR	ODE2	30	0.02	4.5924	-1187.20	30.00	-734.67	30.00	1506.80	30.00	2054.20	30.00
CR	ODE3	30	0.02	6.3244	-1389.20	30.00	-769.41	30.00	2084.30	30.00	2620.30	30.00
CR	ODE4	30	0.02	8.3045	-1390.10	30.00	-770.14	30.00	2085.80	30.00	2622.20	30.00
CR	ODE5	30	0.02	12.239	-1661.20	30.00	-929.40	30.00	2372.10	30.00	3041.40	30.00
CR	ODE45	30	Adaptive	4.3121	-	-	-	-	-	-	-	-

Path	Integration Method	Path Length (s)	Step Size	Clock Time	Lat-distance max (ft)	Time @ Max (s)	Lon-distance max (ft)	Time @ Max (s)	Alt-distance max (ft)	Time @ Max (s)	RSS - Distance max (ft)	Time @ Max (s)
LR	Euler	30	0.005	7.2104	-14.24	16.58	-16.19	30.00	19.89	30.00	25.88	30.00
LR	AB	30	0.005	7.2227	-11.02	14.82	-13.86	30.00	19.78	30.00	24.17	30.00
LR	ODE2	30	0.005	16.6858	5.96	30.00	-9.19	26.29	19.48	30.00	22.30	30.00
LR	ODE3	30	0.005	25.1326	-22.54	19.71	-20.44	30.00	24.24	30.00	35.03	30.00
LR	ODE4	30	0.005	33.4353	-22.95	19.66	-21.01	30.00	25.11	30.00	36.00	30.00
LR	ODE5	30	0.005	47.3202	5.96	30.00	-9.56	26.29	19.93	30.00	22.87	30.00
LR	ODE45	30	Adaptive	4.849	-	-	-	-	-	-	-	-
LR	Euler	30	0.0075	4.7869	-16.70	16.79	-14.33	30.00	17.55	29.06	23.98	26.90
LR	AB	30	0.0075	4.7379	-11.92	14.54	-10.87	29.82	17.37	29.06	20.52	29.69
LR	ODE2	30	0.0075	10.8417	-5.92	12.84	-6.09	26.87	17.01	29.69	18.58	29.80
LR	ODE3	30	0.0075	16.2635	-22.31	19.64	-17.13	30.00	22.04	29.72	31.94	27.54
LR	ODE4	30	0.0075	21.9316	-22.94	19.62	-17.88	30.00	23.10	29.72	33.18	27.55
LR	ODE5	30	0.0075	31.9929	-6.25	12.85	-6.69	26.91	17.71	29.69	19.42	29.81
LR	ODE45	30	Adaptive	4.6671	-	-	-	-	-	-	-	-
LR	Euler	30	0.01	3.6204	-20.13	18.56	-16.71	30.00	16.66	30.00	26.73	26.66
LR	AB	30	0.01	3.5474	-13.56	16.32	-12.13	30.00	16.41	30.00	20.85	30.00
LR	ODE2	30	0.01	8.2773	-6.47	13.39	-6.58	30.00	16.42	30.00	17.91	30.00
LR	ODE3	30	0.01	12.0485	-23.10	20.18	-17.75	30.00	21.39	30.00	32.39	30.00
LR	ODE4	30	0.01	16.0248	-23.85	20.16	-18.60	30.00	22.56	30.00	33.80	30.00
LR	ODE5	30	0.01	24.5623	-6.88	13.40	-7.43	30.00	17.36	30.00	19.10	30.00
LR	ODE45	30	Adaptive	4.7729	-	-	-	-	-	-	-	-
LR	Euler	30	0.0125	2.8831	-26.34	21.06	-25.48	30.00	19.72	30.00	37.17	30.00
LR	AB	30	0.0125	2.8393	-17.22	18.20	-19.79	30.00	19.40	30.00	29.03	30.00
LR	ODE2	30	0.0125	6.7361	-8.52	16.74	-13.81	30.00	19.69	30.00	24.06	30.00
LR	ODE3	30	0.0125	9.8547	-27.23	21.61	-25.41	30.00	24.92	30.00	40.75	30.00
LR	ODE4	30	0.0125	12.9127	-28.05	21.53	-26.42	30.00	26.29	30.00	42.40	30.00
LR	ODE5	30	0.0125	19.2791	-8.73	16.71	-14.64	30.00	20.88	30.00	25.49	30.00
LR	ODE45	30	Adaptive	4.6781	-	-	-	-	-	-	-	-
LR	Euler	30	0.015	2.353	-29.20	13.11	39.24	30.00	20.44	13.95	43.70	30.00
LR	AB	30	0.015	2.3703	-20.46	20.12	-22.25	30.00	16.26	30.00	30.56	30.00
LR	ODE2	30	0.015	5.5402	-30.96	12.29	102.02	30.00	34.35	13.70	105.70	30.00
LR	ODE3	30	0.015	8.1498	-28.66	22.11	-23.79	30.00	23.04	30.00	39.91	30.00
LR	ODE4	30	0.015	10.8914	-29.64	22.01	-25.08	30.00	24.71	30.00	41.90	30.00
LR	ODE5	30	0.015	16.0772	-54.06	17.73	-31.01	22.40	56.46	20.07	81.60	19.89
LR	ODE45	30	Adaptive	4.9938	-	-	-	-	-	-	-	-
LR	Euler	30	0.02	1.755	-161.97	16.30	-66.24	20.52	139.73	17.40	218.77	17.24
LR	AB	30	0.02	1.7845	-52.04	12.84	29.74	30.00	39.12	13.40	65.18	13.16
LR	ODE2	30	0.02	4.2286	-201.00	17.40	-121.14	22.04	202.59	19.32	300.55	19.22
LR	ODE3	30	0.02	6.1932	-32.65	22.34	-27.51	30.00	23.73	30.00	44.65	30.00
LR	ODE4	30	0.02	8.1331	-34.09	21.64	-29.80	30.00	27.97	30.00	48.45	30.00
LR	ODE5	30	0.02	12.3397	-250.95	21.30	-423.89	30.00	289.83	28.68	531.31	30.00
LR	ODE45	30	Adaptive	4.6322	-	-	-	-	-	-	-	-

Appendix B. Euler vs Adams-Bashforth Path Integration Comparison for Off-Nominal Flight

The initial conditions for off-nominal flight were at the following trim conditions:

Trim Condition 1:

Airspeed: 300 KTAS	Altitude: 1,5663 ft	Heading: 35
Gamma: -10°	Beta: 0°	Phi: 0°
Fuel Total: 4580.3 lbs	Fuel Wing Tip: 1919.4 lbs	

Trim Condition 2:

Airspeed: 300 KTAS	Altitude: 1,5663 ft	Heading: 35
Gamma: 0°	Beta: 0°	Phi: 45°
Fuel Total: 4580.3 lbs	Fuel Wing Tip: 1919.4 lbs	

Trim Condition 3:

Airspeed: 300 KTAS	Altitude: 1,5663 ft	Heading: 35
Gamma: 10°	Beta: -10°	Phi: -45°
Fuel Total: 4580.3 lbs	Fuel Wing Tip: 1919.4 lbs	

The following tabulated data compare the RSS error over the forward look-ahead time for the Euler and Adams-Bashforth integration methods at different time steps. The time steps were increased until RSS divergence occurred. The results were used to select the best integration method balancing RSS error and computational speed for implementation into the LJ-25D Auto-GCAS algorithm.

Trim Condition 1

Path	Integration Method	Path Length (s)	Step Size	Clock Time	RSS - Distance max (ft)	Time @ Max (s)
LL	Euler	30	0.01	3.788077341	36.89177437	30
LL	AB	30	0.01	3.797462266	31.98375553	30
LL	ODE45	30	Adaptive	5.199011886	-	-
LL	Euler	30	0.0125	3.025729784	36.26380974	28.9
LL	AB	30	0.0125	2.973573814	29.46056861	28.9
LL	ODE45	30	Adaptive	5.161787221	-	-
LL	Euler	30	0.015	2.530827726	36.56937044	12.96
LL	AB	30	0.015	2.500295014	33.9258686	30
LL	ODE45	30	Adaptive	4.910222799	-	-
LL	Euler	30	0.016	2.281594484	96.50555002	30
LL	AB	30	0.016	2.287888994	31.25987563	29.984
LL	ODE46	30	Adaptive	4.784474049	-	-
LL	Euler	30	0.017	2.177137303	118.6271122	30.005
LL	AB	30	0.017	2.176795385	33.87188782	17.102
LL	ODE46	30	Adaptive	4.915770934	-	-

Trim Condition 1

Path	Integration Method	Path Length (s)	Step Size	Clock Time	RSS - Distance max (ft)	Time @ Max (s)
CL	Euler	30	0.01	3.949061493	6.884698687	30
CL	AB	30	0.01	3.857222555	5.831719085	30
CL	ODE45	30	Adaptive	4.635659848	-	-
CL	Euler	30	0.0125	3.100193432	8.412460883	30
CL	AB	30	0.0125	3.067428609	6.633040099	30
CL	ODE45	30	Adaptive	4.752782323	-	-
CL	Euler	30	0.015	2.637834389	217.5039909	30
CL	AB	30	0.015	2.545511213	11.63174772	30
CL	ODE45	30	Adaptive	5.079057334	-	-
CL	Euler	30	0.016	2.411697285	391.1137272	30
CL	AB	30	0.016	2.416981529	12.79127565	30
CL	ODE45	30	Adaptive	4.797524804	-	-
CL	Euler	30	0.017	2.296425844	355.9214413	30.005
CL	AB	30	0.017	2.197150039	142.5619964	30.005
CL	ODE45	30	Adaptive	4.78380804	-	-

Trim Condition 1

Path	Integration Method	Path Length (s)	Step Size	Clock Time	RSS - Distance max (ft)	Time @ Max (s)
FC	Euler	30	0.01	3.848345832	58.74708131	12.73
FC	AB	30	0.01	3.757268757	61.12920523	12.68
FC	ODE45	30	Adaptive	5.420998045	-	-
FC	Euler	30	0.0125	3.075446152	57.38322055	12.7375
FC	AB	30	0.0125	3.122695742	60.27431145	12.675
FC	ODE45	30	Adaptive	5.255554052	-	-
FC	Euler	30	0.015	2.558682954	53.37867575	24.87
FC	AB	30	0.015	2.535533631	109.4268055	30
FC	ODE45	30	Adaptive	5.326709277	-	-
FC	Euler	30	0.016	2.256160446	42.11686364	12.896
FC	AB	30	0.016	2.23617781	64.01743865	24.352
FC	ODE45	30	Adaptive	5.531591051	-	-

FC	Euler	30	0.017	2.247237842	138.0900578	26.027
FC	AB	30	0.017	2.275290623	182.8104585	30.005
FC	ODE45	30	Adaptive	5.16338167	-	-

Trim Condition 1

Path	Integration Method	Path Length (s)	Step Size	Clock Time	RSS - Distance max (ft)	Time @ Max (s)
CR	Euler	30	0.01	3.800988114	8.10952273	30
CR	AB	30	0.01	3.724635441	7.087819124	30
CR	ODE45	30	Adaptive	4.654459797	-	-
CR	Euler	30	0.0125	2.986223911	10.25067492	30
CR	AB	30	0.0125	3.009293746	8.830183895	30
CR	ODE45	30	Adaptive	4.662055641	-	-
CR	Euler	30	0.015	2.497283796	219.9002108	30
CR	AB	30	0.015	2.436262209	14.68586363	30
CR	ODE45	30	Adaptive	4.570085488	-	-
CR	Euler	30	0.016	2.280111378	401.5365048	30
CR	AB	30	0.016	2.26701854	14.63220946	30
CR	ODE45	30	Adaptive	4.602622074	-	-
CR	Euler	30	0.017	2.172915051	300.8091871	30.005
CR	AB	30	0.017	2.198478259	132.725719	30.005
CR	ODE45	30	Adaptive	4.629122197	-	-

Trim Condition 1

Path	Integration Method	Path Length (s)	Step Size	Clock Time	RSS - Distance max (ft)	Time @ Max (s)
LR	Euler	30	0.01	3.956341721	29.33122946	30
LR	AB	30	0.01	3.940780643	26.19172231	30
LR	ODE45	30	Adaptive	5.466259833	-	-
LR	Euler	30	0.0125	3.033679528	24.57858467	21.15
LR	AB	30	0.0125	2.93659083	19.75314474	21.15
LR	ODE45	30	Adaptive	4.705384861	-	-
LR	Euler	30	0.015	2.562598649	40.85256803	30
LR	AB	30	0.015	2.5014137	20.68445897	21.045
LR	ODE45	30	Adaptive	4.971275364	-	-
LR	Euler	30	0.016	2.35531205	96.6150656	30
LR	AB	30	0.016	2.389189715	31.49434355	27.6
LR	ODE45	30	Adaptive	5.066559786	-	-
LR	Euler	30	0.017	2.17588974	117.4182618	30.005
LR	AB	30	0.017	2.16744699	35.32209106	15.47
LR	ODE45	30	Adaptive	4.923649664	-	-

Trim Condition 2

Path	Integration Method	Path Length (s)	Step Size	Clock Time	RSS - Distance max (ft)	Time @ Max (s)
LL	Euler	30	0.01	4.308380415	13.03409551	12.17
LL	AB	30	0.01	4.2539409	17.08519844	30
LL	ODE45	30	Adaptive	5.741541104	-	-
LL	Euler	30	0.0125	3.230230479	16.89333513	16.1875
LL	AB	30	0.0125	3.273538365	13.86936537	30
LL	ODE45	30	Adaptive	5.663852904	-	-
LL	Euler	30	0.015	2.687422758	44.22787387	30

LL	AB	30	0.015	2.661754344	12.19327843	30
LL	ODE45	30	Adaptive	5.473139987	-	-
LL	Euler	30	0.016	2.432611282	157.0107218	30
LL	AB	30	0.016	2.399520613	16.58244141	30
LL	ODE46	30	Adaptive	5.656678174	-	-
LL	Euler	30	0.017	2.310798098	217.4898144	30.005
LL	AB	30	0.017	2.325573641	18.40858449	13.923
LL	ODE46	30	Adaptive	5.518537958	-	-

Trim Condition 2

Path	Integration Method	Path Length (s)	Step Size	Clock Time	RSS - Distance max (ft)	Time @ Max (s)
CL	Euler	30	0.01	4.168898243	16.07240379	30
CL	AB	30	0.01	4.023371132	17.42593391	30
CL	ODE45	30	Adaptive	5.456874616	-	-
CL	Euler	30	0.0125	3.256416738	15.21890444	30
CL	AB	30	0.0125	3.216784326	16.75971206	30
CL	ODE45	30	Adaptive	5.179547972	-	-
CL	Euler	30	0.015	2.706275894	173.7272798	30
CL	AB	30	0.015	2.660083036	14.57582782	30
CL	ODE45	30	Adaptive	5.245817858	-	-
CL	Euler	30	0.016	2.420293167	341.0368911	30
CL	AB	30	0.016	2.489417924	12.18566042	30
CL	ODE45	30	Adaptive	5.389685935	-	-
CL	Euler	30	0.017	2.296395159	528.1832109	30.005
CL	AB	30	0.017	2.341609897	78.22944569	30.005
CL	ODE45	30	Adaptive	5.489529559	-	-

Trim Condition 2

Path	Integration Method	Path Length (s)	Step Size	Clock Time	RSS - Distance max (ft)	Time @ Max (s)
FC	Euler	30	0.01	4.185535048	88.27417435	15.22
FC	AB	30	0.01	4.01038993	90.52171279	15.18
FC	ODE45	30	Adaptive	5.976978676	-	-
FC	Euler	30	0.0125	3.260183099	85.4261283	15.225
FC	AB	30	0.0125	3.211060557	88.31990818	15.175
FC	ODE45	30	Adaptive	5.867243096	-	-
FC	Euler	30	0.015	2.727217361	21.51737077	30
FC	AB	30	0.015	2.648712941	86.46939319	15.21
FC	ODE45	30	Adaptive	5.671311397	-	-
FC	Euler	30	0.016	2.539469197	93.11141309	29.968
FC	AB	30	0.016	2.413521141	124.6143743	30
FC	ODE45	30	Adaptive	5.775483062	-	-
FC	Euler	30	0.017	2.306959263	124.8125195	29.818
FC	AB	30	0.017	2.324219119	165.2630703	30.005
FC	ODE45	30	Adaptive	5.625977426	-	-

Trim Condition 2

Path	Integration Method	Path Length (s)	Step Size	Clock Time	RSS - Distance max (ft)	Time @ Max (s)
CR	Euler	30	0.01	4.209737012	13.50132517	30
CR	AB	30	0.01	3.996875394	14.83363099	30
CR	ODE45	30	Adaptive	5.124030976	-	-
CR	Euler	30	0.0125	3.157661408	14.95965138	30

CR	AB	30	0.0125	3.143197391	16.45490333	30
CR	ODE45	30	Adaptive	5.20038891	-	-
CR	Euler	30	0.015	2.68220193	167.2820431	30
CR	AB	30	0.015	2.625472439	16.11425516	30
CR	ODE45	30	Adaptive	5.230331009	-	-
CR	Euler	30	0.016	2.436608218	326.1848633	30
CR	AB	30	0.016	2.45345748	15.18188599	30
CR	ODE45	30	Adaptive	5.311649679	-	-
CR	Euler	30	0.017	2.337257015	514.5639899	30.005
CR	AB	30	0.017	2.299203564	77.70178154	30.005
CR	ODE45	30	Adaptive	5.187142356	-	-

Trim Condition 2

Path	Integration Method	Path Length (s)	Step Size	Clock Time	RSS - Distance max (ft)	Time @ Max (s)
LR	Euler	30	0.01	3.971975273	14.21457833	14.03
LR	AB	30	0.01	3.870987539	15.37430769	30
LR	ODE45	30	Adaptive	5.333914984	-	-
LR	Euler	30	0.0125	3.090534973	17.77637623	14.5875
LR	AB	30	0.0125	3.084714473	12.34837802	30
LR	ODE45	30	Adaptive	5.189368623	-	-
LR	Euler	30	0.015	2.611850359	47.67147199	30
LR	AB	30	0.015	2.569851406	12.2904585	30
LR	ODE45	30	Adaptive	5.059394115	-	-
LR	Euler	30	0.016	2.318492427	154.5116376	30
LR	AB	30	0.016	2.32757284	13.51010449	30
LR	ODE45	30	Adaptive	5.217497679	-	-
LR	Euler	30	0.017	2.176517174	219.736193	30.005
LR	AB	30	0.017	2.19415314	17.27146805	12.852
LR	ODE45	30	Adaptive	5.193433943	-	-

Trim Condition 3

Path	Integration Method	Path Length (s)	Step Size	Clock Time	RSS - Distance max (ft)	Time @ Max (s)
LL	Euler	30	0.01	3.851715918	1308.305139	30
LL	AB	30	0.01	4.018728058	1307.35257	30
LL	ODE45	30	Adaptive	6.312954229	-	-
LL	Euler	30	0.0125	3.012603631	1430.440083	30
LL	AB	30	0.0125	2.930662787	1429.380212	30
LL	ODE45	30	Adaptive	6.321607974	-	-
LL	Euler	30	0.015	2.519793704	291.8763941	30
LL	AB	30	0.015	2.46403152	1229.442269	30
LL	ODE45	30	Adaptive	6.445295863	-	-
LL	Euler	30	0.016	2.470926578	242.1670484	30
LL	AB	30	0.016	2.27553698	1492.348002	30
LL	ODE46	30	Adaptive	6.279627724	-	-
LL	Euler	30	0.017	2.252004824	464.6766884	30.005
LL	AB	30	0.017	2.183345895	1332.803408	30.005
LL	ODE46	30	Adaptive	6.352398732	-	-

Trim Condition 3

Path	Integration Method	Path Length (s)	Step Size	Clock Time	RSS - Distance max (ft)	Time @ Max (s)
CL	Euler	30	0.01	3.974267586	23.98512415	30
CL	AB	30	0.01	3.806607263	6.756903733	30
CL	ODE45	30	Adaptive	7.297067891	-	-
CL	Euler	30	0.0125	3.051806745	31.33557268	30
CL	AB	30	0.0125	3.011757311	8.146370336	30
CL	ODE45	30	Adaptive	7.345235107	-	-
CL	Euler	30	0.015	2.527030972	37.59737456	30
CL	AB	30	0.015	2.478922496	9.272068943	30
CL	ODE45	30	Adaptive	7.269401155	-	-
CL	Euler	30	0.016	2.367704393	1171.719626	30
CL	AB	30	0.016	2.390706429	8.820271617	30
CL	ODE45	30	Adaptive	7.525839811	-	-
CL	Euler	30	0.017	2.180830604	1238.351239	30.005
CL	AB	30	0.017	2.275762587	12.2224179	30.005
CL	ODE45	30	Adaptive	7.310187614	-	-

Trim Condition 3

Path	Integration Method	Path Length (s)	Step Size	Clock Time	RSS - Distance max (ft)	Time @ Max (s)
FC	Euler	30	0.01	3.828854448	902.0692601	30
FC	AB	30	0.01	3.725214656	875.4727674	30
FC	ODE45	30	Adaptive	5.222457539	-	-
FC	Euler	30	0.0125	3.030354154	874.0512028	30
FC	AB	30	0.0125	3.0209666	908.4605848	30
FC	ODE45	30	Adaptive	5.266854011	-	-
FC	Euler	30	0.015	2.585172264	757.2558956	30
FC	AB	30	0.015	2.443317413	833.5120619	30
FC	ODE45	30	Adaptive	5.12711087	-	-
FC	Euler	30	0.016	2.324950005	140.6128784	17.248
FC	AB	30	0.016	2.347577977	848.6542047	30
FC	ODE45	30	Adaptive	5.398220155	-	-
FC	Euler	30	0.017	2.194258054	207.0666153	17.34
FC	AB	30	0.017	2.165195006	1062.284301	30.005
FC	ODE45	30	Adaptive	5.220845555	-	-

Trim Condition 3

Path	Integration Method	Path Length (s)	Step Size	Clock Time	RSS - Distance max (ft)	Time @ Max (s)
CR	Euler	30	0.01	3.883089105	1021.120489	30
CR	AB	30	0.01	3.860446522	1024.331773	30
CR	ODE45	30	Adaptive	5.72903888	-	-
CR	Euler	30	0.0125	3.015108693	1151.833436	30
CR	AB	30	0.0125	3.01664528	1159.557363	30
CR	ODE45	30	Adaptive	5.732548948	-	-
CR	Euler	30	0.015	2.560937569	117.1286711	30
CR	AB	30	0.015	2.5137625	1172.356743	30
CR	ODE45	30	Adaptive	5.980034315	-	-
CR	Euler	30	0.016	2.343864512	231.8823247	30
CR	AB	30	0.016	2.328157315	1102.790619	30
CR	ODE45	30	Adaptive	5.87589801	-	-
CR	Euler	30	0.017	2.199316105	324.2832349	30.005

CR	AB	30	0.017	2.242858074	1325.445425	30.005
CR	ODE45	30	Adaptive	6.157287344	-	-

Trim Condition 3

Path	Integration Method	Path Length (s)	Step Size	Clock Time	RSS - Distance max (ft)	Time @ Max (s)
LR	Euler	30	0.01	3.786333266	44.45690581	30
LR	AB	30	0.01	3.706859493	49.44127166	30
LR	ODE45	30	Adaptive	6.838436925	-	-
LR	Euler	30	0.0125	2.98897796	33.6183028	30
LR	AB	30	0.0125	2.992575699	41.79688391	30
LR	ODE45	30	Adaptive	6.726692502	-	-
LR	Euler	30	0.015	2.57789379	1573.653148	30
LR	AB	30	0.015	2.525838642	45.41957462	30
LR	ODE45	30	Adaptive	7.020913705	-	-
LR	Euler	30	0.016	2.525560139	1706.394374	30
LR	AB	30	0.016	2.321861637	46.58906346	30
LR	ODE45	30	Adaptive	6.746329713	-	-
LR	Euler	30	0.017	2.124886064	1939.102805	30
LR	AB	30	0.017	2.115578875	52.86950643	30
LR	ODE45	30	Adaptive	6.779703852	-	-

Appendix C. Test Terrain for Extended Forward Look-Ahead Time: Euler vs Adams-Bashforth Integration Comparison

The Euler and Adams-Bashforth trajectory prediction were compared in a simulated test terrain box. The test terrain box included vertical cliff walls and high sloped pyramids to force multiple Auto-GCAS activations. The simulations lasted 200 seconds and any Height above Terrain less than zero in that time span resulted in a collision with terrain count against the algorithm.

LJ-25D Auto-GCAS MATLAB / SIMULINK BREAKDOWN

Test Matrix

Run Num	Speed [KTAS]	Altitude Above Ground @ Start (ft)	Buffer Height (ft)	Look Ahead Time (s)	Path Integration	Simulation Time (s)	Heading	Lat Start	Lon Start	Comp HZ	Height Above Terrain (HaT) Below Zero	Over-G any maneuver [Y/N] (i.e. + 2.3G)	Comments	Crash Count:	Over-G count:
1	200	150	50	30	Euler	200	30	35.6	-116.3	10.49	Y	N	Over 12 deg AoA	24	4
2	200	150	250	30	Euler	200	30	35.6	-116.3		Y	N	Over 12 deg AoA Failed at Cliff Wall only though	1	0
3	200	150	500	30	Euler	200	30	35.6	-116.3		-	-	Veered off grid from start...AGL start below buffer	0	0
4	200	350	50	30	Euler	200	30	35.6	-116.3		Y	N	Over 12 deg AoA Failed at Cliff Wall & Obstacle 6	1	0
5	200	350	250	30	Euler	200	30	35.6	-116.3		Y	Y	Over 12 deg AoA Reversed @ Dived through Obstacle 1	1	1
6	200	350	500	30	Euler	200	30	35.6	-116.3		Y	N	Went straight through cliff (not enough look ahead time) Over 12 deg AoA	1	0
7	200	600	50	30	Euler	200	30	35.6	-116.3		Y	Y	Failed at 60 deg bank turn	1	1
8	200	600	250	30	Euler	200	30	35.6	-116.3		Y	N	Failed at turning for Obstacle 6 & Cliff	1	0
9	200	600	500	30	Euler	200	30	35.6	-116.3		Y	N	Over 12 deg AoA Cleared Obstalce 1 but ran into Cliff	1	0
10	250	150	50	30	Euler	200	30	35.6	-116.3		Y	N	Over 12 deg AoA Ran into Obstalce 1 and 6, continuos climb	1	0
11	250	150	250	30	Euler	200	30	35.6	-116.3		Y	N	Ran into cliff fence walls	1	0
12	250	150	500	30	Euler	200	30	35.6	-116.3		-	-	Veered off grid from start...AGL start below buffer	0	0
13	250	350	50	30	Euler	200	30	35.6	-116.3		Y	N	Obstacle 1 & 5, cliff wall	1	0
14	250	350	250	30	Euler	200	30	35.6	-116.3		N	N	Over 12 deg AoA, continuous climb at end	0	0
15	250	350	500	30	Euler	200	30	35.6	-116.3		Y	N	Only initial cliff wall, cleared obstacle 5 barely	1	0
16	250	600	50	30	Euler	200	30	35.6	-116.3		Y	N	Hit obstacle 1	1	0
17	250	600	250	30	Euler	200	30	35.6	-116.3		Y	N	Hit obstacle 4 (barely) & cliff wall	1	0
18	250	600	500	30	Euler	200	30	35.6	-116.3		N	N	Over 12 deg AoA, continuous climb at end	0	0
19	300	150	50	30	Euler	200	30	35.6	-116.3		Y	N	Hit obstacle 4 & cliff wall	1	0
20	300	150	250	30	Euler	200	30	35.6	-116.3		N	N	Over 12 deg AoA, continuous climb at end	0	0
21	300	150	500	30	Euler	200	30	35.6	-116.3		-	-	Veered off grid from start...AGL start below buffer	0	0
22	300	350	50	30	Euler	200	30	35.6	-116.3		N	N	Over 12 deg AoA, continuous climb at end	0	0
23	300	350	250	30	Euler	200	30	35.6	-116.3		N	N	Over 12 deg AoA, continuous climb at end	0	0
24	300	350	500	30	Euler	200	30	35.6	-116.3		Y	N	Cleared Obstacle 2, hit 2 cliffs	1	0
25	300	600	50	30	Euler	200	30	35.6	-116.3		N	N	Over 12 deg AoA, continuous climb at end	0	0
26	300	600	250	30	Euler	200	30	35.6	-116.3		N	Y	Good moves! G-spike	0	1
27	300	600	500	30	Euler	200	30	35.6	-116.3		N	Y	Over 12 deg AoA, G-spike	0	1
28	350	150	50	30	Euler	200	30	35.6	-116.3		Y	N	Over 12 deg AoA, hit Obstacle 1 barely	1	0
29	350	150	250	30	Euler	200	30	35.6	-116.3		N	N	Over 12 deg AoA, continuous climb at end	0	0
30	350	150	500	30	Euler	200	30	35.6	-116.3		-	-	Veered off grid from start...AGL start below buffer	0	0
31	350	350	50	30	Euler	200	30	35.6	-116.3		Y	N	Over 12 deg AoA, hit Obstacle 1 barely	1	0
32	350	350	250	30	Euler	200	30	35.6	-116.3		N	N	Over 12 deg AoA,	0	0
33	350	350	500	30	Euler	200	30	35.6	-116.3		Y	N	Hit cliff wall w/60 deg bank	1	0
34	350	600	50	30	Euler	200	30	35.6	-116.3		Y	N	Barely hit Obstacle 1	1	0
35	350	600	250	30	Euler	200	30	35.6	-116.3		N	N		0	0
36	350	600	500	30	Euler	200	30	35.6	-116.3		N	N	Over 12 deg AoA,	0	0
37	400	150	50	30	Euler	200	30	35.6	-116.3		Y	N	Barely hit Obstacle 1	1	0
38	400	150	250	30	Euler	200	30	35.6	-116.3		Y	N	Hit cliff wall w/60 deg bank	1	0
39	400	150	500	30	Euler	200	30	35.6	-116.3		-	-	Veered off grid from start...AGL start below buffer	0	0
40	400	350	50	30	Euler	200	30	35.6	-116.3		Y	N	Hit obstacle 1, obstacle	1	0
41	400	350	250	30	Euler	200	30	35.6	-116.3		N	N		0	0
42	400	350	500	30	Euler	200	30	35.6	-116.3		N	N	cleared cliffs with 60 deg bank	0	0
43	400	600	50	30	Euler	200	30	35.6	-116.3		Y	N	Barely hit Obstacle 1 & cliff front	1	0
44	400	600	250	30	Euler	200	30	35.6	-116.3		N	N		0	0
45	400	600	500	30	Euler	200	30	35.6	-116.3		N	N		0	0
														Crash Count:	Over-G count:
										7.045				22	0
1	200	150	50	45	Euler	200	30	35.6	-116.3		Y	N	Over 12 deg AoA, continuous climb at end	1	0
2	200	150	250	45	Euler	200	30	35.6	-116.3		N	N	Over 12 deg AoA, continuous climb at end	0	0
3	200	150	500	45	Euler	200	30	35.6	-116.3		-	-	Veered off grid from start...AGL start below buffer	0	0
4	200	350	50	45	Euler	200	30	35.6	-116.3		Y	N	hit cliff wall, obstalce 6	1	0
5	200	350	250	45	Euler	200	30	35.6	-116.3		Y	N	hit cliff wall barely, over 12deg AoA	1	0
6	200	350	500	45	Euler	200	30	35.6	-116.3		Y	N	hit cliff wall on fwd climb, over 12deg AoA	1	0
7	200	600	50	45	Euler	200	30	35.6	-116.3		Y	N	hit obstacle 1 (early handback to autopilot), obstacle 5, cliff wall	1	0
8	200	600	250	45	Euler	200	30	35.6	-116.3		Y	N	hit cliff wall barely (early handback to autopilot)	1	0
9	200	600	500	45	Euler	200	30	35.6	-116.3		N	N	over 12deg AoA, continous climb at end	0	0
10	250	150	50	45	Euler	200	30	35.6	-116.3		N	N	continous climb at end	0	0
11	250	150	250	45	Euler	200	30	35.6	-116.3		Y	N	barely hits cliff wall	1	0
12	250	150	500	45	Euler	200	30	35.6	-116.3		-	-	Veered off grid from start...AGL start below buffer	0	0
13	250	350	50	45	Euler	200	30	35.6	-116.3		Y	N	Hits obstacle 1 and 4	1	0
14	250	350	250	45	Euler	200	30	35.6	-116.3		N	N	Over 12 deg AoA, continuous climb at end	0	0
15	250	350	500	45	Euler	200	30	35.6	-116.3		N	N		0	0
16	250	600	50	45	Euler	200	30	35.6	-116.3		Y	N	Close to ground at start, Hit obstacle 1 and cliff wall	1	0
17	250	600	250	45	Euler	200	30	35.6	-116.3		Y	N	early handback at obstacle 4	1	0
18	250	600	500	45	Euler	200	30	35.6	-116.3		N	N	Over 12 deg AoA, continuous climb at end	0	0
19	300	150	50	45	Euler	200	30	35.6	-116.3		Y	N	Hits obstacle 4	1	0
20	300	150	250	45	Euler	200	30	35.6	-116.3		N	N	Over 12 deg AoA, continuous climb at end	0	0
21	300	150	500	45	Euler	200	30	35.6	-116.3		-	-	Veered off grid from start...AGL start below buffer	0	0
22	300	350	50	45	Euler	200	30	35.6	-116.3		Y	N	clears obstacle 1 barely, early handback at cliff wall	1	0
23	300	350	250	45	Euler	200	30	35.6	-116.3		N	N		0	0
24	300	350	500	45	Euler	200	30	35.6	-116.3		Y	N	barely hits cliff walls (early handback)	1	0
25	300	600	50	45	Euler	200	30	35.6	-116.3		N	N	barely doesn't hit ground though (obstacle 4)...barely!	0	0
26	300	600	250	45	Euler	200	30	35.6	-116.3		Y	N	barely hits terrain (early handback)	1	0
27	300	600	500	45	Euler	200	30	35.6	-116.3		Y	N	barely hits terrain once	1	0
28	350	150	50	45	Euler	200	30	35.6	-116.3		Y	N	hits obstacle 1 barely	1	0
29	350	150	250	45	Euler	200	30	35.6	-116.3		N	N	continous climb at end	0	0
30	350	150	500	45	Euler	200	30	35.6	-116.3		-	-	Veered off grid from start...AGL start below buffer	0	0
31	350	350	50	45	Euler	200	30	35.6	-116.3		Y	N	hits obstacle 1 barely, over 12 deg AoA	1	0
32	350	350	250	45	Euler	200	30	35.6	-116.3		N	N	over 12 deg AoA	0	0
33	350	350	500	45	Euler	200	30	35.6	-116.3		N	N		0	0
34	350	600	50	45	Euler	200	30	35.6	-116.3		Y	N	barely hits obstacle 1	1	0
35	350	600	250	45	Euler	200	30	35.6	-116.3		N	N		0	0
36	350	600	500	45	Euler	200	30	35.6	-116.3		N	N	over 12deg AoA	0	0
37	400	150	50	45	Euler	200	30	35.6	-116.3		Y	N		1	0
38	400	150	250	45	Euler	200	30	35.6	-116.3		Y	N	barely hits cliff wall (early handback)	1	0
39	400	150	500	45	Euler	200	30	35.6	-116.3		-	-	Veered off grid from start...AGL start below buffer	0	0
40	400	350	50	45	Euler	200	30	35.6	-116.3		Y	N		1	0
41	400	350	250	45	Euler	200	30	35.6	-116.3		N	N		0	0
42	400	350	500	45	Euler	200	30	35.6	-116.3		N	N		0	0
43	400	600	50	45	Euler	200	30	35.6	-116.3		Y	N	barely hits	1	0
44	400	600	250	45	Euler	200	30	35.6	-116.3		N	N		0	0
45	400	600	500	45	Euler	200	30	35.6	-116.3		N	N		0	0
														Crash Count:	Over-G count:
										3.682				22	6
1	200	150	50	90	Euler	200	30	35.6	-116.3		Y	Y	over 12deg AoA, fails obstacle 4	1	1
2	200	150	250	90	Euler	200	30	35.6	-116.3		N	N	over 12deg AoA	0	0
3	200	150	500	90	Euler	200	30	35.6	-116.3		-	-	Veered off grid from start...AGL start below buffer	0	0
4	200	350	50	90	Euler	200	30	35.6	-116.3		Y	Y	fails obstacle 4	1	1
5	200	350	250	90	Euler	200	30	35.6	-116.3		Y	Y	fails obstacle 4	1	1
6	200	350	500	90	Euler	200	30	35.6	-116.3		-	-	Veered off grid from start...AGL start below buffer	0	0
7	200	600	50	90	Euler	200	30	35.6	-116.3		Y	Y	over 12deg AoA, fails obstacle 4	1	1
8	200	600	250	90	Euler	200	30	35.6	-116.3		Y	Y	over 12deg AoA, fails obstacle 4	1	1
9	200	600	500	90	Euler	200	30	35.6	-116.3		N	Y	over 12deg AoA...same path as above but doesn't hit obstacle 4	0	1
10	250	150	50	90	Euler	200	30	35.6	-116.3		N	N	continous climb at end	0	0

11	250	150	250	90	Euler	200	30	35.6	-116.3		Y	N	over 12deg AoA, barely...hits cliff wall	1	0
12	250	150	500	90	Euler	200	30	35.6	-116.3		-	-	Veered off grid from start...AGL start below buffer	0	0
13	250	350	50	90	Euler	200	30	35.6	-116.3		Y	N	hits first moutain and obstacle 4	1	0
14	250	350	250	90	Euler	200	30	35.6	-116.3		Y	N	barely, hits obstacle 5	1	0
15	250	350	500	90	Euler	200	30	35.6	-116.3		N	N		0	0
16	250	600	50	90	Euler	200	30	35.6	-116.3		Y	N	hits obstacle 1 and cliff wall	1	0
17	250	600	250	90	Euler	200	30	35.6	-116.3		Y	N	hits obstacle 4	1	0
18	250	600	500	90	Euler	200	30	35.6	-116.3		N	N		0	0
19	300	150	50	90	Euler	200	30	35.6	-116.3		Y	N	early handback at obstacle 4	1	0
20	300	150	250	90	Euler	200	30	35.6	-116.3		N	N	continous climb at end	0	0
21	300	150	500	90	Euler	200	30	35.6	-116.3		-	-	Veered off grid from start...AGL start below buffer	0	0
22	300	350	50	90	Euler	200	30	35.6	-116.3		Y	N	early handback at end	1	0
23	300	350	250	90	Euler	200	30	35.6	-116.3		N	N		0	0
24	300	350	500	90	Euler	200	30	35.6	-116.3		Y	N	over 12deg AoA, barely fails at early handback cliff wall	1	0
25	300	600	50	90	Euler	200	30	35.6	-116.3		N	N	barley passes! At obstacle 4	0	0
26	300	600	250	90	Euler	200	30	35.6	-116.3		Y	N		1	0
27	300	600	500	90	Euler	200	30	35.6	-116.3		Y	N		1	0
28	350	150	50	90	Euler	200	30	35.6	-116.3		Y	N	over 12deg AoA, barely fails with fwd climb	1	0
29	350	150	250	90	Euler	200	30	35.6	-116.3		N	N	continous climb at end	0	0
30	350	150	500	90	Euler	200	30	35.6	-116.3		-	-	Veered off grid from start...AGL start below buffer	0	0
31	350	350	50	90	Euler	200	30	35.6	-116.3		Y	N	over 12deg AoA, barely fails with fwd climb	1	0
32	350	350	250	90	Euler	200	30	35.6	-116.3		N	N	right at 12deg AoA	0	0
33	350	350	500	90	Euler	200	30	35.6	-116.3		N	N	right at 12deg AoA...if ran for longer, would get a true box canyon sc	0	0
34	350	600	50	90	Euler	200	30	35.6	-116.3		Y	N	barely fails on initial climb obstacle 1	1	0
35	350	600	250	90	Euler	200	30	35.6	-116.3		N	N		0	0
36	350	600	500	90	Euler	200	30	35.6	-116.3		N	N	over 12deg AoA	0	0
37	400	150	50	90	Euler	200	30	35.6	-116.3		Y	N	barely fails on climbs	1	0
38	400	150	250	90	Euler	200	30	35.6	-116.3		N	N	over 12deg AoA	0	0
39	400	150	500	90	Euler	200	30	35.6	-116.3		-	-	Veered off grid from start...AGL start below buffer	0	0
40	400	350	50	90	Euler	200	30	35.6	-116.3		Y	N	barely fails on climbs	1	0
41	400	350	250	90	Euler	200	30	35.6	-116.3		N	N		0	0
42	400	350	500	90	Euler	200	30	35.6	-116.3		Y	N	barely fails on early handback, over 12deg AoA	1	0
43	400	600	50	90	Euler	200	30	35.6	-116.3		Y	N	barely fails on climbs (early handback)	1	0
44	400	600	250	90	Euler	200	30	35.6	-116.3		N	N		0	0
45	400	600	500	90	Euler	200	30	35.6	-116.3		N	N		0	0
														Crash Count:	**Over-G count:**
										10.42				24	3
1	200	150	50	30	Adam-Bash (4th) Learjet Euler	200	30	35.6	-116.3		Y	N	over 12deg AoA, continous climb at end	1	0
2	200	150	250	30	Adam-Bash (4th)	200	30	35.6	-116.3		Y	Y	over 12deg AoA, not early enough escape maneuver for clearance	1	1
3	200	150	500	30	Adam-Bash (4th)	200	30	35.6	-116.3		-	-	Veered off grid from start...AGL start below buffer	0	0
4	200	350	50	30	Adam-Bash (4th)	200	30	35.6	-116.3		Y	N		1	0
5	200	350	250	30	Adam-Bash (4th)	200	30	35.6	-116.3		Y	Y	way over 12deg AoA	1	1
6	200	350	500	30	Adam-Bash (4th)	200	30	35.6	-116.3		Y	Y		1	1
7	200	600	50	30	Adam-Bash (4th)	200	30	35.6	-116.3		Y	N		1	0
8	200	600	250	30	Adam-Bash (4th)	200	30	35.6	-116.3		Y	N		1	0
9	200	600	500	30	Adam-Bash (4th)	200	30	35.6	-116.3		Y	N		1	0
10	250	150	50	30	Adam-Bash (4th)	200	30	35.6	-116.3		Y	N	continous climb at end	1	0
11	250	150	250	30	Adam-Bash (4th)	200	30	35.6	-116.3		Y	N	not early enough initiation, continuous climb at end	1	0
12	250	150	500	30	Adam-Bash (4th)	200	30	35.6	-116.3		-	-	Veered off grid from start...AGL start below buffer	0	0
13	250	350	50	30	Adam-Bash (4th)	200	30	35.6	-116.3		Y	N	not early enough initiation, early handback	1	0
14	250	350	250	30	Adam-Bash (4th)	200	30	35.6	-116.3		N	N	continous climb at end	0	0
15	250	350	500	30	Adam-Bash (4th)	200	30	35.6	-116.3		Y	N	barely fails, not early enough initiation	1	0
16	250	600	50	30	Adam-Bash (4th)	200	30	35.6	-116.3		Y	N	not early enough initiation	1	0
17	250	600	250	30	Adam-Bash (4th)	200	30	35.6	-116.3		Y	N	barely fails, not early enough initiation	1	0
18	250	600	500	30	Adam-Bash (4th)	200	30	35.6	-116.3		N	N	continous climb at end	0	0
19	300	150	50	30	Adam-Bash (4th)	200	30	35.6	-116.3		Y	N	not early enough initiation	1	0
20	300	150	250	30	Adam-Bash (4th)	200	30	35.6	-116.3		N	N	continous climb at end	0	0
21	300	150	500	30	Adam-Bash (4th)	200	30	35.6	-116.3		-	-	Veered off grid from start...AGL start below buffer	0	0
22	300	350	50	30	Adam-Bash (4th)	200	30	35.6	-116.3		N	N	continous climb at end	0	0
23	300	350	250	30	Adam-Bash (4th)	200	30	35.6	-116.3		N	N	continous climb at end	0	0
24	300	350	500	30	Adam-Bash (4th)	200	30	35.6	-116.3		Y	N	barely fails	1	0
25	300	600	50	30	Adam-Bash (4th)	200	30	35.6	-116.3		N	N	continous climb at end	0	0
26	300	600	250	30	Adam-Bash (4th)	200	30	35.6	-116.3		N	N	continous climb at end	0	0
27	300	600	500	30	Adam-Bash (4th)	200	30	35.6	-116.3		N	N	poor handback on 60 deg turn	0	0
28	350	150	50	30	Adam-Bash (4th)	200	30	35.6	-116.3		Y	N	barely fails on initial climb obstacle 1	1	0
29	350	150	250	30	Adam-Bash (4th)	200	30	35.6	-116.3		N	N	continous climb at end	0	0
30	350	150	500	30	Adam-Bash (4th)	200	30	35.6	-116.3		-	-	Veered off grid from start...AGL start below buffer	0	0
31	350	350	50	30	Adam-Bash (4th)	200	30	35.6	-116.3		Y	N	barely fails on initial climb obstacle 1	1	0
32	350	350	250	30	Adam-Bash (4th)	200	30	35.6	-116.3		N	N	over 12deg AoA	0	0
33	350	350	500	30	Adam-Bash (4th)	200	30	35.6	-116.3		Y	N	barely fails by running into side wall	1	0
34	350	600	50	30	Adam-Bash (4th)	200	30	35.6	-116.3		Y	N	barely fails on initial climb obstacle 1	1	0
35	350	600	250	30	Adam-Bash (4th)	200	30	35.6	-116.3		N	N		0	0
36	350	600	500	30	Adam-Bash (4th)	200	30	35.6	-116.3		N	N	over 12deg AoA	0	0
37	400	150	50	30	Adam-Bash (4th)	200	30	35.6	-116.3		Y	N	barely fails on initial climb obstacle 1	1	0
38	400	150	250	30	Adam-Bash (4th)	200	30	35.6	-116.3		Y	N	barely fails, not early enough initiation	1	0
39	400	150	500	30	Adam-Bash (4th)	200	30	35.6	-116.3		-	-	Veered off grid from start...AGL start below buffer	0	0
40	400	350	50	30	Adam-Bash (4th)	200	30	35.6	-116.3		Y	N	barely fails	1	0
41	400	350	250	30	Adam-Bash (4th)	200	30	35.6	-116.3		N	N		0	0
42	400	350	500	30	Adam-Bash (4th)	200	30	35.6	-116.3		N	N		0	0
43	400	600	50	30	Adam-Bash (4th)	200	30	35.6	-116.3		Y	N	barely fails	1	0
44	400	600	250	30	Adam-Bash (4th)	200	30	35.6	-116.3		N	N		0	0
45	400	600	500	30	Adam-Bash (4th)	200	30	35.6	-116.3		N	N		0	0
														Crash Count:	**Over-G count:**
										7.039				22	0
1	200	150	50	45	Adam-Bash (4th)	200	30	35.6	-116.3		Y	N	over 12deg AoA	1	0
2	200	150	250	45	Adam-Bash (4th)	200	30	35.6	-116.3		N	N	over 12deg AoA, continous climb at end	0	0
3	200	150	500	45	Adam-Bash (4th)	200	30	35.6	-116.3		-	-		0	0
4	200	350	50	45	Adam-Bash (4th)	200	30	35.6	-116.3		Y	N	over 12degAoA, early handback to pilot causing collision	1	0
5	200	350	250	45	Adam-Bash (4th)	200	30	35.6	-116.3		Y	N	only fails at sidewall	1	0
6	200	350	500	45	Adam-Bash (4th)	200	30	35.6	-116.3		Y	N	continous climb, fails	1	0
7	200	600	50	45	Adam-Bash (4th)	200	30	35.6	-116.3		Y	N	early handback fail, fails at sidewall	1	0
8	200	600	250	45	Adam-Bash (4th)	200	30	35.6	-116.3		Y	N	fails at sidewall	1	0
9	200	600	500	45	Adam-Bash (4th)	200	30	35.6	-116.3		N	N		0	0
10	250	150	50	45	Adam-Bash (4th)	200	30	35.6	-116.3		N	N	over 12deg AoA, continous climb at end	0	0
11	250	150	250	45	Adam-Bash (4th)	200	30	35.6	-116.3		Y	N	fails at sidewall	1	0
12	250	150	500	45	Adam-Bash (4th)	200	30	35.6	-116.3		-	-		0	0
13	250	350	50	45	Adam-Bash (4th)	200	30	35.6	-116.3		Y	N		1	0
14	250	350	250	45	Adam-Bash (4th)	200	30	35.6	-116.3		N	N	over 12deg AoA, continous climb at end	0	0
15	250	350	500	45	Adam-Bash (4th)	200	30	35.6	-116.3		N	N		0	0
16	250	600	50	45	Adam-Bash (4th)	200	30	35.6	-116.3		Y	N		1	0
17	250	600	250	45	Adam-Bash (4th)	200	30	35.6	-116.3		Y	N	barely fails, early handback	1	0
18	250	600	500	45	Adam-Bash (4th)	200	30	35.6	-116.3		N	N	over 12deg AoA, continous climb at end	0	0
19	300	150	50	45	Adam-Bash (4th)	200	30	35.6	-116.3		Y	N	barely fails, early handback	1	0
20	300	150	250	45	Adam-Bash (4th)	200	30	35.6	-116.3		N	N	over 12deg AoA, continous climb at end	0	0
21	300	150	500	45	Adam-Bash (4th)	200	30	35.6	-116.3		-	-		0	0
22	300	350	50	45	Adam-Bash (4th)	200	30	35.6	-116.3		Y	N	barely fails, early handback	1	0
23	300	350	250	45	Adam-Bash (4th)	200	30	35.6	-116.3		N	N		0	0
24	300	350	500	45	Adam-Bash (4th)	200	30	35.6	-116.3		Y	N	not early enough initiation and early handback fail	1	0
25	300	600	50	45	Adam-Bash (4th)	200	30	35.6	-116.3		N	N		0	0
26	300	600	250	45	Adam-Bash (4th)	200	30	35.6	-116.3		Y	N		1	0
27	300	600	500	45	Adam-Bash (4th)	200	30	35.6	-116.3		Y	N	barely fails, not early enough initiation	1	0
28	350	150	50	45	Adam-Bash (4th)	200	30	35.6	-116.3		Y	N	barely fails	1	0
29	350	150	250	45	Adam-Bash (4th)	200	30	35.6	-116.3		N	N	over 12deg AoA, continous climb at end	0	0
30	350	150	500	45	Adam-Bash (4th)	200	30	35.6	-116.3		-	-		0	0
31	350	350	50	45	Adam-Bash (4th)	200	30	35.6	-116.3		Y	N	barely fails	1	0

32	350	350	250	45	Adam-Bash (4th)	200	30	35.6	-116.3		N	N		0	0
33	350	350	500	45	Adam-Bash (4th)	200	30	35.6	-116.3		N	N		0	0
34	350	600	50	45	Adam-Bash (4th)	200	30	35.6	-116.3		Y	N	barely fails	1	0
35	350	600	250	45	Adam-Bash (4th)	200	30	35.6	-116.3		N	N		0	0
36	350	600	500	45	Adam-Bash (4th)	200	30	35.6	-116.3		N	N	over 12deg AoA	0	0
37	400	150	50	45	Adam-Bash (4th)	200	30	35.6	-116.3		Y	N	barely fails	1	0
38	400	150	250	45	Adam-Bash (4th)	200	30	35.6	-116.3		Y	N	barely fails, early handback	1	0
39	400	150	500	45	Adam-Bash (4th)	200	30	35.6	-116.3		-	-		0	0
40	400	350	50	45	Adam-Bash (4th)	200	30	35.6	-116.3		Y	N	barely fails	1	0
41	400	350	250	45	Adam-Bash (4th)	200	30	35.6	-116.3		N	N		0	0
42	400	350	500	45	Adam-Bash (4th)	200	30	35.6	-116.3		N	N		0	0
43	400	600	50	45	Adam-Bash (4th)	200	30	35.6	-116.3		Y	N		1	0
44	400	600	250	45	Adam-Bash (4th)	200	30	35.6	-116.3		N	N		0	0
45	400	600	500	45	Adam-Bash (4th)	200	30	35.6	-116.3		N	N		0	0
														Crash Count:	**Over-G count:**
										6.24				15	3
1	200	150	50	(45 forward, 30 rest)	Adam-Bash (4th)	200	30	35.6	-116.3		Y	N	Over 12 deg AoA, continuous climb at end	1	0
2	200	150	250	(45 forward, 30 rest)	Adam-Bash (4th)	200	30	35.6	-116.3		N	N	Over 12 deg AoA, continuous climb at end	0	0
3	200	150	500	(45 forward, 30 rest)	Adam-Bash (4th)	200	30	35.6	-116.3		Y	Y	Barely hits cliff wall...improvement over previous ones, g-spike	1	1
4	200	350	50	(45 forward, 30 rest)	Adam-Bash (4th)	200	30	35.6	-116.3		N	N		0	0
5	200	350	250	(45 forward, 30 rest)	Adam-Bash (4th)	200	30	35.6	-116.3		N	N		0	0
6	200	350	500	(45 forward, 30 rest)	Adam-Bash (4th)	200	30	35.6	-116.3		N	Y		0	1
7	200	600	50	(45 forward, 30 rest)	Adam-Bash (4th)	200	30	35.6	-116.3		Y	N	hit obstalce 1, cleared other obstacles...improvement	1	0
8	200	600	250	(45 forward, 30 rest)	Adam-Bash (4th)	200	30	35.6	-116.3		N	N	over 12deg AoA, continous climb at end	0	0
9	200	600	500	(45 forward, 30 rest)	Adam-Bash (4th)	200	30	35.6	-116.3		N	N	continous climb at end	0	0
10	250	150	50	(45 forward, 30 rest)	Adam-Bash (4th)	200	30	35.6	-116.3		N	N	continous climb	0	0
11	250	150	250	(45 forward, 30 rest)	Adam-Bash (4th)	200	30	35.6	-116.3		Y	N	barely hits obstacle 3	1	0
12	250	150	500	(45 forward, 30 rest)	Adam-Bash (4th)	200	30	35.6	-116.3		Y	N	Hits obstacle 1 and 4	1	0
13	250	350	50	(45 forward, 30 rest)	Adam-Bash (4th)	200	30	35.6	-116.3		Y	N	Changed from continous climb back to pilot...hit obstacle 4 & cliff wa	1	0
14	250	350	250	(45 forward, 30 rest)	Adam-Bash (4th)	200	30	35.6	-116.3		Y	N	Changed from continous climb back to pilot...hit obstacle 4 & cliff wa	1	0
15	250	350	500	(45 forward, 30 rest)	Adam-Bash (4th)	200	30	35.6	-116.3		N	N	cleared obstacle 1 & cliff walls (change from before)	0	0
16	250	600	50	(45 forward, 30 rest)	Adam-Bash (4th)	200	30	35.6	-116.3		Y	N	still hit but much improvement w/cliff walls, early handback on obsta	1	0
17	250	600	250	(45 forward, 30 rest)	Adam-Bash (4th)	200	30	35.6	-116.3		N	N	changed to under 12 deg AoA & non-continuous climb at end	0	0
18	250	600	500	(45 forward, 30 rest)	Adam-Bash (4th)	200	30	35.6	-116.3		N	N		0	0
19	300	150	50	(45 forward, 30 rest)	Adam-Bash (4th)	200	30	35.6	-116.3		Y	N	early handback obstacle 4	1	0
20	300	150	250	(45 forward, 30 rest)	Adam-Bash (4th)	200	30	35.6	-116.3		N	N		0	0
21	300	150	500	(45 forward, 30 rest)	Adam-Bash (4th)	200	30	35.6	-116.3		N	N	clears obstacle 1 barely, early handback at cliff wall	0	0
22	300	350	50	(45 forward, 30 rest)	Adam-Bash (4th)	200	30	35.6	-116.3		N	N	continous climb at end	0	0
23	300	350	250	(45 forward, 30 rest)	Adam-Bash (4th)	200	30	35.6	-116.3		N	N	continous climb at end	0	0
24	300	350	500	(45 forward, 30 rest)	Adam-Bash (4th)	200	30	35.6	-116.3		N	N		0	0
25	300	600	50	(45 forward, 30 rest)	Adam-Bash (4th)	200	30	35.6	-116.3		N	N		0	0
26	300	600	250	(45 forward, 30 rest)	Adam-Bash (4th)	200	30	35.6	-116.3		N	N	continous climb at end	0	0
27	300	600	500	(45 forward, 30 rest)	Adam-Bash (4th)	200	30	35.6	-116.3		N	N		0	0
28	350	150	50	(45 forward, 30 rest)	Adam-Bash (4th)	200	30	35.6	-116.3		Y	N	barely hits obstacle 1	1	0
29	350	150	250	(45 forward, 30 rest)	Adam-Bash (4th)	200	30	35.6	-116.3		N	N	continous climb at end	0	0
30	350	150	500	(45 forward, 30 rest)	Adam-Bash (4th)	200	30	35.6	-116.3		N	N	continous climb at end	0	0
31	350	350	50	(45 forward, 30 rest)	Adam-Bash (4th)	200	30	35.6	-116.3		Y	N	barely hits obstacle 1	1	0
32	350	350	250	(45 forward, 30 rest)	Adam-Bash (4th)	200	30	35.6	-116.3		N	N		0	0
33	350	350	500	(45 forward, 30 rest)	Adam-Bash (4th)	200	30	35.6	-116.3		N	N		0	0
34	350	600	50	(45 forward, 30 rest)	Adam-Bash (4th)	200	30	35.6	-116.3		Y	N	barely hits obstacle 1	1	0
35	350	600	250	(45 forward, 30 rest)	Adam-Bash (4th)	200	30	35.6	-116.3		N	N	over 12deg AoA	0	0
36	350	600	500	(45 forward, 30 rest)	Adam-Bash (4th)	200	30	35.6	-116.3		N	N		0	0
37	400	150	50	(45 forward, 30 rest)	Adam-Bash (4th)	200	30	35.6	-116.3		Y	N	barely hits obstacle 1	1	0
38	400	150	250	(45 forward, 30 rest)	Adam-Bash (4th)	200	30	35.6	-116.3		N	N		0	0
39	400	150	500	(45 forward, 30 rest)	Adam-Bash (4th)	200	30	35.6	-116.3		N	N		0	0
40	400	350	50	(45 forward, 30 rest)	Adam-Bash (4th)	200	30	35.6	-116.3		Y	Y	barely hits obstacle 1 and obstacle 4	1	1
41	400	350	250	(45 forward, 30 rest)	Adam-Bash (4th)	200	30	35.6	-116.3		N	N		0	0
42	400	350	500	(45 forward, 30 rest)	Adam-Bash (4th)	200	30	35.6	-116.3		N	N		0	0
43	400	600	50	(45 forward, 30 rest)	Adam-Bash (4th)	200	30	35.6	-116.3		Y	N	barely hits	1	0
44	400	600	250	(45 forward, 30 rest)	Adam-Bash (4th)	200	30	35.6	-116.3		N	N		0	0
45	400	600	500	(45 forward, 30 rest)	Adam-Bash (4th)	200	30	35.6	-116.3		N	N		0	0

Appendix D. Piloted Study Test Plan in AFRL Multi-Crew Cockpit Simulator (MCCS)

Results for one test subject are shown in the below figures. Each test subject flew the escape-maneuver three times. Each run calculated the time to collision at anxiety point and time to collision at the minimum distance along the escape-maneuver. Calculations were based on the aircraft U-body velocity and heading at the anxiety point.

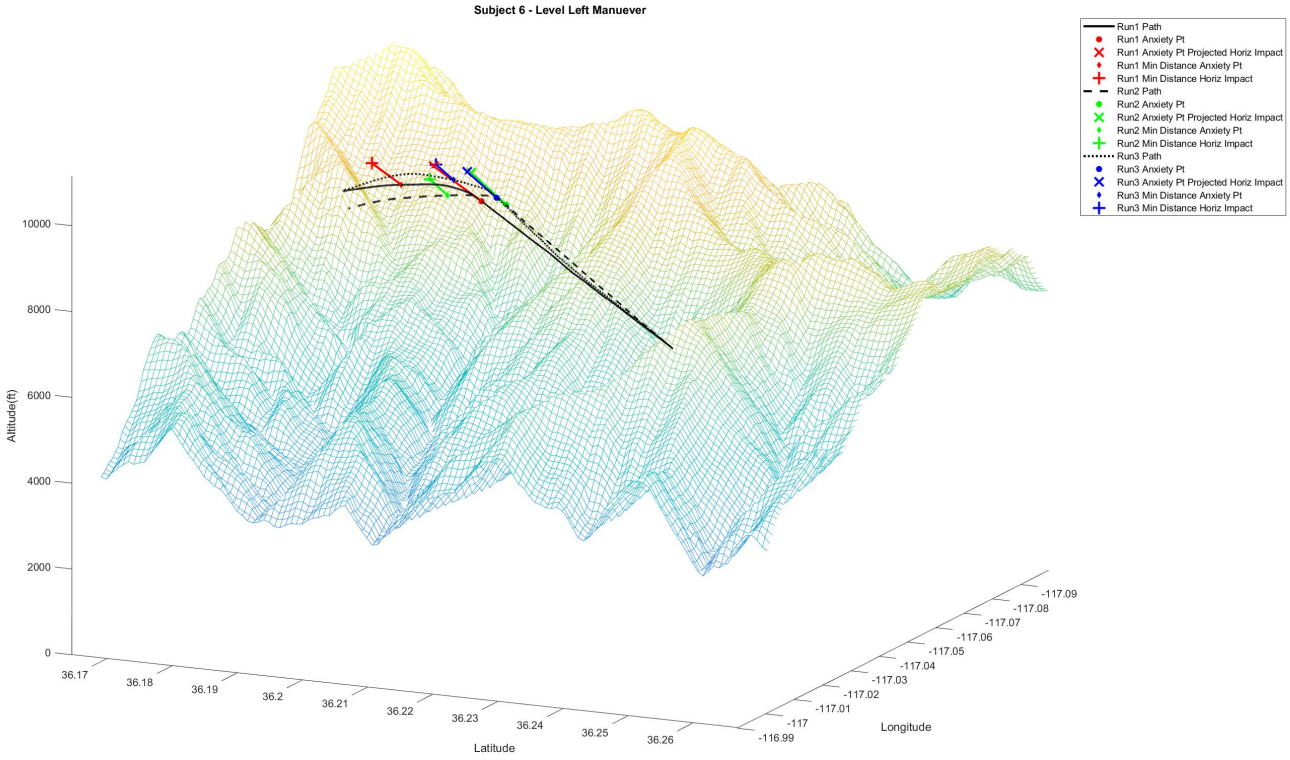

Figure 54. Test Subject 6 - Level Left Escape-Maneuvers and Projected Time to Collision Points

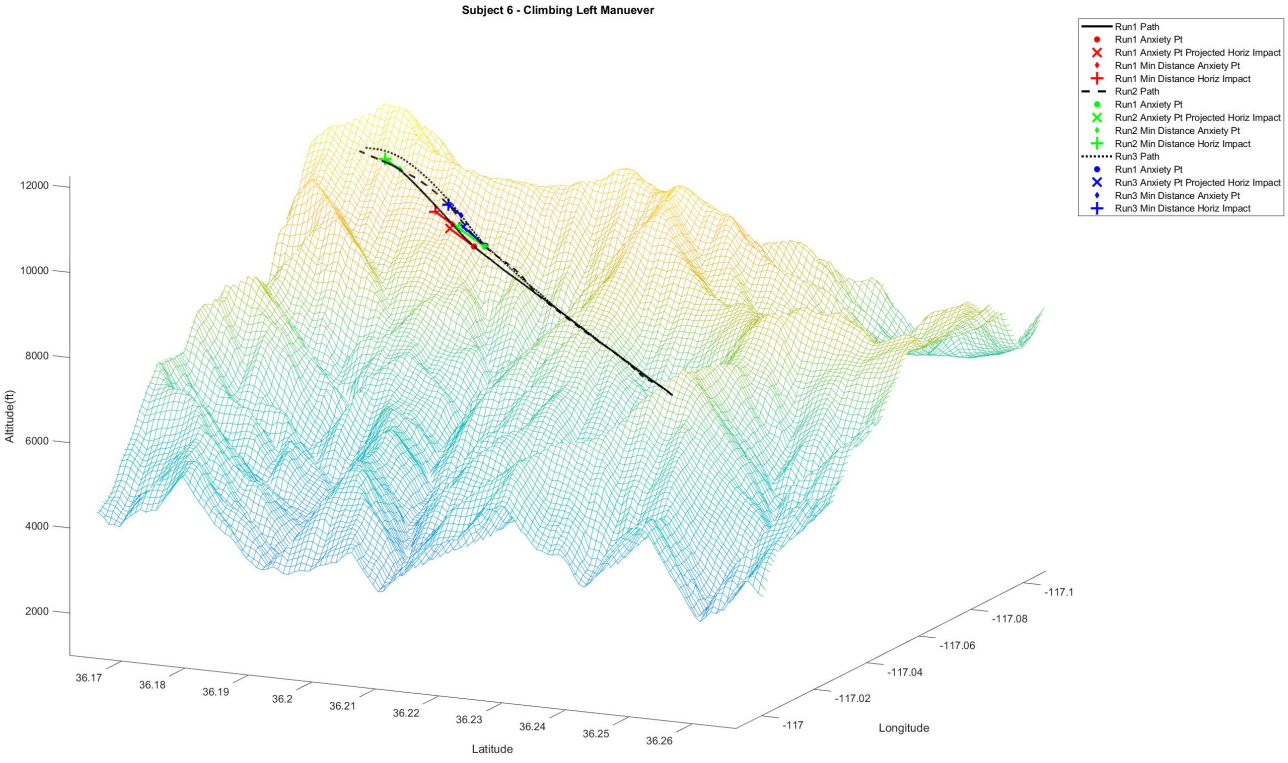

Figure 55. Test Subject 6 - Climbing Left Escape-Maneuvers and Projected Time to Collision Points

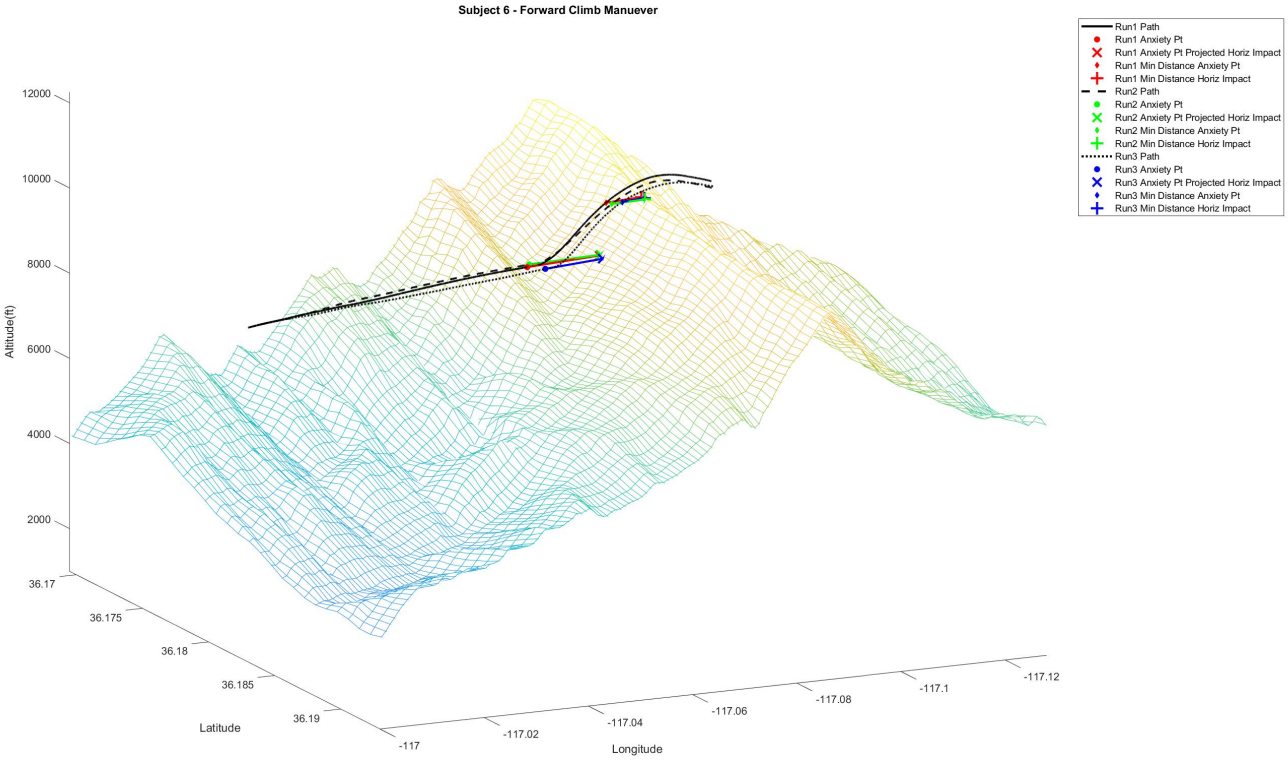

Figure 56. Test Subject 6 - Forward Climb Escape-Maneuvers and Projected Time to Collision Points

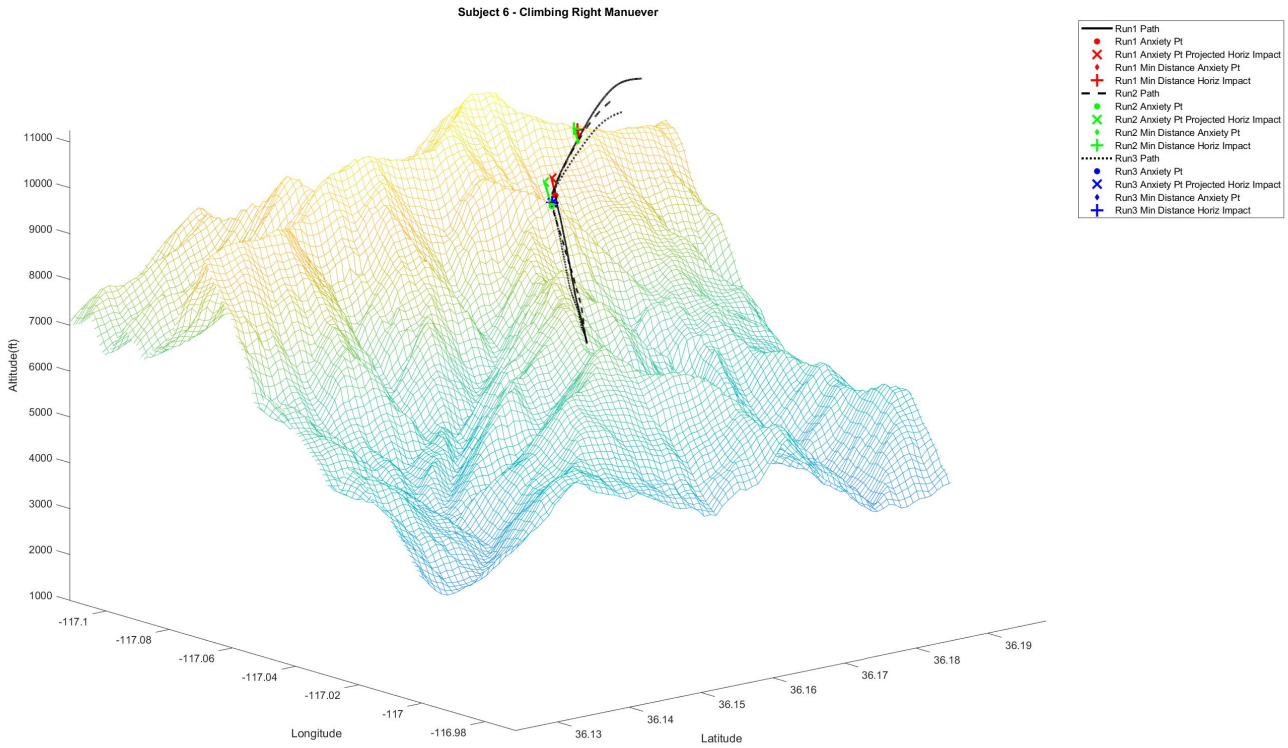

Figure 57. Test Subject 6 - Climbing Right Escape-Maneuvers and Projected Time to Collision Points

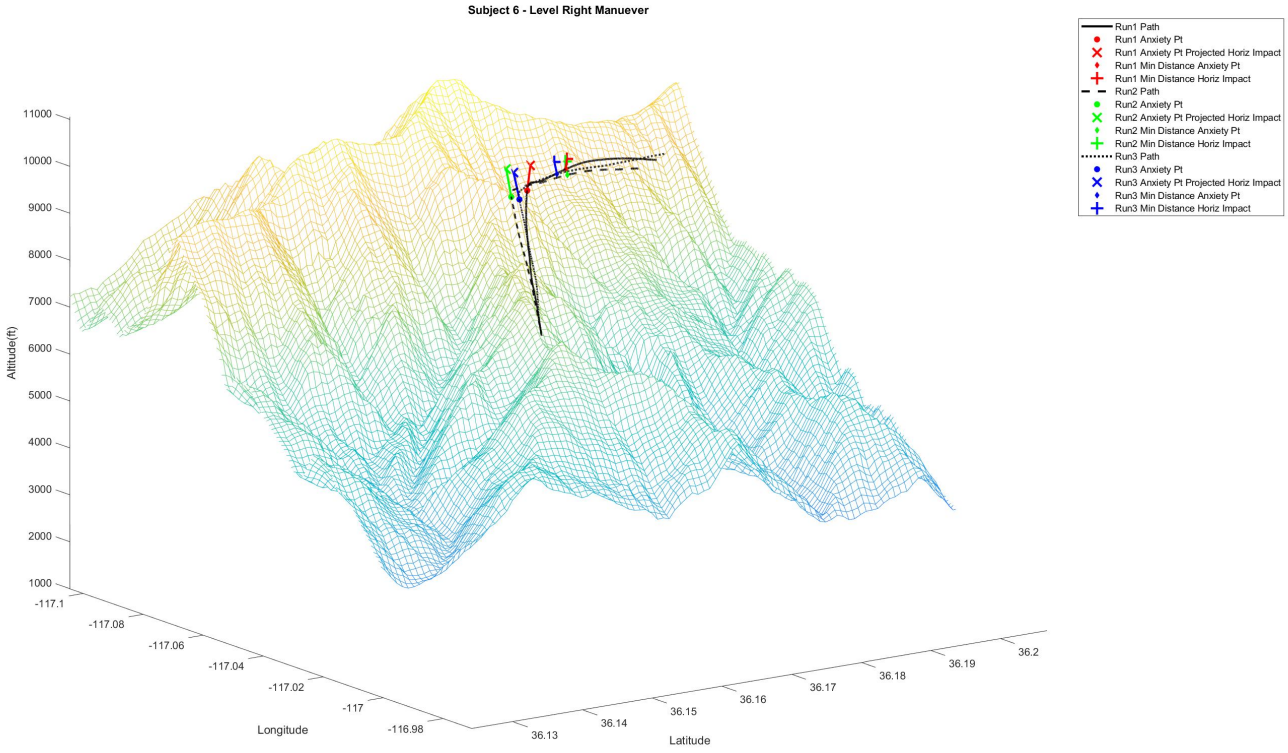

Figure 58. Test Subject 6 - Level Right Escape-Maneuvers and Projected Time to Collision Points

Multi-Crew Cockpit Simulator (MCCS) Study

Initial Nuisance and Display Evaluation of an Automatic Ground Collision Avoidance System (auto-GCAS) for Performance Limited Aircraft

Study Conductor(s):

Auto-GCAS algorithm:	Jim Carpenter, AFIT/ENY
MCC Integration & Coding:	Zach Demers, AFRL/RQQD
MCC Display & Operation:	Tom Danube, AFRL/RQQD

Study Participants:

All participants are current or retired cargo (C-17 and C-130) aircraft pilots. Members include C-17 pilots from the 89 AS, previous test pilots, and AFIT faculty / students.

Overall Study Goals:

The first goal is to develop an initial Design Criteria Limit (nuisance boundary) for the LJ-25D aircraft through the LJ-25D model hosted on the MCCS. This is Task 2 of the study.

The second goal is to receive feedback on initial concept displays, the situational awareness level desired by pilots, warning indicators leading up to Auto-GCAS activation, and also the take-over control of the Auto-GCAS. This is Task 3 of the study.

Test Item Description:

The aircraft model flown is a Learjet LJ-25D developed through Air Force Test Pilot School in conjunction with Textron Aviation and Calspan. Additionally, the auto-GCAS algorithm has been flight tested on the LJ-25D in September 2018. The Auto-GCAS algorithm system logic is represented in Figure 1. The algorithm takes the current aircraft position and state variables (Euler angles, body velocity vectors, latitude/longitude position, etc) from the LJ-25D model and projects the future aircraft spatial location. For each projected location, the algorithm calculates five spatial-escape paths from pre-determined escape maneuvers.

Path Number	Maneuver Term	Description	Look Ahead Time
Path 1	Level Left (LL)	60º bank, 0º climb angle	30s
Path 2	Climbing Left (CL)	15º bank with 10 º AoA	30s
Path 3	Forward Climb (FC)	Roll to wings level, at under 10º bank-starts climb at 2-g pull to 10 º AoA climb	45s
Path 4	Climbing Right (CR)	15º bank with 10 º AoA	30s
Path 5	Level Right (LR)	60º bank, 0º climb angle	30s

All 5 escape-path altitudes are compared to the Digital Terrain Elevation Data (DTED) altitude plus a 250-ft safety buffer, at a refresh rate of 7.15 Hz as represented in Figure 2. This differential height comparison represents Height Above Terrain (HAT). If HAT is less than zero (including the safety buffer), the escape path is closed. Once all paths are closed, the algorithm triggers the last open escape path and transfers aircraft control from the pilot to the autopilot maneuvers in

order for the aircraft's digital flight controls to execute the selected escape path. The algorithm continues executing and transferring between escape paths until the forward climb path is open, at which point the control is handed back to the pilot as demonstrated in Figure 3.

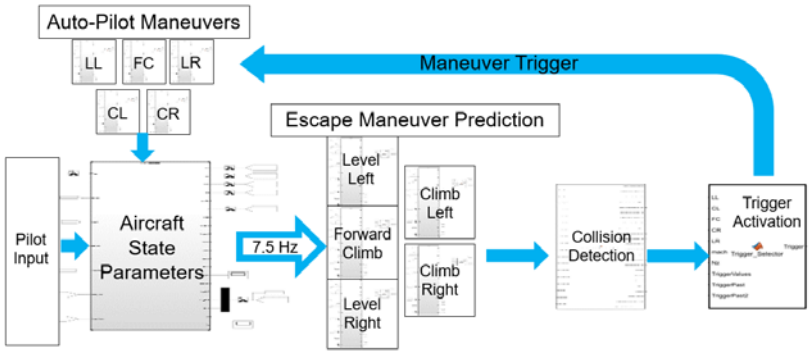

Figure 1: Auto-GCAS algorithm system logic

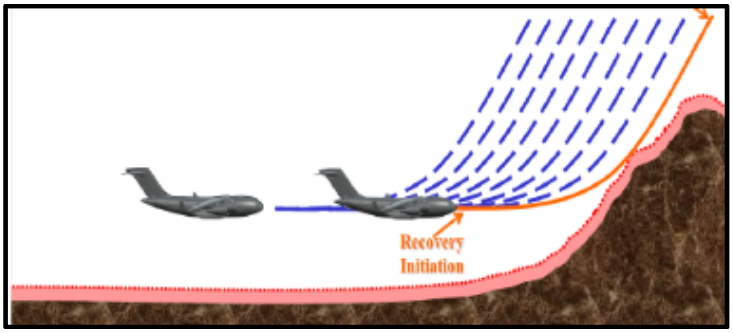

Figure 2: Auto-GCAS refresh rate for terrain collision calculations

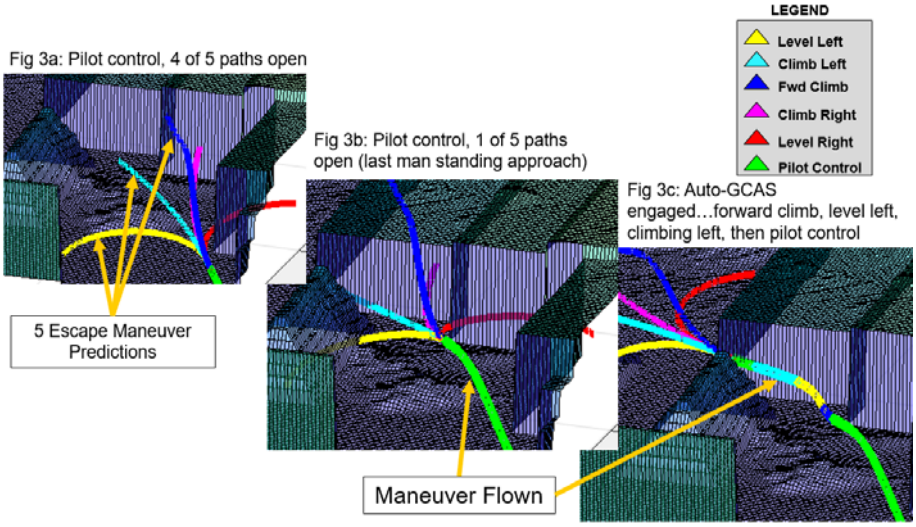

Figure 3: Collision avoidance progression

Switchology:

The left simulator seat will be the test participant chair. The stick is left hand controlled with two specific buttons used for Auto-GCAS testing. The pinkie button on the back of the

stick disconnects the Auto-GCAS algorithm (ref Figure 4). The button has to be held down to continue disconnect, and once released will run the Auto-GCAS algorithm again. When this button is depressed, the green indicator light will turn off in the upper right portion of the Multi-Function Display MFD. The thumb button on the front of the stick will be a time stamp for Design Criteria Limit, where the pilot will press and hold the button to indicate when they would initiate the maneuver to avoid terrain. When this button is depressed, a red indicator light will turn on in the upper left portion of the MFD. The Auto-GCAS display is viewed on the MFD by pressing the "GCAS" button on the top right MFD page options. The 4 different Auto-GCAS displays can be toggled by selecting a small representative icon of each display on the right side of the MFD.

Figure 4: MCCS aircraft stick

Simulator Intricacies:

Below are a few non-standard items specific to the simulator at the time of the study:

- The HUD horizon line is slightly angled to visual terrain horizon line (projector scaling issue)
- The HUD g-force readout has a delay for short abrupt maneuvers
- The rudder pedals do not have yaw input control, only use pitch and roll inputs through stick
- The stick may give out on load pressure during operations, just continue flying if possible, and the stick resistance will be reloaded after that task

Test Location Description:

The primary test location will be between N37 and N36 latitude, and W118 and W117 longitude (ref Figure 5). A red outlined box is overlaid on the MFD topographical map to indicate this range. This covers the terrain in Death Valley National Park where the max altitude is 11,050 ft (Telescope Peak), and the min altitude is -252 ft (Badwater Basin). The terrain was chosen for aggressive mountain terrain and steep valleys in order to encourage auto-GCAS activations against varying terrain. Any Lat / Lon flown outside this location will still have imagery shown in the simulator, but the Auto-GCAS algorithm will not-engage before ground contact because the algorithm does not have the DTED information to work.

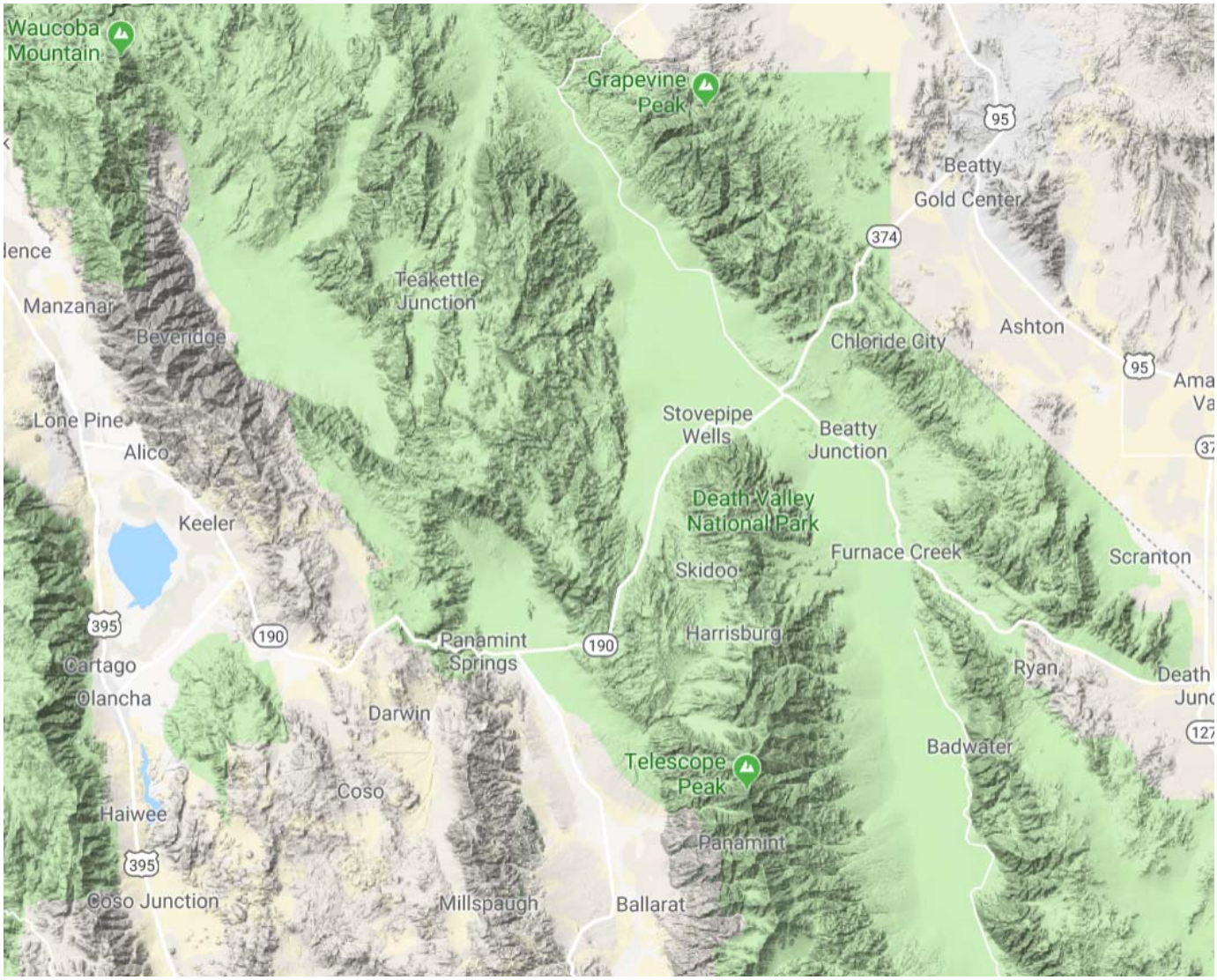

Figure 5: DTED map loaded, N37 – N36 and W118 to W117

TASK 1: Simulator Familiarity

1. Initial Questionnaire & Familiarity with Simulator

Approximately how many flight hours do you have in a cargo aircraft? _____ **hrs**

Approximately, when was the last time you conducted low-level (<500 ft AGL) mountainous flying? (N/A if not applicable) _____ **(yrs/months)**

What cargo platform(s) have you flown? _____

2. Simulator Familiarity

Objective: Verbal confirmation from pilot that they are comfortable with simulator displays, switches, and aircraft controls before proceeding to recorded tasks.

Initial Condition (Scenario 1):

Auto-GCAS turned off, no MFD displays showing, and all warnings muted.
Lat: 36.3
Lon: -116.95
Altitude: 8300 ft
Heading: 215
Airspeed: 300 knots
Paths: [0 0 0 0 0]

Task:

Have pilot be able to maintain constant airspeed, level flight, and level heading. Have pilot perform standard turns at 30º bank while maintaining altitude and speed. Have pilot perform the 5 paths manually. Have pilot fly close to terrain to see feeling of ground rush, and also what it means to go through the terrain. Have pilot press pinkie button and thumb button to see MFD light.

Check points for familiarity, get verbal Y/N before proceeding to Task 2:

1. Comfortable with readouts of the HUD? (airspeed, altitude, heading, g-load, horizon line) _____ (Y / N)
2. Comfortable with readouts of the internal instruments (airspeed, altitude, lat / lon location, heading, VVI) _____ (Y / N)
3. Comfortable with stick control? Do your inputs to the aircraft match expected outcome? _____ (Y / N)
4. Comfortable with switch used to turn on / off the Auto-GCAS algorithm (pinkie button)? _____ (Y / N)
5. Comfortable with switch used to turn on/ off the Design Criteria Limit (thumb button)? _____ (Y / N)

TASK 2: Design Criteria Limit

Objective: Determine initial Design Criteria Limit (nuisance boundary) for heavy aircraft through the LJ25-D simulator by calculating the time until impact for each escape maneuver. The time until impact is the Design Criteria Limit, where the Auto-GCAS activation needs to occur after in order to avoid a nuisance activation to the pilot.

Measure of Performance: The time until impact is the time between when the pilot initiates their escape maneuver (by pressing the thumb button) and how long it would have taken from that position to impact the terrain in front of them (i.e. if the pilot did not put in an input, how long would it have taken them to impact the terrain from where they felt "uncomfortable" not executing the escape maneuver).

Method of Evaluation: The auto-GCAS algorithm will be turned off. Participant will fly towards Telescope Peak (N36.17, W117.09) three times for each path. When the pilot feels like the maneuver should be activated to safely steer away from terrain, they will depress the thumb button for recording and perform the specified maneuver (level left, climbing left, forward climb, climbing right, or level right) while holding the thumb button down. Once they feel safe from impacting the terrain, they will release the thumb button. This will be repeated three times for each escape maneuver, for a total of 15 recorded test points collected per participant. After each test pass, the pilot will be asked for an anxiety rating per the following scale.

Anxiety Rating Scale:

Anxiety Value	Anxiety Rating
1	Was never more than casually aware of the ground
2	Would have felt comfortable with a recovery at a lower altitude
3	Recovery went as anticipated
4	Recovery went lower than personal comfort levels allow
5	Sensations of life threatening conditions

Test Card 1	**Path 1 – Level Left Turn**		**Comments**	
Starting Initial Conditions	Lat	36.57		
(Scenario #1)	Lon	-116.99		
Subject #____	Altitude	8682	*8668 on MFD instrument	
	Heading	225		
	Airspeed	300		
	Paths	[0 0 0 0 0]		
Data Collected	Anxiety Rating (circle)	Red Recording Light On	Run File #	
Test 1	1 2 3 4 5	Y / N		
Test 2	1 2 3 4 5	Y / N		
Test 3	1 2 3 4 5	Y / N		

Test Card 2	**Path 2 – Climbing Left Turn**		**Comments**	
Starting Initial Conditions	Lat	36.57		
(Scenario #1)	Lon	-116.99		
Subject #____	Altitude	8682	*8668 on MFD instrument	
	Heading	225		
	Airspeed	300		
	Paths	[0 0 0 0 0]		
Data Collected	Anxiety Rating (circle)	Red Recording Light On	Run File #	
Test 1	1 2 3 4 5	Y / N		
Test 2	1 2 3 4 5	Y / N		
Test 3	1 2 3 4 5	Y / N		

Test Card 3	**Path 3 – Forward Climb**		**Comments**	
Starting Initial Conditions	Lat	36.183		
(Scenario #2)	Lon	-117.00		
Subject #____	Altitude	8855	8886 on MFD instrument	
	Heading	265		
	Airspeed	300		
	Paths	[0 0 0 0 0]		
Data Collected	Anxiety Rating (circle)	Red Recording Light On	Run File #	
Test 1	1 2 3 4 5	Y / N		
Test 2	1 2 3 4 5	Y / N		
Test 3	1 2 3 4 5	Y / N		

Test Card 4	**Path 4 – Climbing Right Turn**		**Comments**	
Starting Initial Conditions	Lat	36.134		
(Scenario #3)	Lon	-116.97		
Subject #____	Altitude	9135	9112 on MFD instrument	
	Heading	296		
	Airspeed	300		
	Paths	[0 0 0 0 0]		
Data Collected	Anxiety Rating (circle)	Red Recording Light On	Run File #	
Test 1	1 2 3 4 5	Y / N		
Test 2	1 2 3 4 5	Y / N		
Test 3	1 2 3 4 5	Y / N		

Test Card 5	**Path 5 – Level Right Turn**		**Comments**	
Starting Initial Conditions	Lat	36.134		
(Scenario #3)	Lon	-116.97		
Subject #____	Altitude	9135	9112 on MFD instrument	
	Heading	296		
	Airspeed	300		
	Paths	[0 0 0 0 0]		
Data Collected	Anxiety Rating (circle)	Red Recording Light On	Run File #	
Test 1	1 2 3 4 5	Y / N		
Test 2	1 2 3 4 5	Y / N		
Test 3	1 2 3 4 5	Y / N		

TASK 3: Display Options

Objective: Feedback on auto-GCAS activation and displays in order to determine what information a pilot prefers for situational awareness and if current display ideas are nuisance free.

Measure of Performance: Participant comments on the pre-initiation warnings, the activation phase, and the handback phase. Particularly interested in warning sequence and situational awareness.

Method of Evaluation: Participant will fly along a ridge line (staying close to 300 ft AGL), go up west up a canyon at the indicated test point conditions (Lat / Lon), and purposefully steer the aircraft towards the ground to activate any of the 5 paths. This will be repeated for each of the 4 displays, and comments recorded on how each participant was warned during the pre-initiation phase, the activation phase, and the handback phase.

*** Note: The two primary MFDs in front of the pilot will not have auto-GCAS selected. This is because when the system activates, it should override one of the primary displays to inform the pilot the system is activated. This is in addition to the HUD and the center console MFD warnings. However, the right primary MFD needs to be selected to be the same as the center console.**

**** Put display on upper center console MFD, ensure pilot's console does not have display**

Explanation of Display Stages:
(1) No-Initiation: The algorithm is running, but not escape paths are closed off
(2) Partial Initiation: Some Paths are closed but algorithm not activated
(3) Pre-Initiation: Only one path remaining, algorithm likely to engage
    - Chevron warning in HUD of only 1 path left to inform pilot
(4) Initiation: All paths closed, algorithm engaged
    - Audio / Visual Warning to inform pilot of escape path

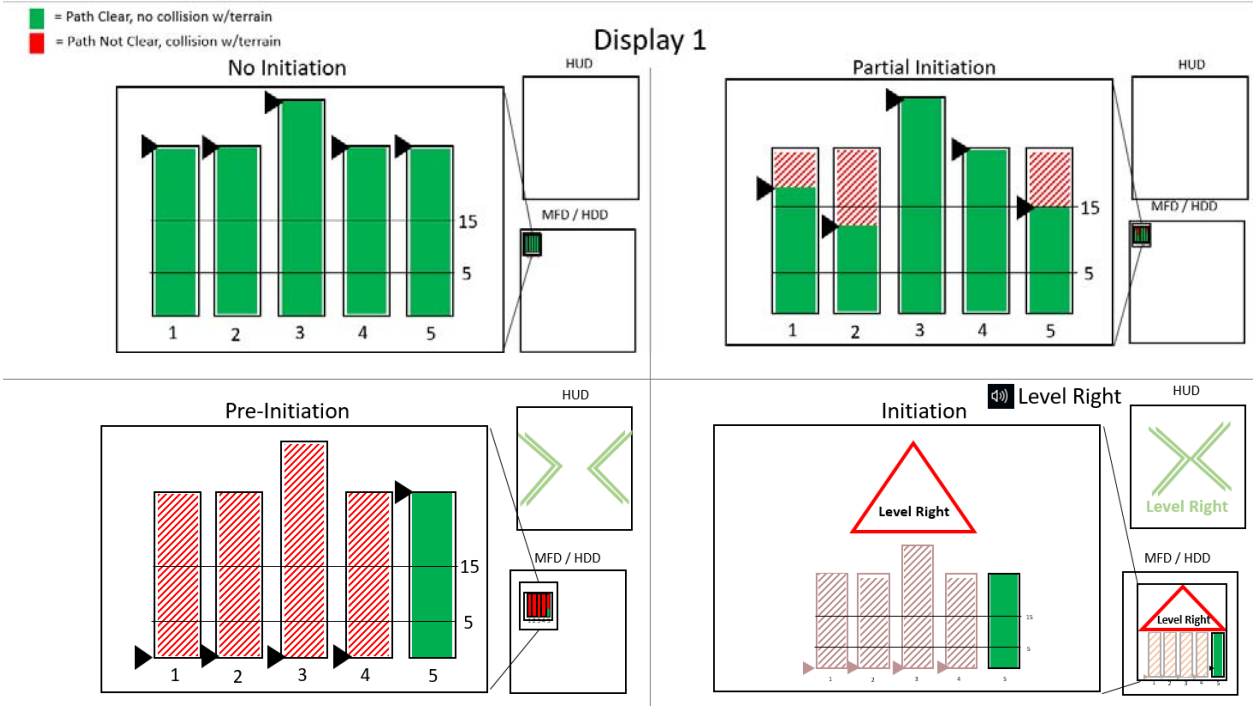
= Path Clear, no collision w/terrain
= Path Not Clear, collision w/terrain
Display 1
No Initiation
HUD
MFD / HDD
15
5
1
2
3
4
5
Partial Initiation
Pre-Initiation
Initiation
Level Right

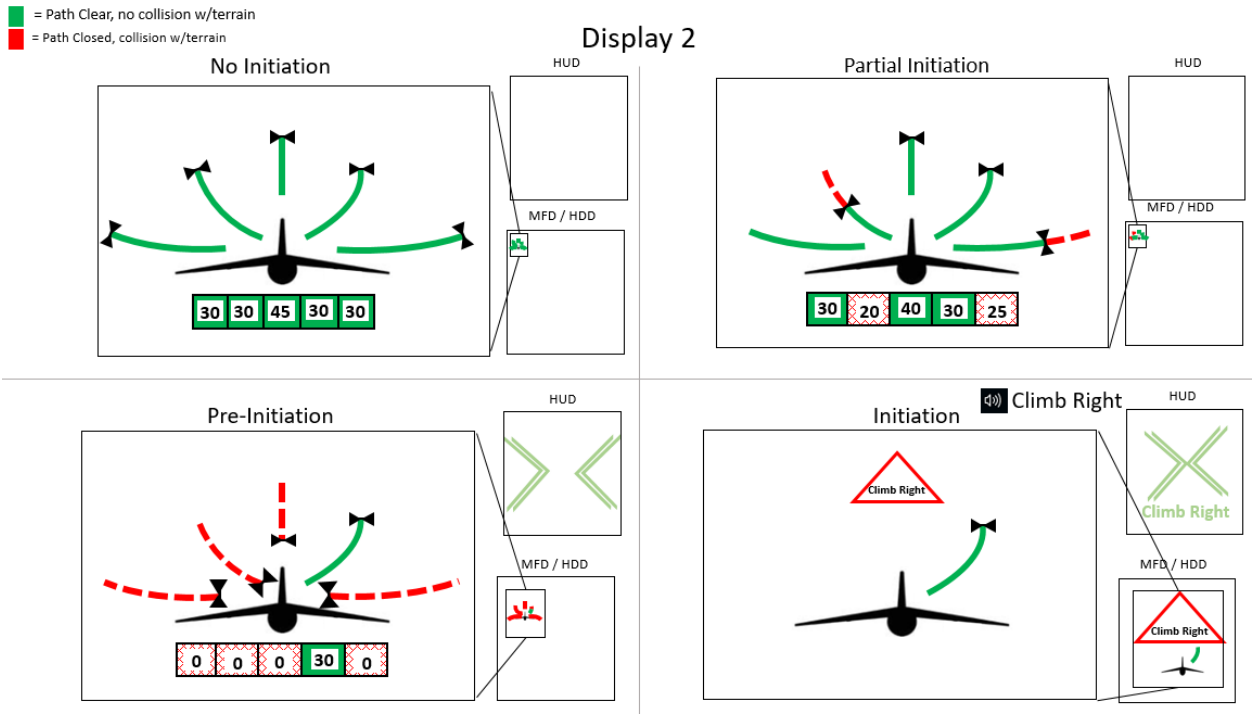
= Path Clear, no collision w/terrain
= Path Closed, collision w/terrain
Display 2
No Initiation
HUD
MFD / HDD
30 30 45 30 30
Partial Initiation
30 20 40 30 25
Pre-Initiation
0 0 0 30 0
Initiation
Climb Right

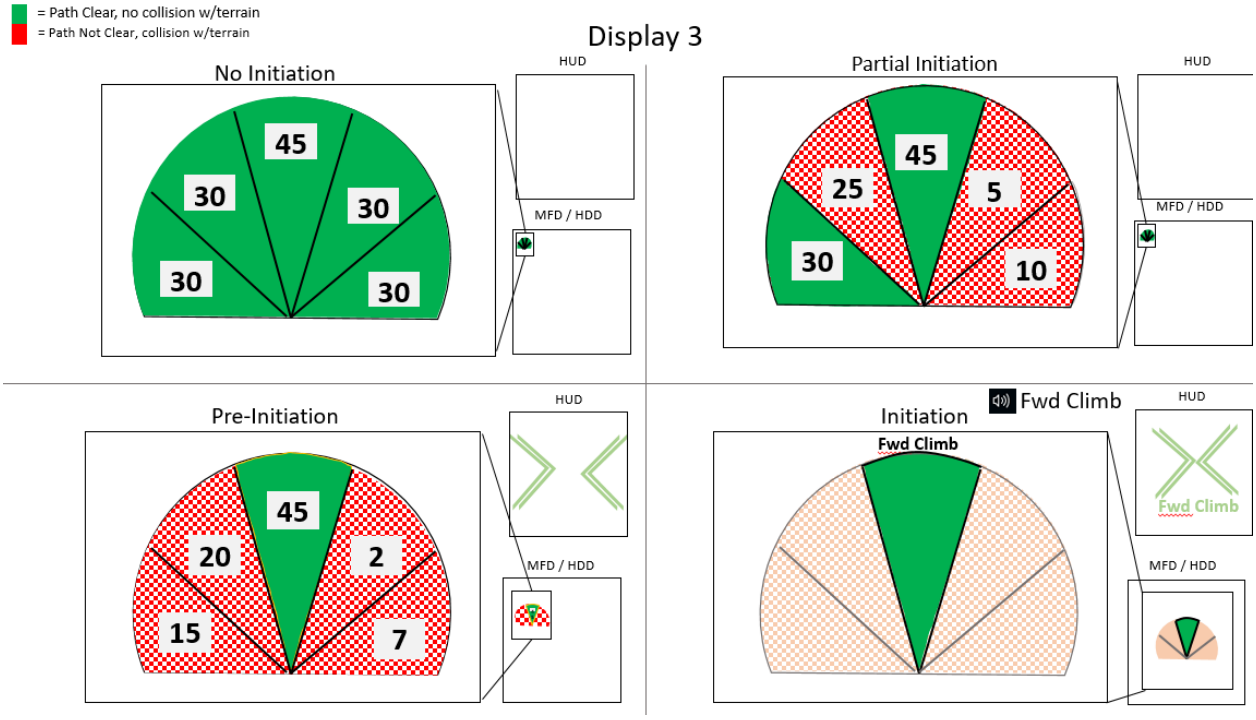
= Path Clear, no collision w/terrain
= Path Not Clear, collision w/terrain
Display 3
No Initiation
HUD
MFD / HDD
45
30
30
30
30
Partial Initiation
HUD
MFD / HDD
45
25
5
30
10
Pre-Initiation
HUD
MFD / HDD
45
20
2
15
7
Initiation
Fwd Climb
HUD
MFD / HDD
Fwd Climb
Fwd Climb

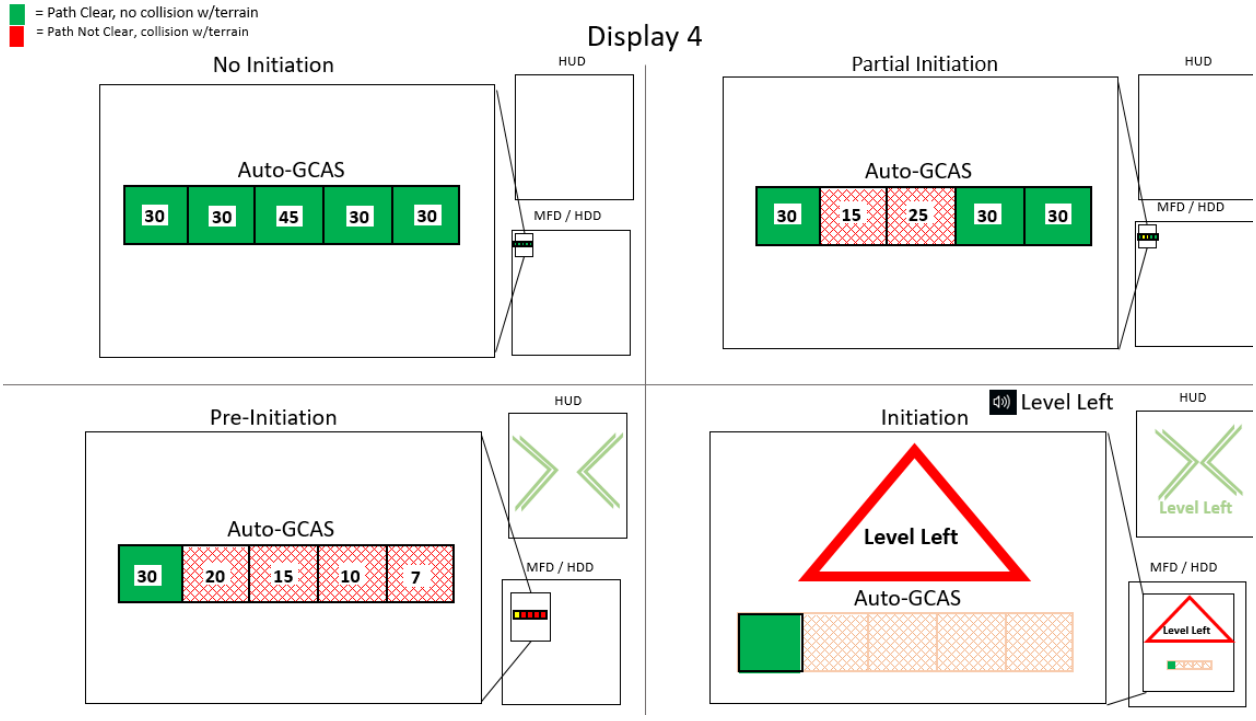
= Path Clear, no collision w/terrain
= Path Not Clear, collision w/terrain
Display 4
No Initiation
HUD
MFD / HDD
Auto-GCAS
30
30
45
30
30
Partial Initiation
HUD
MFD / HDD
Auto-GCAS
30
15
25
30
30
Pre-Initiation
HUD
MFD / HDD
Auto-GCAS
30
20
15
10
7
Initiation
Level Left
HUD
MFD / HDD
Level Left
Auto-GCAS
Level Left
Level Left

Test Card 6	Any Path Activation Possible		Comments
Starting Initial Conditions	Lat	36.8	* Rolling hill terrain
(Scenario #4)	Lon	-117.92	
Subject #____	Altitude	3996	
	Heading	270	
	Airspeed	300	
	Paths	[1 1 1 1 1]	
Data Collected			
Display 1	Was it clear which paths were closed before activation?	Y / N	
	Was it clear which path was selected?	Y / N	
	Did Auto-GCAS activate at a reasonable time?	Y / N	
	Would you have chosen a different path to avoid terrain?	Y / N	If Yes, which path:
Display 2	Was it clear which paths were closed before activation?	Y / N	
	Was it clear which path was selected?	Y / N	
	Did Auto-GCAS activate at a reasonable time?	Y / N	
	Would you have chosen a different path to avoid terrain?	Y / N	If Yes, which path:

Test Card 7	Any Path Activation Possible		Comments
Starting Initial Conditions	Lat	36.8	* Mountainous terrain
(Scenario #5)	Lon	-117.92	
Subject #____	Altitude	3996	
	Heading	270	
	Airspeed	300	
	Paths	[1 1 1 1 1]	
Data Collected			
Display 3	Was it clear which paths were closed before activation?	Y / N	
	Was it clear which path was selected?	Y / N	
	Did Auto-GCAS activate at a reasonable time?	Y / N	
	Would you have chosen a different path to avoid terrain?	Y / N	If Yes, which path:
Display 4	Was it clear which paths were closed before activation?	Y / N	
	Was it clear which path was selected?	Y / N	
	Did Auto-GCAS activate at a reasonable time?	Y / N	
	Would you have chosen a different path to avoid terrain?	Y / N	If Yes, which path:

Display Questions:

Between the 4 displays, rank them compared to each other for the following attributes overall from best to worst. (Best being 1 and worst being 4).

	Display 1	Display 2	Display 3	Display 4
Situational Awareness				
Clarity of Information				
Overall Ranking				

Is there information missing from the MFD display design, if so, what?

_____

_____

_____

_____

_____

Is there information missing from the HUD display design, if so, what?

_____

_____

_____

_____

_____

Any final comments on the display designs?

_____

_____

_____

_____

_____

AFRL IR Protocol Number: FWR20190014N

IRB Reviewer Basis for Determination/Comments:

The data collected will be specific to operators of heavy aircraft with A-GCAS displays. The results will not generalize outside of this single operational community. Pilots and retired pilots will be evaluating a simulated collision avoidance system to determine nuisance and noise. Pilot comments will only be identified by a subject number and not as personally identifiable information. This project does not meet the definition of research per 32 CFR 219 as the data not intended to contribute to generalizable knowledge but will only apply to operators of heavy aircraft that have this specific display.

There may be other approvals that are required (i.e. safety review board) that are outside of the purview of the IRB.

THIS PAGE TO BE COMPLETED BY AFRL IRB MEMEBER

This purpose of this worksheet is limited to consideration of whether an activity falls under the purview of the AFRL IRB in accordance with 32 CFR 219, DoDD 3216.2, AFI 40-402, and related human research subject regulations. The AFRL IRB is not responsible for the oversight of activities that are determined not to be research involving human subjects (e.g., test and evaluation activities). Any modifications to this activity must first be reviewed by the AFRL IRB.

If this activity is a survey, attitude or opinion poll, questionnaire, or interview, it might require approval by the Air Force Survey Office (HQ AFPC/DSYS). See AFI 38-501, Air Force Survey Program. Contact HQ AFPC/DSYS with questions: af.surveys@us.af.mil.

Other reviews and determinations may be required before this activity can begin. If other reviews are required, they should be pursued separately (note, AFRLI 61-103 v.2).

Contact the AFRL Safety Officer, Mr. Keith Vossler, AFRL/SE, regarding requirements applicable to test and evaluation: keith.vossler@us.af.mil.

REVIEWER DETERMINATION:

Based on the information provided, the IRB reviewer has determined:

☐ The activity does not meet the definition of "research" under the Common Rule (32 CFR 219).

☐ The activity is research but does not involve "human subjects" under the Common Rule (32 CFR 219).

☐ The activity needs review by the IRB Chair for the following reasons:

☐ The activity is research involving Human Subjects under the common rule (32 CFR 219).

☐ The activity involves use of protected health information (PHI) for research purposes.

☐ The activity appears to be subject to FDA regulations.

IRB Reviewer Signature

ALLEN.RHONDA.COLLEEN.1395901547 Digitally signed by ALLEN.RHONDA.COLLEEN.1395901547 Date: 2018.10.25 11:28:34 -04'00'

Date

Bibliography

[1] Federal Aviation Administration. "Airworthiness Criteria for the Installation Approval of a Terrain Awareness and Warning System (TAWS) for Part 25 Airplanes". In: *Advisory Circular* (2000). ISSN: 1002185X.

[2] International Air Transport Association (IATA). *IATA Controlled Flight Into Terrain Accident Analysis Report 2008-2017 Data 2018 Edition*. 2018.

[3] Randy Gibb and Wes Olson. "Classification of Air Force Aviation Accidents: Mishap Trends and Prevention". In: CI04-1814 (June 2006).

[4] Angela Suplisson. AFTC Deputy Commander: Personal Communication, 2018.

[5] JK Evans. "Frequency of Specific Categories of Aviation Accidents and Incidents During 2001-2010". In: (Mar. 2014). URL: `http://ntrs.nasa.gov/search.jsp?R=20140012710`.

[6] Boeing Commercial Airplanes. "Statistical Summary of Commercial Jet Airplane Accidents - Worldwide Operations 1959 – 2014". In: (2010), p. 24. URL: `http://www.boeing.com/commercial/safety/investigate.html`.

[7] Donald Rumsfeld. "Reducing Preventable Accidents". In: *'Secretary of Defense Memorandum'* (May 2003).

[8] E.M. Griffin et al. ""Automatic ground collision avoidance system design for pre-block 40 F-16 configurations"". In: *IEEE Aerospace and Electronic Systems Magazine* (May 2012), pp. 4–15.

[9] Arthur Barfield. AFRL Auto GCAS Chief Engineer: Personal Communication, 2018.

[10] Kenneth C. Gahan. "Multi-Path Automatic Ground Collision Avoidance System for Performance Limited Aircraft with Flight Tests: Project HAVE MEDUSA". Air Force Institute of Technology, Mar. 2019. Unpublished.

[11] J K Kuchar and a C Drumm. "The traffic alert and collision avoidance system". In: *Lincoln Laboratory Journal* 16.2 (2007), pp. 277–296.

[12] Angela W. Suplisson. "Optimal Recovery Trajectories for Automatic Ground Collision Avoidance Systems (Auto GCAS)". PhD thesis. Air Force Institute of Technology, Mar. 2015.

[13] John V Trombetta. "Multi-Trajectory Automatic Ground Collision Avoidance System with Flight Tests (Project Have ESCAPE)". Air Force Institute of Technology, 2016.

[14] Stéphane Mondoloni. "Aircraft Trajectory Prediction Errors: Including a Summary of Error Sources and Data". In: *FAA/Eurocontrol Action Plan 16 Common Trajectory Prediction Capabilities* (July 2006). URL: `https://acy.tc.faa.gov/data/_uploaded/Publications/tjm/TP_Sens_v02.pdf`.

[15] Aaron M.U. Church. “”The Science of Avoidance””. In: (Feb. 2016). URL: http://www.airforcemag.com/MagazineArchive/Pages/2016/February%5C%202016/The-Science-of-Avoidance-.aspx.

[16] Neil Campbell. “The Use of Enhanced Ground Proximity Warning System (EGPWS) Data for Aviation Safety Investigation”. In: (2005). URL: http://scholar.google.com/scholar?hl=en&btnG=Search&q=intitle:The+Use+of+Enhanced+Ground+Proximity+Warning+System+(+EGPWS+)+Data+for+Aviation+Safety+Investigation#0.

[17] Honeywell. “MK V and MK VII EGPWS”. In: (2011).

[18] Mikael Karanikas and Agne Widholm. “Accident involving a Royal Norwegian Air Force aircraft of type C-130 with call sign HAZE 01, on 15 March 2012 at Kebnekaise, Norrbotten County, Sweden.” In: (2013).

[19] Barry C Breen. *The Avionics Handbook*. CRC Press LLC, 2001. Chap. Enhanced Situation Awareness.

[20] Robert C. Nelson. *Flight Stability and Automatic Control*. 2nd. McGraw Hill, Feb. 1998.

[21] Brian L Stevens and Frank L Lewis. *Aircraft Control and Simulations*. 2nd. John Wiley sons, Inc., 2003.

[22] Donald L. Kunz. *Intermediate Dynamics for Aeronautics Astronautics*. Centerville, OH: Headmaster Press, 2015.

[23] Karen Kemp. *Encyclopedia of Geographic Information Science*. SAGE Publications, 2007, pp. 107–109. ISBN: 1452265607.

[24] Department of Defense. “Performance Specification Digital Terrain Elevation Data (DTED)”. In: *MIL-PRF-89020B* (2000). URL: https://dds.cr.usgs.gov/srtm/version2_1/Documentation/MIL-PDF-89020B.pdf.

[25] Paul Sorokowski et al. “Small UAV Automatic Ground Collision Avoidance System Design Considerations and Flight Test Results”. In: *NASA/TM-2015-218732* June (2015).

[26] D. E. Swihart et al. “Design, integration and flight test of an autonomous ground collision avoidance system”. In: *Gyroscopy and Navigation* 2.2 (2011), pp. 84–91. DOI: 10.1134/S2075108711020088.

[27] Donald E. Swihart et al. “Automatic ground collision avoidance system design, integration, & flight test”. In: *IEEE Aerospace and Electronic Systems Magazine* 26.5 (2011), pp. 4–11. DOI: 10.1109/MAES.2011.5871385.

[28] Kenneth C. Gahan et al. “A Limited Evaluation of an Automatic Ground Collision Avoidance System for Performance Limited Aircraft (Project Have MEDUSA)”. In: (2018).

[29] Guy Norris. "Auto-GCAS Saves Unconscious F-16 Pilot—Declassified USAF Footage". In: *Aviation Week Space Technology* (Sept. 2016). URL: http://aviationweek.com/air-combat-safety/auto-gcas-saves-unconscious-f-16-pilot-declassified-usaf-footage.

[30] Lisa F. Weinstein et al. "Standardization of Aircraft Control and Performance Symbology on the USAF Head-Up Display". In: *AL/CF-TR-1993-0088 AD-A274283* (1993). URL: http://www.dtic.mil/dtic/tr/fulltext/u2/AD-A274283.pdf.

[31] Major Foster Bitton and Major Rick Evans. "Head-Up Display Symbology Standardization". In: (1990). URL: http://www.dtic.mil/dtic/tr/fulltext/u2/a235818.pdf.

[32] Kimberlee H. Shish et al. "Trajectory Prediction and Alerting for Aircraft Mode and Energy State Awareness". In: *AIAA Infotech at Aerospace* (2015), pp. 1–19. URL: http://arc.aiaa.org/doi/10.2514/6.2015-1113.

[33] Daniel Delahaye et al. "Mathematical Models for Aircraft Trajectory Design : A Survey". In: *Lecture Notes in Electrical Engineering, 290 (Part V)* (2014), pp. 205–247. DOI: 10.1007/978-4-431-54475-3_12.

[34] T Ota, M Nagati, and D C Lee. "Aircraft collision avoidance trajectory generation". In: *Proceedings of the AIAA Guidance, Navigation, and Control Conference* (1998), pp. 828–837. URL: http://dx.doi.org/10.2514/6.1998-4241.

[35] Amos Gilat and Vish Subramaniam. *Numerical Methods for Engineers and Scientists: An Introduction with Applications Using MATLAB*. John Wiley sons, Inc., 2008.

[36] Åke Bjorck Dahlquist Germund. *Numerical Methods in Scientific Computing*. Vol. 1. 2008.

[37] John T. Betts. "Survey of Numerical Methods for Trajectory Optimization". In: *Journal of Guidance, Control, and Dynamics* 21.2 (1998), pp. 193–207. DOI: 10.2514/2.4231. URL: http://arc.aiaa.org/doi/10.2514/2.4231.

[38] Silvana Ilie, Gustaf Söderlind, and Robert M. Corless. "Adaptivity and computational complexity in the numerical solution of ODEs". In: *Journal of Complexity* 24.3 (2008), pp. 341–361. DOI: 10.1016/j.jco.2007.11.004.

[39] Vladimir Dobrushkin. *MATHEMATICA TUTORIAL for the First Course*. 2015. URL: http://www.cfm.brown.edu/people/dobrush/am33/Mathematica/RK3.html (visited on 12/15/2018).

[40] Tom Berger et al. "Development and Validation of a Flight-Identified Full-Envelope Business Jet Simulation Model Using a Stitching Architecture". In: *AIAA Modeling and Simulation Technologies Conference* (2017), pp. 1–34. DOI: 10.2514/6.2017-1550. URL: http://arc.aiaa.org/doi/10.2514/6.2017-1550.

[41] Global Air. "LJ-25D Technical Specificaitons". In: (). URL: https://www.globalair.com/aircraft-for-sale/Specifications?specid=15.

[42] MathWorks. "Choose a Solver". In: (). URL: https://www.mathworks.com/help/simulink/ug/types-of-solvers.html#f11-42611.

[43] P.J. Prince Dormand J.R. "A family of Embedded Runge-Kutta Formulae". In: *Journal of Computational and Applied Mathematics* 6 (1980).

[44] Stephanie Simon. AFRL Aerospace Engineer: Personal Communication, 2019.

REPORT DOCUMENTATION PAGE

Form Approved
OMB No. 0704–0188

1. REPORT DATE *(DD–MM–YYYY)*	2. REPORT TYPE	3. DATES COVERED *(From — To)*
03–21–2019	Master's Thesis	October 2017 — March 2019

4. TITLE AND SUBTITLE

Simulation and Piloted Simulator Study of an Automatic Ground Collision Avoidance System for Performance Limited Aircraft

5a. CONTRACT NUMBER

5b. GRANT NUMBER

5c. PROGRAM ELEMENT NUMBER

6. AUTHOR(S)

Capt James D. Carpenter

5d. PROJECT NUMBER

5e. TASK NUMBER

5f. WORK UNIT NUMBER

7. PERFORMING ORGANIZATION NAME(S) AND ADDRESS(ES)

Air Force Institute of Technology
Graduate School of Engineering and Management (AFIT/EN)
2950 Hobson Way
WPAFB OH 45433-7765

8. PERFORMING ORGANIZATION REPORT NUMBER

AFIT-ENY-MS-19-M-207

9. SPONSORING / MONITORING AGENCY NAME(S) AND ADDRESS(ES)

Aerospace Systems Directorate
2130 8th Street
WPAFB OH 45433-7765
DSN 798-4601
Email: amy.burns.3@us.af.mil

10. SPONSOR/MONITOR'S ACRONYM(S)

AFOSR / AFRL/RQ

11. SPONSOR/MONITOR'S REPORT NUMBER(S)

12. DISTRIBUTION / AVAILABILITY STATEMENT

DISTRIBUTION STATEMENT A:
APPROVED FOR PUBLIC RELEASE; DISTRIBUTION UNLIMITED.

13. SUPPLEMENTARY NOTES

14. ABSTRACT

The F-16 Automatic-Ground Collision Avoidance System (Auto-GCAS) has been a resounding success since implementation in Nov 2014, saving 8 pilots and 7 aircraft from Controlled Flight into Terrain (CFIT). However, there is no implemented Auto-GCAS for "heavy" performance limited aircraft. This research endeavors to expand on the success of F-16 Auto-GCAS to other aircraft in the Air Force inventory such as the C-130, C-17, and B-1. MIL-STD-1797 classifies performance limited aircraft as large, heavy, and low to medium maneuverability. Using a stitched Learjet-25D model (LJ-25D), an Auto-GCAS algorithm was developed to predict multiple escape-maneuver trajectories, compare these paths to digital terrain elevation data (DTED), and trigger the most aggressive escape path upon predicted terrain collision. Multiple numerical integration methods were compared to balance computational speed vs. accuracy. The Adams-Bashforth multi-step method showed improved accuracy and increased speed than the previous Euler Explicit method. Simulations in a modified DTED terrain map evaluated differences in Auto-GCAS algorithm design, principally forward look-ahead time. Results showed extending the forward look-ahead time past 45 s did not decrease collision prevention, but changing the trigger activation to the forward-open method successfully reduced the number of collisions. An algorithm was developed to vary trajectory prediction based on airspeed and performance variables without increasing computational cost. This Trajectory Prediction Algorithm (TPA) was able to extend the forward climb look-ahead time approximately 20 seconds at slower airspeeds and successfully escape a box canyon where previous methods failed. Preliminary pilot feedback was collected through a piloted simulator study at Air Force Research Laboratory's (AFRL) Multi-Crew Cockpit Simulator (MCCS).

15. SUBJECT TERMS

Auto-GCAS, Trajectory Prediction Algorithm, Terrain Collision Prediction, Numerical Integration, Piloted Simulator Study

16. SECURITY CLASSIFICATION OF:			17. LIMITATION OF ABSTRACT	18. NUMBER OF PAGES	19a. NAME OF RESPONSIBLE PERSON
a. REPORT	b. ABSTRACT	c. THIS PAGE			Dr. Richard G. Cobb, AFIT/ENY
U	U	U	U	113	19b. TELEPHONE NUMBER *(include area code)* (937) 255-3636 x4559 richard.cobb@afit.edu